EFFECT OF MATERIAL CONTRAST ON ANISOTROPY AND DISPERSION OF LAYERED PERIODIC MEDIUM

A Thesis

Presented to

the Faculty of the Department of Earth and Atmospheric Sciences

University of Houston

In Partial Fulfillment

of the Requirements for the Degree

Master of Science

By

Yuandi Gan

December 2014

EFFECT OF MATERIAL CONTRAST ON ANISOTROPY AND DISPERSION OF LAYERED PERIODIC MEDIUM

Yuandi Gan

APPROVED:

Dr. Evgeny Chesnokov, Chairman
Department of Earth and Atmospheric Sciences

Dr. Aibing Li
Department of Earth and Atmospheric Sciences

Dr. Donald Kouri
Department of Physics

Dean, College of Natural Sciences and Mathematics

Acknowledgements

Thanks is due to my advisor, Dr. Evgeny Chesnokov, for giving me the guidance on finding my way on research. Thanks to other committee members, Dr. Aibing Li, and Dr. Donald Kouri, for their insightful recommendations on my research. Thanks to Rui Zhou and Zhao Li, who gave me much help when I faced obstacles during research.

Finally, thank you to my father, Tao Gan, my mother, Xiaoyan Ji, and my girlfriend Linyu Li, who gave me patient support and endless love, which provide courage and strength for me when frustrations or setbacks would occur.

EFFECT OF MATERIAL CONTRAST ON ANISOTROPY AND DISPERSION OF LAYERED PERIODIC MEDIUM

An Abstract of a Thesis

Presented to

the Faculty of the Department of Earth and Atmospheric Sciences

University of Houston

In Partial Fulfillment

of the Requirements for the Degree

Master of Science

By

Yuandi Gan

December 2014

Abstract

In order to research the anisotropy and dispersion features of media with aligned fractures, models which approximately describe the media are constructed. For the case in which crack density is very high and aspect ratio may be very low, the cracked medium can be described as a layered periodic medium, in which the aligned fractures in question are described as layers.

Given a layered periodic medium consisting of all solid layers, the effect of the contrast between individual layers on the behavior of anisotropy is examined. The effect of shear modulus contrast on anisotropy is essential. If shear moduli of two layers are equal, the effective medium is isotropic. The increase of bulk modulus contrast shifts the maximum S_V-wave velocity point to that of smaller angle.

For the layered periodic medium consisting of alternating solid and fluid layers, the effects on both anisotropy and frequency dispersion are then examined. There will be dispersion for propagating P-wave, and thereby stop-bands exist. For the wave propagates perpendicular to the layering, the stop-bands as a function of physical properties of individual layers are studied. When wavelength is much greater than the spatial period of the medium, there are two modes of P-wave, the fast and slow P-wave.

For cases in which crack density is low and aspect ratio is relatively high, the anisotropy is characterized using the Eshelby-Cheng method. The increase of bulk modulus contrast will increase the anisotropy of the effective medium. As the aspect ratio increases from 0.1 to 0.5, the anisotropy of P-wave and S_V-wave increases.

Contents

Chapter 1

Introduction

Layered media theory is a significant topic of exploration geophysics. Layering exists in sedimentary basins at multiple scales, from microscopic to macroscopic. This thesis will focus on periodic layering and the effect of material contrast on the behavior of the anisotropy and dispersion of velocity in periodic media. Emphasis will be placed not only on layered media consisting of all solid layers, but also on media consisting of alternating solid and fluid layers.

On the small scale, shales, which commonly exist in sedimentary basins, can be treated as a layered medium. Vernik and Nur (1992) show that kerogen-rich shales can be effectively modeled using alternating layers of illite and kerogen.

On the large scale, cyclical geological processes can generate periodic sections. Figure 1.1 shows an aggradational parasequence set formed by the rise and fall of local sea level, which can be indicated by periodic media. And as shown in Figure 1.2, cyclical climatic changes create sedimentary layers consisting of alternating limestones and mudstones.

For the sake of simplicity, in this thesis the x_3 axis of the coordinate system is always set to be perpendicular with respect to layering; the layers themselves are always assumed to be infinite in both x_1 and x_2 directions.

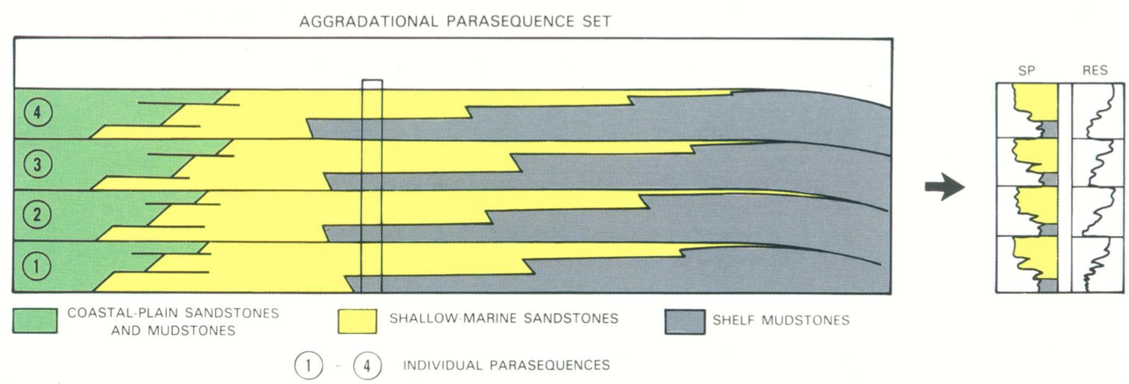

Figure 1.1: Aggradational parasequence set modified from Van Wagoner et al. (1990)

Chapter 2 discusses a simple case in which all the layers of the periodic media are solid and the wavelength is much greater than the period of the media. For the long wavelength case, effective anisotropy is researched with the focus on how different material contrasts control the behavior of the anisotropy of phase and group velocities.

Chapter 3 considers more complex scenarios in which the periodic media consist of alternating solid and fluid layers. Such consideration extends to taking into account cases of differing wavelengths. As the velocity changes with the frequency, stop-bands can be observed, which are the frequency bands which only make allowance for waves in a state of decay. Under certain conditions, the periodic media consisting of alternating solid and fluid layers can approximately describe the media with aligned, penny-shape fractures which have low aspect ratio and high crack density.

Chapter 4 studies the long wavelength limit of the periodic media with alternating solid and fluid layers.

Chapter 5 considers the media with aligned, penny-shape fractures having low

Figure 1.2: Interbedded limestones and mudstones from Coe (2003)

crack density.

It is assumed that readers here have a basic knowledge of elastic wave equations associated with anisotropic media.

Chapter 2

Layered Periodic Media with All Solid Layer at Conditions of Long Wavelength

2.1 Background model

In order to study wave propagation occurring in layered media, we should start from the simplest and most studied case, which involves periodic media consisting of thin layers. It is a problem carrying with it a long history that has been researched in various fields, such as materials science, engineering, and geophysics (Postma, 1955; Backus, 1962; Delph et al., 1978; Berryman, 1979). In this chapter, we will focus on a case in which all layers are solid. The layered periodic media is composed of two alternating layers of isotropic and homogeneous materials. Each layer is characterized by its elastic constants C_{ijkl}, density ρ, and thickness d. The spatial period of the alternating layers is H. In this study, intrinsic attenuation is ignored. The word 'thin' indicates a situation in which the seismic wavelength is much greater than the period of the given media. The thin layering conduction is illustrated in Figure 2.1.

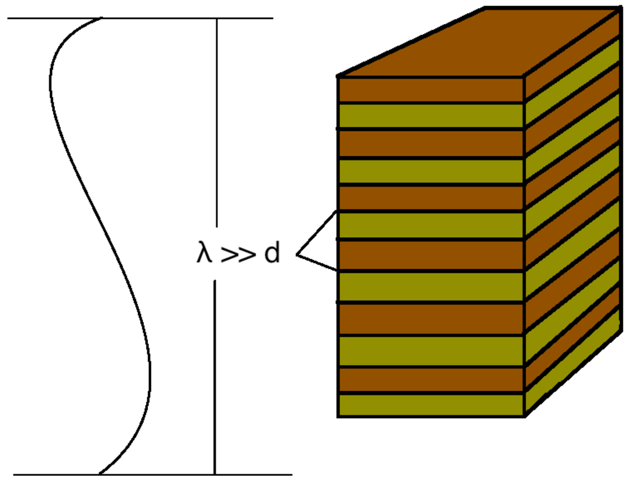

Figure 2.1: Model in which wavelength much greater than the period of the media

For the case in which the individual layers are isotropic, the effective symmetry type of the layered periodic media is transversely isotropic. Whereas a multitude of previous research has covered this topic, there are two basic methods to characterize the elastic constants of the effective media and the corresponding wave propagation in the layered media. Backus' method is one of the most significant works to characterize the behavior of elastic waves in thin layered media (Backus, 1962). There are two major advantages to Backus' average method. First, it provides explicit expression for the stiffness as an average calculated in algebraic quantities. Second, this method is able to extend to non-periodic layered media with more than two constituents, including media that may be anisotropic. However, Backus' average method only considers scenarios involving long wavelength; nominally, these occurrences indicate no dispersion effect. Backus' method is a generalization of Postma's method, in which only two periodic constituents are discussed (Postma, 1955).

2.2 Elastic waves: Isotropic constituents

Elastic wave propagation in homogeneous and isotropic media is controlled by Lamé parameters, λ and μ, and density ρ. The thickness for each layer, d_1 and d_2, in the periodic layered media must also be considered. Usually, the bulk modulus K is more frequently used instead of λ. In the isotropic and homogeneous conditions, phase velocity is expressed as follows:

$$V_p = \sqrt{\frac{\lambda + 2\mu}{\rho}} = \sqrt{\frac{K + \frac{4}{3}\mu}{\rho}} \tag{2.1}$$

$$V_s = \sqrt{\frac{\mu}{\rho}} \tag{2.2}$$

For a case involving long wavelength, according to Postma's method, the stiffness of the effective media can be expressed explicitly with the parameters of the constituent layers as such:

$$\begin{aligned}
c_{11} =& \frac{1}{D}\{(d_1 + d_2)^2(\lambda_1 + 2\mu_1)(\lambda_2 + 2\mu_2) \\
& + 4d_1d_2(\mu_1 - \mu_2)[(\lambda_1 + \mu_1) - (\lambda_2 + \mu_2)]\} \\
c_{12} =& \frac{1}{D}\{(d_1 + d_2)^2\lambda_1\lambda_2 + 2(\lambda_1 d_1 + \lambda_2 d_2)(\mu_2 d_1 + \mu_1 d_2)\} \\
c_{13} =& \frac{1}{D}\{(d_1 + d_2)[\lambda_1 d_1(\lambda_2 + 2\mu_2) + \lambda_2 d_2(\lambda_1 + 2\mu_1)]\} \\
c_{33} =& \frac{1}{D}\{(d_1 + d_2)^2(\lambda_1 + 2\mu_1)(\lambda_2 + 2\mu_2)\} \\
c_{44} =& \frac{(d_1 + d_2)\mu_1\mu_2}{d_1\mu_2 + d_2\mu_1} \\
c_{66} =& \frac{\mu_1 d_1 + \mu_2 d_2}{d_1 + d_2}
\end{aligned} \tag{2.3}$$

where

$$D = (d_1 + d_2)[d_1(\lambda_2 + 2\mu_2) + d_2(\lambda_1 + 2\mu_1)]$$

The Backus formulae are generalizations pointing to higher number of constituent layers and VTI constituents:

$$
\begin{aligned}
C_{11} &= < c_{11} - c_{13}^2 c_{33}^{-1} > + < c_{33}^{-1} >^{-1} < c_{13} c_{33}^{-1} >^2 \\
C_{12} &= < c_{12} - c_{13}^2 c_{33}^{-1} > + < c_{33}^{-1} >^{-1} < c_{13} c_{33}^{-1} >^2 \\
C_{13} &= < c_{33}^{-1} >^{-1} < c_{13} c_{33}^{-1} > \\
C_{33} &= < c_{33}^{-1} >^{-1} \\
C_{44} &= < c_{44}^{-1} >^{-1} \\
C_{66} &= < c_{66} >
\end{aligned}
\tag{2.4}
$$

where the average notation $<>$ represents thickness weighted average, shown as Equation 2.5. The upper case C on the left side represents the stiffness of the effective medium, and lower case c on the right side represents the stiffness of the given constituent layer.

$$
< c > = \frac{\sum_{n=1}^{N} d_n c_n}{\sum_{n=1}^{N} d_n} \tag{2.5}
$$

In VTI media, three phase velocities can be calculated with these six (five independent) elastic constants. The value of the velocities can be obtained from the Green Christoffel equation (Equation 2.6).

$$
(\Gamma_{ik} - \rho V^2 \delta_{ik}) U_k = 0 \tag{2.6}
$$

where Γ is called the first Green-Christoffel tensor, and **U** make up the eigenvectors of Γ, physically representing the direction of particle displacement. Γ is calculated using stiffness and the direction of wave propagation:

$$
\Gamma_{ik} = C_{ijkl} n_j n_l \tag{2.7}
$$

where **n** is the unit vector representing the direction of wave propagation. The modulus of phase velocities can be calculated from the eigenvalues of Γ with known density. Additionally, the group velocities can be calculated as follows:

$$V_j^{(group)} = \frac{1}{\rho|\mathbf{V}^{(phase)}|} C_{ijkl} U_i U_k n_l \tag{2.8}$$

For the case of VTI media, the phase velocities can be expressed explicitly in the form indicated below (Thomsen, 1986):

$$V_P^2(\theta) = \frac{1}{2\rho}[c_{33} + c_{44} + (c_{11} - c_{33})sin^2\theta + D] \tag{2.9}$$

$$V_{S_V}^2(\theta) = \frac{1}{2\rho}[c_{33} + c_{44} + (c_{11} - c_{33})sin^2\theta - D] \tag{2.10}$$

$$V_{S_H}^2(\theta) = \frac{1}{\rho}[c_{44}cos^2\theta + c_{66}sin^2\theta] \tag{2.11}$$

where

$$\begin{aligned} D^2 \equiv &(c_{33} - c_{44})^2 + 2[2(c_{13} + c_{44})^2 - (c_{33} - c_{44})(c_{11} + c_{33} - 2c_{44})]sin^2\theta \\ &+ [(c_{11} + c_{33} - 2c_{44})^2 - 4(c_{13} + c_{44})^2]sin^4\theta \end{aligned} \tag{2.12}$$

There exists a conclusion that it is the shear modulus contrast which dominates the degree of anisotropy. It means that there is no effective anisotropy unless a difference in shear modulus exists, regardless of what differences occur within any other parameters (Mavko et al., 2009; Berryman, 2005). This can be seen by substituting $\mu_1 = \mu_2$ into Equation 2.3. The result is that $c_{11} = c_{33}, c_{13} = c_{12}, c_{11} - c_{12} = 2\mu, c_{44} = c_{66} = \mu$. It becomes an isotropic media with effective λ is given by $\lambda_{eff} = c_{12}$. The consequence is that the essential conditions for layered media showing anisotropy is that μ must vary between layers. For instance, if two layers consistes of identical isotropic rock with different fluid saturations, there would be no shear modulus contrast, therefore it would not show anisotropy. As a result, a difference in Poisson's ratio between layers does not necessarily produce long wavelength layer anisotropy where Poisson's ratio σ is given by:

$$\sigma = \frac{(V_P/V_S)^2 - 2}{2((V_P/V_S)^2 - 1)} \tag{2.13}$$

In order to get a further study on sensitivities of contrast among such elastic constants, a quantitative definition should then be made:

$$anisotropy\ coefficient = \frac{velocity(\theta) - velocity(\theta = 0^\circ)}{velocity(\theta = 0^\circ)} \tag{2.14}$$

where $\theta = 0^\circ$ is perpendicular to the layers and the velocity is phase velocity. The first approach in studying sensitivities is to examine the effect of each parameter separately. However, taking such an approach is not geologically realistic. Such an approach assists with indicating which physical property is more significant in affecting layer-induced anisotropy.

Figure 2.2 indicates the effect on phase velocities of varying shear modulus contrast between two layers, with other parameters remaining constant. The variation of the shear modulus contrast is produced by variation of shear modulus of the second layer. This shows that the angle in which the maximum velocity of S_V-wave occurs causes a shift to smaller values; thus the degree of anisotropy increases as shear modulus contrast increases. Figure 2.3 shows what effect all this has on group velocities. The width of the triplication zone of the S_V-wave and the degree of anisotropy involved both increase as shear modulus contrast increases.

Figure 2.4 illustrates the effect on phase velocities of varying bulk modulus contrast, maintaining a constant shear contrast. The bulk modulus contrast has no effect on the anisotropy of the S_H-wave, the reason being that the S_H-wave velocity

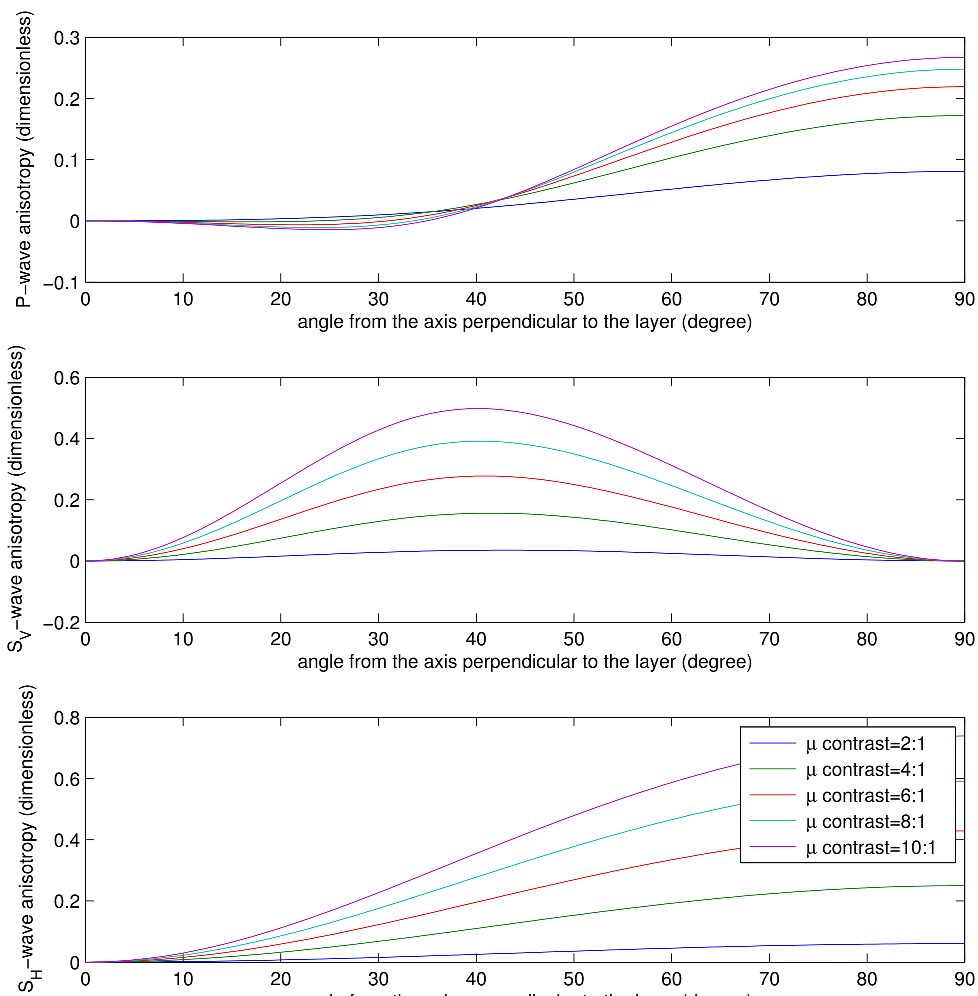

Figure 2.2: Effect of varying shear modulus contrast on angular anisotropy of phase velocities. The first layer: $K = 20.35\,GPa, \mu = 13.24\,GPa, \rho = 2.37\ g/cm^3$; the second layer: $K = 7.13\,GPa, \rho = 2.1\ g/cm^3$. The thickness of the two layers are equal. The legend gives fractional shear modulus contrasts.

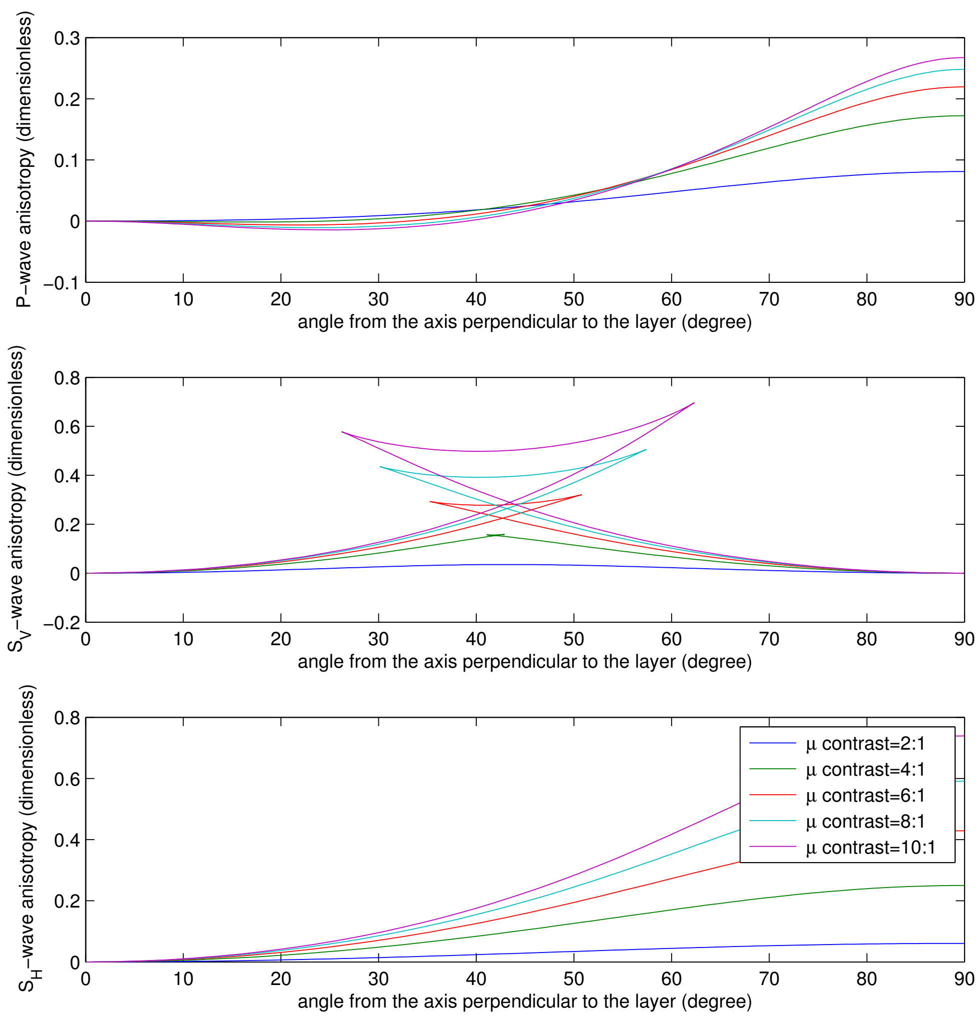

Figure 2.3: Effect of varying shear modulus contrast on angular anisotropy of group velocities. The first layer: $K = 20.35\,GPa, \mu = 13.24\,GPa, \rho = 2.37\ g/cm^3$; the second layer: $K = 7.13\,GPa, \rho = 2.1\ g/cm^3$. The thickness of the two layers are equal. The legend gives fractional shear modulus contrasts.

only depends on c_{44} and c_{66}. It is shown that the angle corresponding to the maximum anisotropy of S_V-wave becomes smaller as bulk modulus contrast increases. Figure 2.5 shows the effect on group velocities.

As thickness contrast increases, the anisotropy will become less significant, because the properties of the whole material will be closer to that of the thicker layer. This behavior can be observed in Figures 2.6 and 2.7, showing cases involving phase and group velocities respectively. Density does not contribute to anisotropy, so there is no need to take such into account.

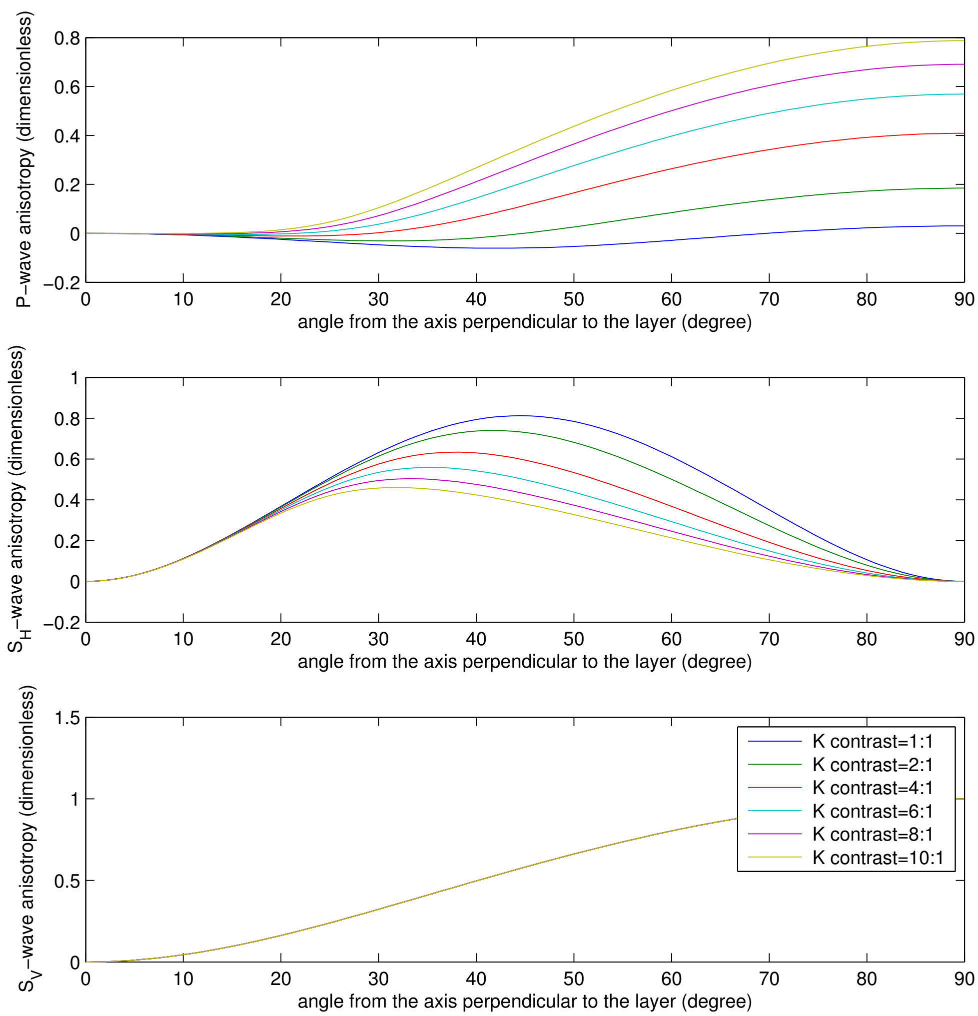

Figure 2.4: Effect of varying bulk modulus contrast on angular anisotropy of phase velocities. The first layer: $K = 20.35\, GPa, \mu = 13.24\, GPa, \rho = 2.37\ g/cm^3$; the second layer: $\mu = 0.95\, GPa, \rho = 2.1\ g/cm^3$. The thickness of the two layers are equal. The legend gives fractional bulk modulus contrast.

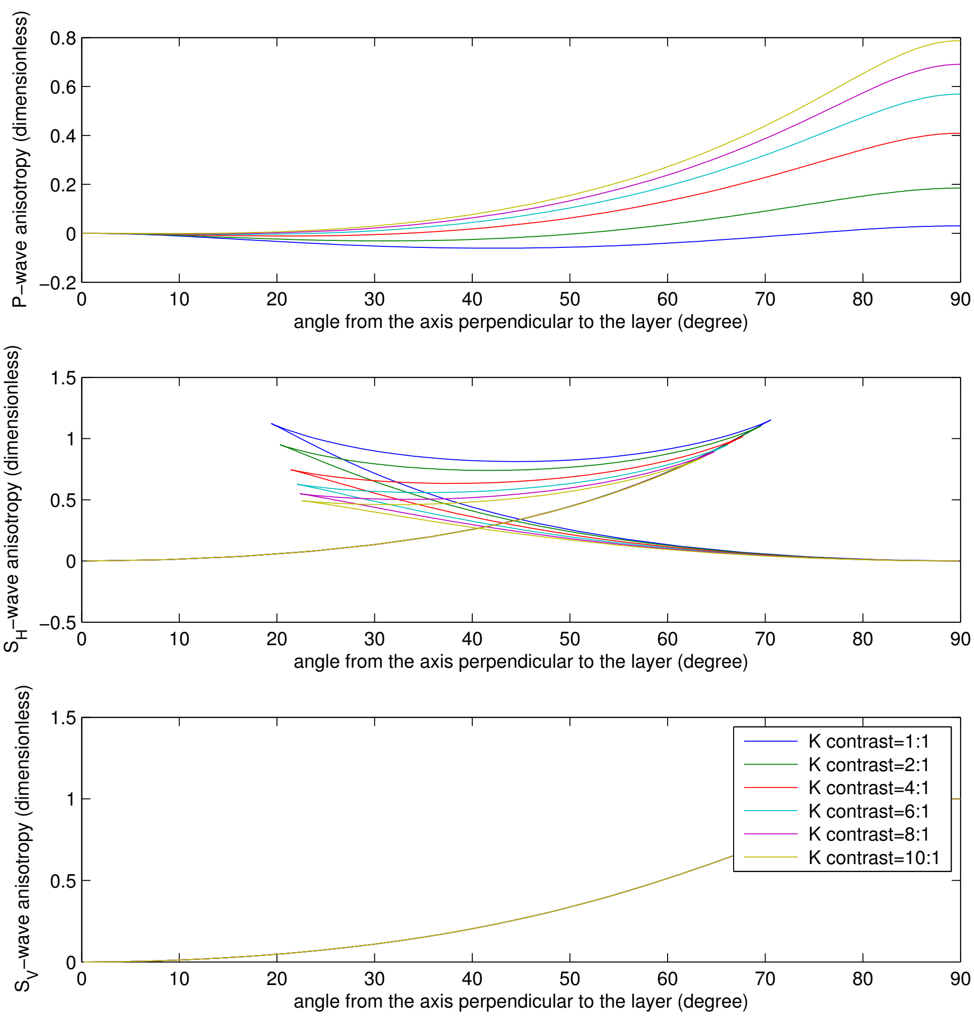

Figure 2.5: Effect of varying bulk modulus contrast on angular anisotropy of group velocities. The first layer: $K = 20.35\,GPa, \mu = 13.24\,GPa, \rho = 2.37\ g/cm^3$; the second layer: $\mu = 0.95\,GPa, \rho = 2.1\ g/cm^3$. The thickness of the two layers are equal. The legend gives fractional bulk modulus contrast.

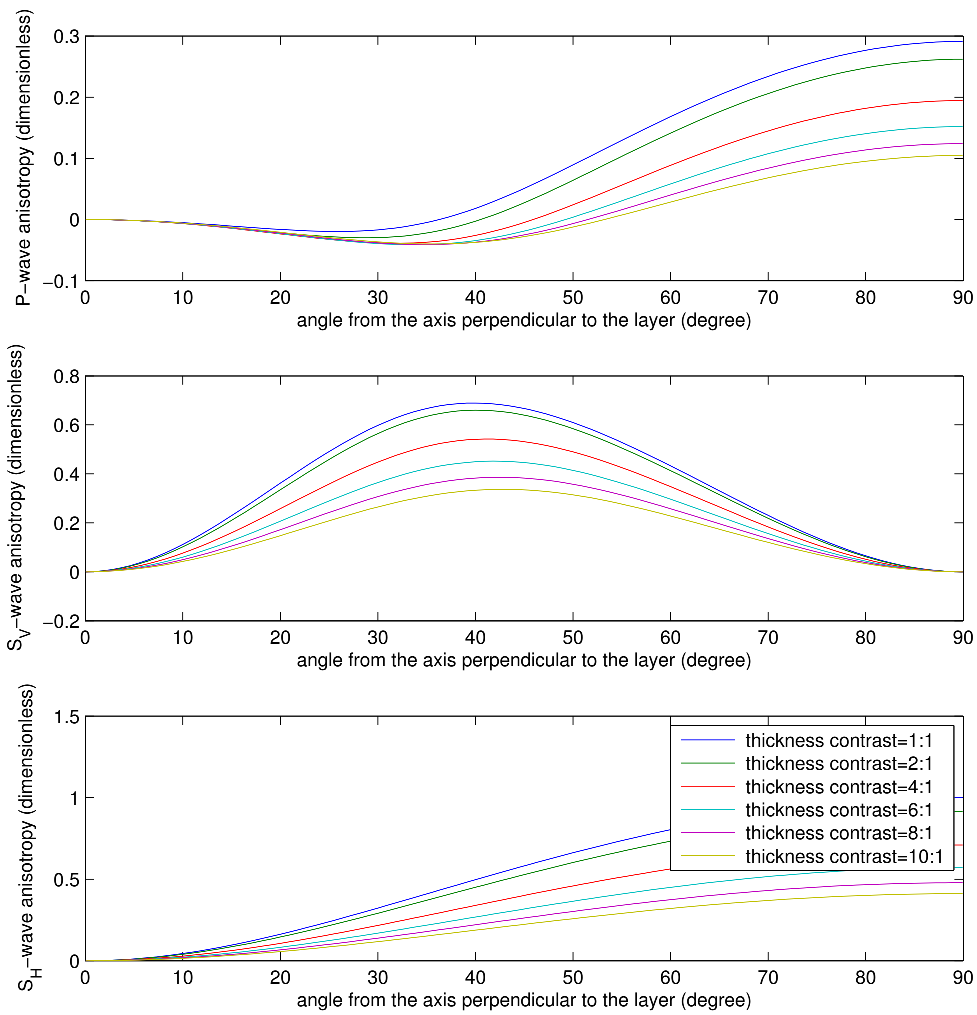

Figure 2.6: Effect of varying layer thickness contrast on angular anisotropy of phase velocities.The first layer: $K = 20.35GPa, \mu = 13.24GPa, \rho = 2.37g/cm^3$; the second layer: $K = 7.13\,GPa, \mu = 0.95\,GPa, \rho = 2.1\,g/cm^3$. The legend gives fractional thickness contrast.

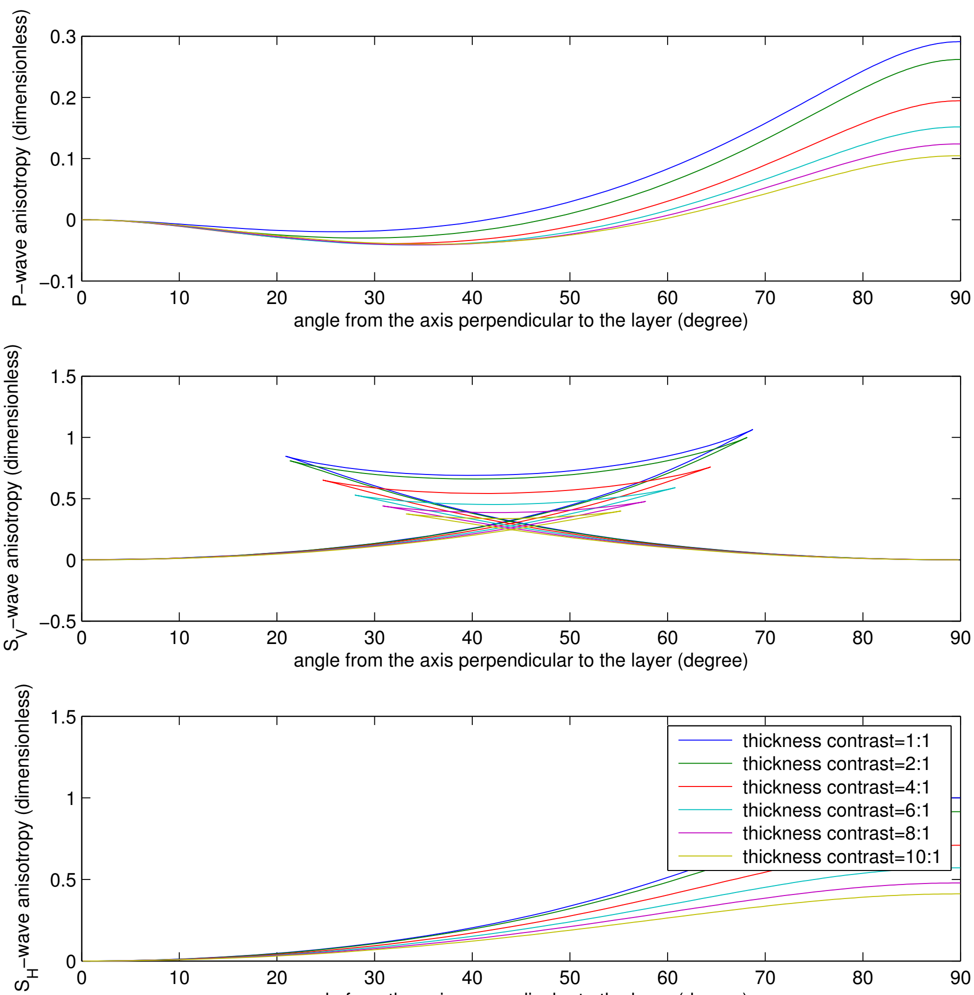

Figure 2.7: Effect of varying layer thickness contrast on angular anisotropy of group velocities.The first layer: $K = 20.35GPa, \mu = 13.24GPa, \rho = 2.37g/cm^3$; the second layer: $K = 7.13\, GPa, \mu = 0.95\, GPa, \rho = 2.1\, g/cm^3$. The legend gives fractional thickness contrast.

Chapter 3

Layered Periodic Media with Alternating Solid and Fluid Layers

3.1 Background of wave propagation in elasto-acoustic medium

In petroleum reservoirs, fractures can significantly increase permeability and consequently enhance production capabilities (Baird et al., 2013). Limited by low resolution, seismic studies are usually unable to effectively image individual fractures. However, the seismic anisotropy produced by the presence of aligned fracture sets can be used as a method to characterize such a reservoir overall (Lynn and Thomsen, 1990). In order to simplify the model, aligned sets of fractures with low aspect ratio can be approximately regarded as thin layers containing fluid. Therefore, Such a model becomes one of layered periodic media, with alternating solid and fluid layers, thus one presenting an elastoacoustic medium (Schoenberg, 1984), as shown in Figure 3.1.

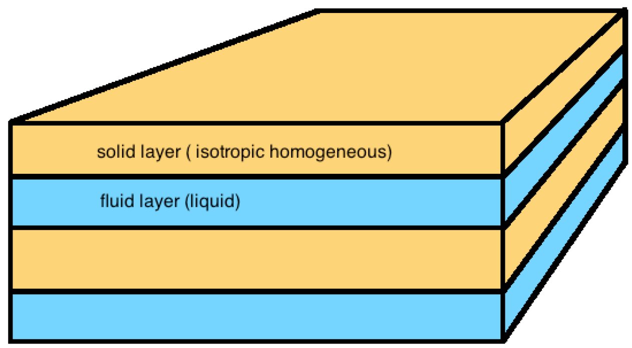

Figure 3.1: the model of periodic layered medium with alternating solid and fluid layers

3.2 Schoenberg's solution for elastoacoustic media

In observing the alternating solid and liquid layers, there are several facts to consider. First, boundary conditions between a solid and ideal (shear stress free) fluid lead to phenomena that differ from one involving a solid-solid case. Second, the exact solution at all frequencies and wave numbers parallel to stratification can help to explain the meaning of theories on wave propagation in porous media (Schoenberg, 1984). The Rytov (1956) approach shows that there is one wave speed for propagation perpendicular to the layering, while for propagation parallel to the layering, there are two speeds, both of which correspond to compressional waves. The existence of two compressional modes is predicted by Biot's theory of wave propagation in porous media. Hereafter such a periodic layered medium composed of alternating elastic solid and ideal fluid layers should then be called an elastoacoustic medium. The 4×4 transfer matrix for an elastic layer of general case can reduce to the 2×2 matrix when applied to an elastic layer, in which shear stress vanishes on both surfaces. In order to solve the problem of wave propagation in periodic layered media, the method of propagator matrices is used (Gilbert and Backus, 1966). A matrix

$\overline{Q}$ relates values of continuous field parameters at one depth in the periodic layered medium to another depth one period deeper in the same medium. For the boundary conditions, the fluid layers are considered to be composed of ideal fluid; therefore viscous shear stress vanishes and tangential displacement at a solid-fluid interface can no longer be continuous. The propagator matrix $\overline{Q}$, which is a 2×2 matrix with a determinant equal to one, describes the relationship of the continuous variables, σ_{33}, the normal stress, and ν_3, the normal particle velocity, between the upper and the lower surfaces of one period (i.e. one solid layer and one fluid layer). In the following, the derivation of $\overline{Q}$ from an elastoacoustic medium is present. The matrix equation across one period, H, is

$$\mathbf{y}(H) = \begin{bmatrix} \sigma_{33} \\ \nu_3 \end{bmatrix}_{x_3=H} = \overline{Q}(s_1,\omega) \begin{bmatrix} \sigma_{33} \\ \nu_3 \end{bmatrix}_{x_3=0} \equiv \overline{Q}\mathbf{y}(0) \tag{3.1}$$

$\overline{Q}$ is decomposed into eigenvector and eigenvalue matrices,

$$\overline{Q} = \overline{V}\cdot\overline{\Lambda}\cdot\overline{V}^{-1} = \begin{bmatrix} v_{11} & v_{12} \\ v_{21} & v_{22} \end{bmatrix} \cdot \begin{bmatrix} \lambda_1 & 0 \\ 0 & \lambda_2 \end{bmatrix} \cdot \begin{bmatrix} v_{22} & -v_{12} \\ -v_{21} & v_{11} \end{bmatrix} / det\,\overline{V} \tag{3.2}$$

where λ_i are the eigenvalues, and $[v_{1i}, v_{2i}]^T$ are the eigenvectors corresponding to λ_i. The equation describing relationship across n periods is

$$\begin{aligned} \mathbf{y}(nH) =& \overline{Q}^n(s_1,\omega)\mathbf{y}(0) = \overline{V} \begin{bmatrix} \lambda_1^n & 0 \\ 0 & \lambda_2^n \end{bmatrix} \overline{V}^{-1}\mathbf{y}(0) \\ =& \left\{ \lambda_1^n \begin{bmatrix} v_{11} \\ v_{21} \end{bmatrix} \begin{bmatrix} v_{22} & -v_{12} \end{bmatrix} + \lambda_2^n \begin{bmatrix} v_{12} \\ v_{22} \end{bmatrix} \begin{bmatrix} -v_{21} & v_{11} \end{bmatrix} \right\} \mathbf{y}(0)/det\,\overline{V} \end{aligned} \tag{3.3}$$

If $\mathbf{y}(0)$ is arbitrary decomposed into a linear combination of eigenvectors,

$$\mathbf{y}(0) = \sum_{i=1}^{2} c_i \begin{bmatrix} v_{1i} \\ v_{2i} \end{bmatrix} \equiv \sum_{i=1}^{2} c_i \mathbf{v}_i \tag{3.4}$$

then $\mathbf{y}$(nH) can be written as

$$\mathbf{y}(nH) = \sum_{i=1}^{2} c_i \lambda_i^n \mathbf{v}_i \tag{3.5}$$

which is the sum of two solutions. For any value of x_3, $(x_3 = (n+\delta)H, 0 \leqslant \delta < 1)$, $\mathbf{y}$ is related to $\mathbf{y}$(nH) by a 2x2 matrix $\overline{Q}'(\delta H)$, with $\overline{Q}'(H) = \overline{Q}$. Then

$$\begin{aligned} \mathbf{y}(x_3) =& \overline{Q}'(\delta H)\mathbf{y}(nH) = \overline{Q}'(\delta H) \sum_{i=1}^{2} c_i \lambda_i^n \mathbf{v}_i = \sum_{i=1}^{2} \lambda_i^{n+\delta} c_i \lambda_i^{-\delta} \overline{Q}'(\delta H) \mathbf{v}_i \\ =& \sum_{i=1}^{2} (\lambda_i^{1/H})^{x_3} c_i (\lambda_i^{1/H})^{-\delta H} \overline{Q}'(\delta H) \mathbf{v}_i \equiv \sum_{i=1}^{2} (\lambda_i^{1/H})^{x_3} \mathbf{f}_i(\delta H) \end{aligned} \tag{3.6}$$

and as $\mathbf{f}_i(0) = \mathbf{f}_i(H) = c_i \boldsymbol{v}_i$, two continuous periodic functions $f_i^p(x_3)$ are induced by period H. As a result, when $x_3 = (n+\delta)H, (0 \leqslant \delta < 1), \mathbf{f}_i^p(x_3) = \mathbf{f}_i(\delta H)$. Then

$$\mathbf{y}(x_3) = \sum_{i=1}^{2} (\lambda_i^{1/H})^{x_3} \mathbf{f}_i^p(x_3) \tag{3.7}$$

$\mathbf{f}_i^p(x_3)$ indicates the mode shapes within each period, each mode being related to a different wave. Because $\overline{Q}$ is a 2x2 matrix whose determinant equal to one, $\lambda_1 \lambda_2 = 1$, and the value of λ_1 and λ_2 are only decided by the trace of $\overline{Q}$. A parameter C is introduced with $C = (q_{11} + q_{22})/2$, representing half the trace of $\overline{Q}$. Then the solution of the quadratic equation can be given such value (in eigenvalues):

$$\lambda^2 - 2C\lambda + 1 = 0 \tag{3.8}$$

For C, there are two cases: (1)$|C| \leqslant 1, \lambda_1, \lambda_2$ are complex conjugates, and their absolute values are equal to one. (2) $|C| > 1, \lambda_1, \lambda_2$ are real reciprocals of each other. For the first case, one has $\lambda = e^{\pm i\omega s_3 H}$, where $\omega s_3 H$ can be calculated from

$$C = cos\, \omega s_3 H \tag{3.9}$$

s_3 is the component of slowness in the x_3 direction, i. e. the real apparent slowness along given x_3 axis. For the second case, let λ_1 be the eigenvalue with smaller absolute value, so that $|\lambda_1| < 1, |\lambda_2| > 1$. Then

$$\begin{aligned} \lambda_1 =& C[1 - (1 - C^{-2})^{\frac{1}{2}}] \\ \lambda_2 =& C[1 + (1 - C^{-2})^{-\frac{1}{2}}] \end{aligned} \tag{3.10}$$

and λ_1 is related to evanescent waves which decay in direction along a positive x_3 axis, and λ_2 ,along a negative x_3 axis. C and λ_i have the same sign. Therefore, if λ_i are negative, there is phase reversal between adjacent periods as the wave decays, but if λ_i are positive, there is no phase reversal.

In what follows, we discuss the periodic layered medium with alternating solid and fluid layers. Consider a periodic layered medium whose spatial period is H in direction along the x_3 axis. Within a period, for example, $0 < x_3 < H$, one layer of the region $0 < x_3 < h_s H$ is formed with a homogeneous isotropic elastic solid whose P-wave velocity is α, S-wave velocity is β, and density is ρ; another layer of the region $h_s H < x_3 < H$, with width $h_f H = (1 - h_s)H$, is formed with ideal fluid whose P-wave velocity is α_f and density is ρ_f. The porosity of this elastoacoustic medium is h_f. Because of an expected x_1 and t dependance, $e^{i\omega(s_1 x_1 - t)}$, there is offered a general solution of the equations of elasticity in a solid layer - a linear combination of $+x_3$ and $-x_3$ propagating or decaying P-waves and S-waves of the form

$$
\mathbf{Y}(x_3) = \begin{bmatrix} \sigma_{33} \\ \sigma_{31} \\ \nu_1 \\ \nu_3 \end{bmatrix}_{x_3} = \overline{B} \cdot \overline{D}(x_3) \cdot \mathbf{A} \tag{3.11}
$$

where

$$
\begin{aligned}
\overline{B} &= \begin{bmatrix} \rho\alpha^2\Gamma & -2\rho\beta^4 s_1 s_s & B_{11} & -B_{12} \\ 2\rho\alpha^2\beta^2 s_1 s_p & \rho\beta^2\Gamma & -B_{21} & B_{22} \\ -\alpha^2 s_1 & -\beta^2 s_s & B_{31} & -B_{32} \\ -\alpha^2 s_p & \beta^2 s_1 & -B_{41} & B_{42} \end{bmatrix} \\
\overline{D}(x_3) &= \begin{bmatrix} e^{i\omega s_p x_3} & 0 & 0 & 0 \\ 0 & e^{i\omega s_s x_3} & 0 & 0 \\ 0 & 0 & e^{-i\omega s_p x_3} & 0 \\ 0 & 0 & 0 & e^{-i\omega s_s x_3} \end{bmatrix} \\
s_s &= (\beta^{-2} - s_1^2)^{\frac{1}{2}} \\
s_p &= (\alpha^{-2} - s_1^2)^{\frac{1}{2}} \\
\Gamma &= 1 - 2\beta^2 s_1^2
\end{aligned} \tag{3.12}
$$

and where $\mathbf{A}$ is the coefficient vector, which equals $\overline{B}^{-1}\mathbf{Y}(0)$. Then

$$
\mathbf{Y}(x_3) = \overline{B} \cdot \overline{D}(x_3) \cdot \overline{B}^{-1} \cdot \mathbf{Y}(0) \equiv \overline{P}(x_3) \cdot \mathbf{Y}(0) \tag{3.13}
$$

where

$$\overline{P} = \begin{bmatrix} \beta^2 s_1^2 C_s + \Gamma C_p & -is_1(2\beta^2 s_s^2 S_s - \Gamma S_p) \\ is_1(2\beta^2 s_p^2 S_p - \Gamma S_s) & 2\beta^2 s_1^2 C_p + \Gamma C_s \\ s_1(C_s - C_p)/\rho & -i(s_s^2 S_s + s_1^2 S_p)/\rho \\ -i(s_p^2 S_p + s_1^2 S_s)/\rho & P_{31} \end{bmatrix.$$

$$\begin{matrix} 2\rho\beta^2 s_1 \Gamma(C_s - C_p) & -i\rho(4\beta^4 s_1^2 s_s^2 S_s + \Gamma^2 S_p) \\ -i\rho(4\beta^2 s_1^2 s_p^2 S_p + \Gamma^2 S_s & P_{13} \\ P_{22} & P_{12} \\ P_{21} & P_{11} \end{matrix} \Bigg] \tag{3.14}$$

$$C_s = cos\, \omega s_s x_3 \qquad C_p = cos\, \omega s_p x_3$$

$$S_s = s_s^{-1} sin\, \omega s_s x_3 \quad S_p = s_p^{-1} sin\, \omega s_p x_3$$

$P(h_s H)$ is the transfer matrix across one solid layer. The value of S_s and S_p are set to be so that as ω approaches 0, $S_s \approx S_p \approx \omega x_3$. Because the solid layer is bounded by ideal fluid on both surfaces, $Y_3 = \nu_1$, the horizontal component of particle velocity ν is not continuous across a solid-fluid interface, and the shear stress, $Y_2 = \sigma_{31}$, becomes zero when $x_3 = 0, h_s H$. Thus, from Equation 3.11(Schoenberg, 1984)

$$0 = P_{21}(h_s H)Y_1(0) + P_{23}(h_s H)Y_3(0) + P_{24}(h_s H)Y_4(0) \tag{3.15}$$

$Y_3(0)$ can be expressed in terms of $Y_1(0)$ and $Y_4(0)$. Substitute $Y_3(0)$ as this expression into the first and fourth elements of Equation 3.11 (as Y_1 and Y_4 must be continuous within the whole medium along x_3 axis). Then

$$
\mathbf{y}(h_sH) = \begin{bmatrix} Y_1 \\ Y_4 \end{bmatrix}_{h_sH} = \begin{bmatrix} P_{11} - \frac{P_{21}P_{13}}{P_{23}} & P_{14} - \frac{P_{24}P_{13}}{P_{23}} \\ P_{41} - \frac{P_{21}P_{43}}{P_{23}} & P_{44} - \frac{P_{24}P_{43}}{P_{23}} \end{bmatrix}_{h_sH} \cdot \begin{bmatrix} Y_1 \\ Y_4 \end{bmatrix}_0
$$

$$
\equiv \overline{q}_s\mathbf{y}(0) = \begin{bmatrix} (4\beta^2 s_1^2 s_p^2 C_s S_p + \Gamma^2 C_p S_s)/\kappa & -i\rho\xi/\kappa \\ -is_p^2 S_s S_p/\rho\kappa & q_{s_{11}} \end{bmatrix} \mathbf{y}(0) \tag{3.16}
$$

where

$$
\begin{aligned}
\xi =& 8\beta^4 s_1^2 \Gamma^2 (1 - C_s C_p) + (16\beta^8 s_1^4 s_S^2 s_p^2 + \Gamma^4) S_s S_p \\
\kappa =& 4\beta^4 s_1^2 s_p^2 S_p + \Gamma^2 S_s
\end{aligned} \tag{3.17}
$$

Here, C_s, C_p, S_s and S_p are calculated at $x_3 = h_sH$. Where $\Gamma^2 = 1 - 4\beta^4 s_1^2 s_s^2$.

For the fluid layer of region $h_sH < x_3 < H$, under the assumption that there exists $e^{i\omega(s_1x_1 - t)}$ dependance on x_1 and t, the general solution can be expressed as a linear combination of $+x_3$ and $-x_3$ propagating or decaying P-waves. Then

$$
\mathbf{y}(x_3) = \begin{bmatrix} \sigma \\ \nu_3 \end{bmatrix}_{x_3} = \overline{bd}(x_3 - h_sH)\mathbf{a} \tag{3.18}
$$

where

$$
\begin{aligned}
\overline{b} &= \rho_f \alpha_f^2 \begin{bmatrix} 1 & 1 \\ -\frac{s_f}{\rho_f} & \frac{s_f}{\rho_f} \end{bmatrix} \\
\overline{d}(\delta) &= \begin{bmatrix} e^{i\omega s_f \delta} & 0 \\ 0 & e^{-i\omega s_f \delta} \end{bmatrix} \\
s_f &= (\alpha_f^{-2} - s_1^2)^{\frac{1}{2}}
\end{aligned} \tag{3.19}
$$

and where σ is the negative of the acoustic pressure, and $\mathbf{a}$ is the coefficient vector describing the relationship between the place at any value of x_3 in the fluid layer and the place at $x_3 = h_sH$. And $\mathbf{a} = \overline{b}^{-1}\mathbf{y}(h_sH)$, $\delta = x_3 - h_sH$, thus

$$\mathbf{y}(x_3) = \overline{bd}(x_3 - h_s H)\overline{b}^{-1}\mathbf{y}(h_s H) \equiv \overline{q}_f(x_3 - h_s H)\mathbf{y}(h_s H) \tag{3.20}$$

where

$$\begin{gathered}\overline{q}_f = \begin{bmatrix} C_f & -i\rho_f S_f \\ -is_f^2 S_f/\rho_f & C_f \end{bmatrix} \\ C_f = cos\,\omega s_f \delta \\ S_f = s_f^{-1} sin\,\omega s_f \delta \end{gathered} \tag{3.21}$$

There are two parameters, both along lines of which $\overline{Q}$ should be expressed: $\overline{q}_s$ - transfer matrix across one solid layers, and $\overline{q}_f$ - transfer matrix across one fluid layer.

$$\overline{Q} = \overline{q}_f(h_f H)\overline{q}_s \tag{3.22}$$

C, which equals to half the trace of $\overline{Q}$, is expressed by

$$\begin{aligned} C &\equiv cos\,\omega s_3 H \\ &= \frac{1}{\kappa}\left[C_f(4\beta^4 s_1^2 s_p^2 C_s S_p + \Gamma^2 C_p S_p) - \frac{1}{2}S_f(\frac{\rho_f}{\rho}s_p^2 S_s S_p + \frac{\rho}{\rho_f}s_f^2 \xi)\right] \end{aligned} \tag{3.23}$$

It shows that C is an even function of ω, s_p, s_s, and s_f. Figure 3.2 describes the behavior of C as a function of horizontal slowness s_1 and angular frequency ω, for a physical model with combination of materials and low velocity contrast . Commonly suggested choices are layers of Plexiglas and water, which are of equal thickness. The plane of frequency and parallel slowness is divided into: (a) regions (white) within which propagating waves exist, (b) regions (\\\\\\\\\\) where there are waves that are evanescent in the perpendicular direction with no phase change between adjacent periods, and (c) regions (/////////) where there are evanescent waves with a 180° phase change between adjacent periods. Lines indicated by the heavy dark lines represent discontinuity of the trace of Q which separates the different modes of propagation (Schoenberg, 1984).

As shown in Figure 3.2, when $|C| < 1$, it corresponds to pass-bands, which are regions on the plane of the s_1 and ω for where waves propagating in the direction of x_3 axis exist. When $C > 1$, corresponding to positive stop-bands, it denotes regions where evanescent waves exist. It is for these waves, from period to period along a line of direction that indicates decaying, that the amplitude of the next period is multiplied by a positive factor λ_i. When $C < -1$, it corresponds to negative stop-bands, where amplitude of waves is multiplied by negative factor λ_i in the same way as that of the former case; this leads to a phase reversal from period to period. In some cases, the value of κ vanishes while the numerator of C is non-zero, which leads to the value of C approaching infinite. This phenomenon is denoted by the heavy black lines in the plane of s_1 and ω, indicating the infinite discontinuity of $C(s_1, \omega)$. The plane is divided by these lines into different modes of propagation. When $s_1 = 0$, the numerator of C also becomes zero at $\omega h_s H/\beta = n\pi$, therefore the lines of discontinuity fade at the ω axis when they intersect the ω axis perpendicularly. For the case of low frequency wave propagation, κ vanishes and C approaches infinity when $s_1^2 = 1/\alpha_{pl}^2$, where α_{pl} is the long wavelength plate velocity of the solid layer. κ must be non-zero for any frequency when $s_1 > 1/\beta$. At low frequencies, as shown in Figure 3.2, the range of s_1 is divided by $1/\alpha_{pl}$ into two possible modes, a fast-wave mode and a slow-wave mode.

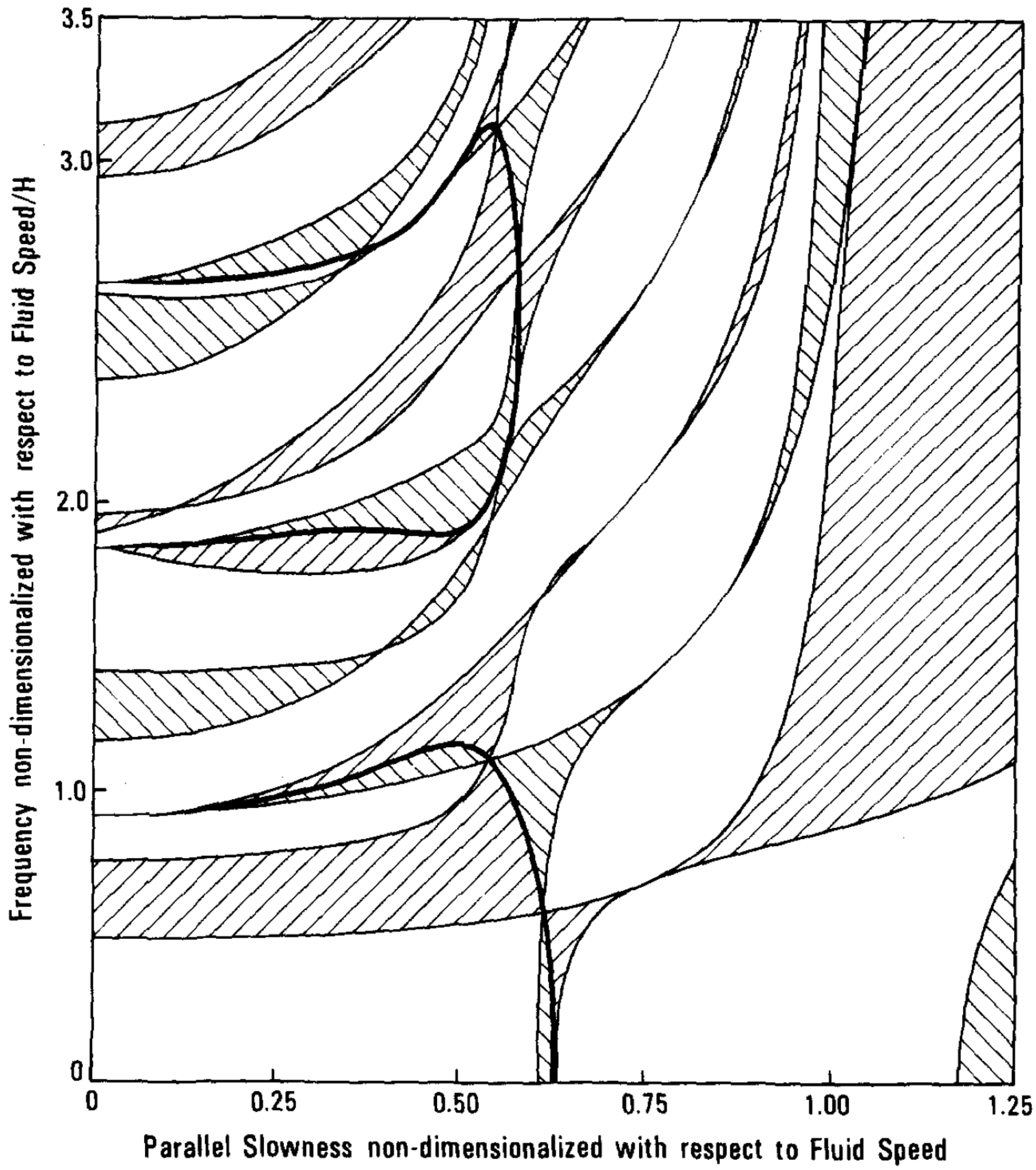

Figure 3.2: A Plexiglas and water model of 50% porosity. White regions: propagating waves exist; regions marked by (\\\\\\\\\\ ): there are waves evanescent in the perpendicular direction with no phase change between adjacent periods; regions marked by (/////////): there are evanescent waves with a 180° phase change between adjacent periods. Lines indicated by the heavy dark lines represent discontinuity of the trace of Q which separates the different modes of propagation. (Schoenberg, 1984)

3.3 Dispersion of wave propagation perpendicular to the layering

L. Brillouin's research is the most comprehensive early work in the field of wave propagation in periodic structures (Brillouin, 1946). The most impressive contribution of his study is the indication of the existence of stop-bands, which appears at the boundaries between the so-called 'Brillouin zones'. Within these frequency bands, waves are attenuated but do not propagate in periodic structures. Brillouin suggests that considering wave number within the range $-\pi/H \leqslant k \leqslant \pi/H$ is enough to fully describe wave behavior in periodic media, where H is the period of the medium and k indicates the wave number. In order to illustrate this, the first case to be studied is for wave propagation perpendicular to the respective layers. For the case in which wave propagation perpendicular to layers, $s_1 = 0$ is substituted into Equation 3.23. Then the equation that describes the relation between frequency ω and wave number k is constructed as follow:

$$C(\omega) = cos(kH) \tag{3.24}$$

where $k = \omega s_3$, and the function $C(\omega)$ can be expressed by the right-hand side of Equation 3.23. For a medium that consists of isotropic shale layers and water layers of equal thickness, the full solution of $\omega - k$ spectrum of real solutions is shown in Figure 3.3.

The frequency bands where there is no real solution for wave number are stop-bands. The equation 3.24 denotes that the dispersion relation is even, therefore there is the following relationship: $\omega(k) = \omega(-k)$. This fully allows description of the dispersion relation by considering wave number within the interval $0 \leqslant k \leqslant \pi/H$. In this way the reduced zone scheme is obtained (Lee and Yang, 1973; Ziman, 1972),

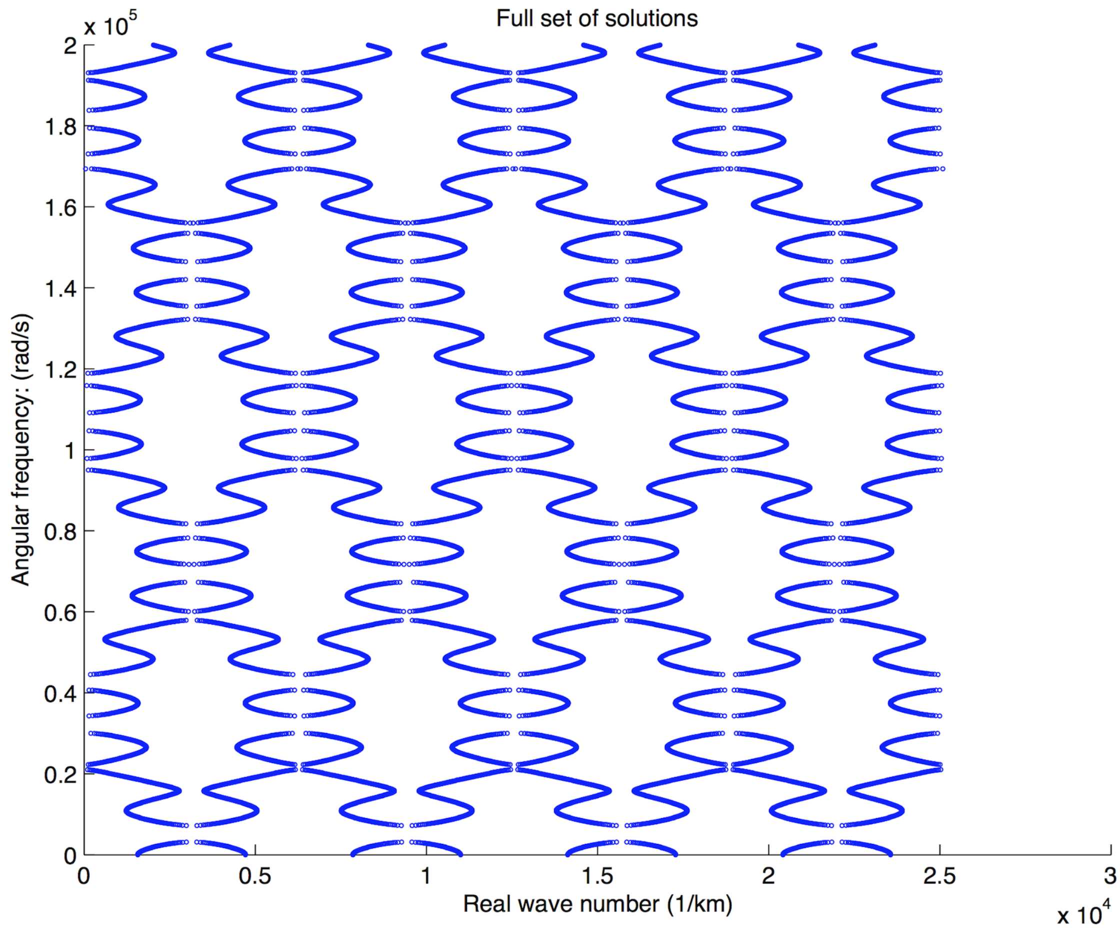

Figure 3.3: Entire frequency spectrum for alternating solid and fluid layer. solid layer: K=7.13 GPa, μ=0.95 GPa, ρ=2.1 g/cm^3, thickness: 0.5 m. liquid layer: K=2.2 GPa, ρ=1g/cm^3, thickness: 0.5 m.

as shown in Figure 3.4.

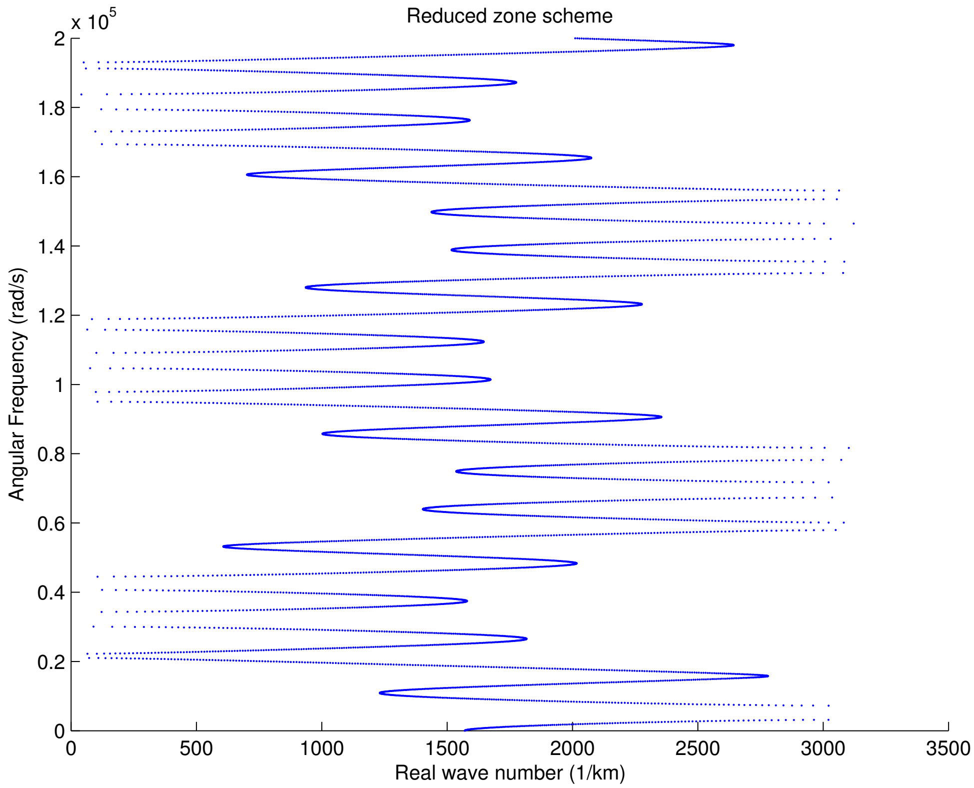

Figure 3.4: Reduced zone frequency spectrum for alternating solid and fluid layer.

Usually, it is convenient to work with wave number k covering all positive real values, leading to the need for an extended diagram (Lee and Yang, 1973). The non-unique solution is due to the fact that observation of a wave only at positions at equal distance from each other does not determine the wavelength, hence wave number and phase velocity cannot be determined either (Brillouin, 1953). The extended representation can be obtained by unfolding the values of $\omega(k)$ on the reduced diagram with respect to the axis $k = \pi/H$ as it is shown in Figure 3.5. The numbers on the side of each curve in this figure show how the curves unfold, with the same numbers representing the same points on the lines. (Perdomo, 2012). This is a diagram only indicating the method of unfolding the curves, with no actual meaning of the curves involved.

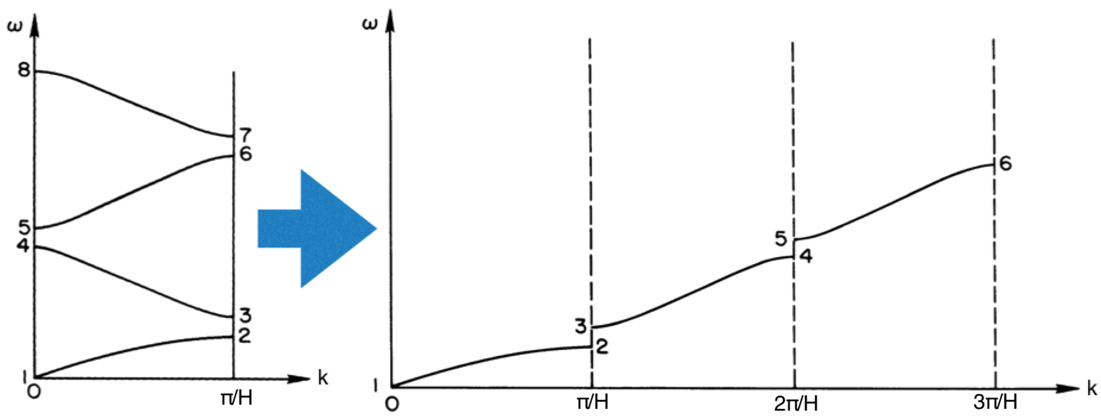

Figure 3.5: Example of the reduced diagram (left) and extended diagram (right). (Lee and Yang, 1973).

From the extended zone scheme, the phase velocities can be evaluated in the normal way where $v = \omega/k$ (Lee and Yang, 1973). This is shown in Figure 3.6. It is now able to examine how the phase velocity varies with frequency and wave number using the extended zone scheme from a calculated dispersion relation.

Figure 3.7 shows the phase velocity of P-wave as a function of angular frequency and Figure 3.8 shows the phase velocity of P-wave as a function of wavelength divided by the period of the layered medium, λ/H.

From the two figures, stop-bands can be clearly observed. As a given frequency increases, or wavelength decreases, the range of the velocity becomes narrower. The velocity finally converges at the limit of high frequency velocity, or at the limit of short wavelength velocity, which is equal to ray velocity.

The behavior of phase velocity as a function of frequency is affected by bulk modulus contrast, density contrast and thickness contrast. In order to examine the

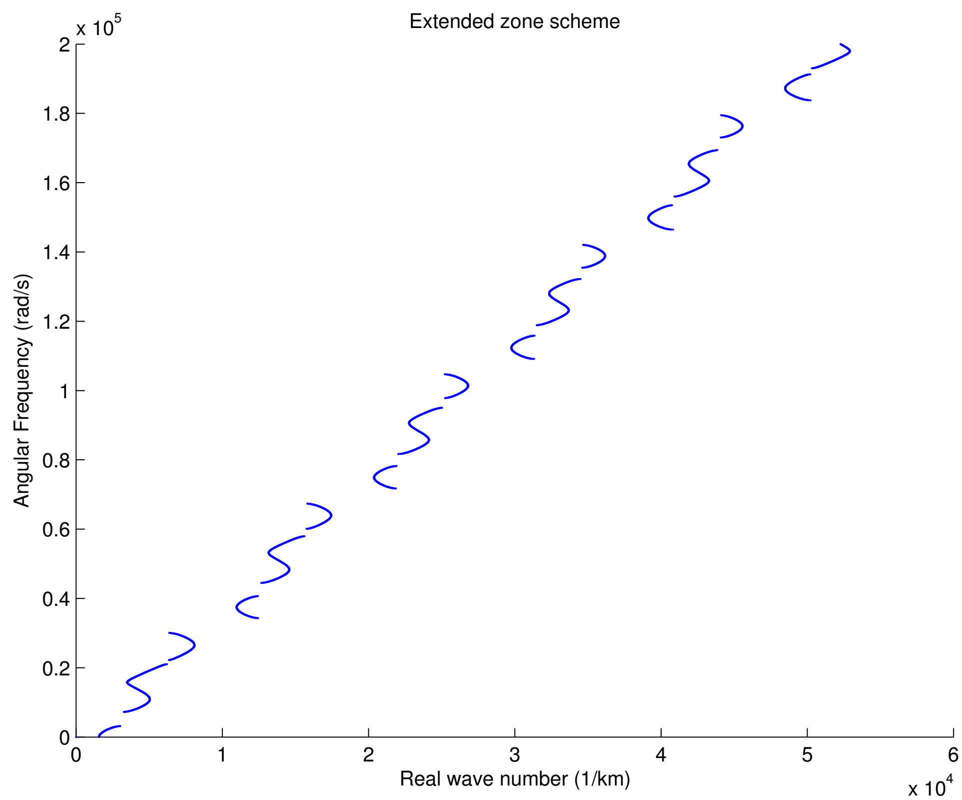

Figure 3.6: Extended zone frequency spectrum for alternating solid and fluid layer.

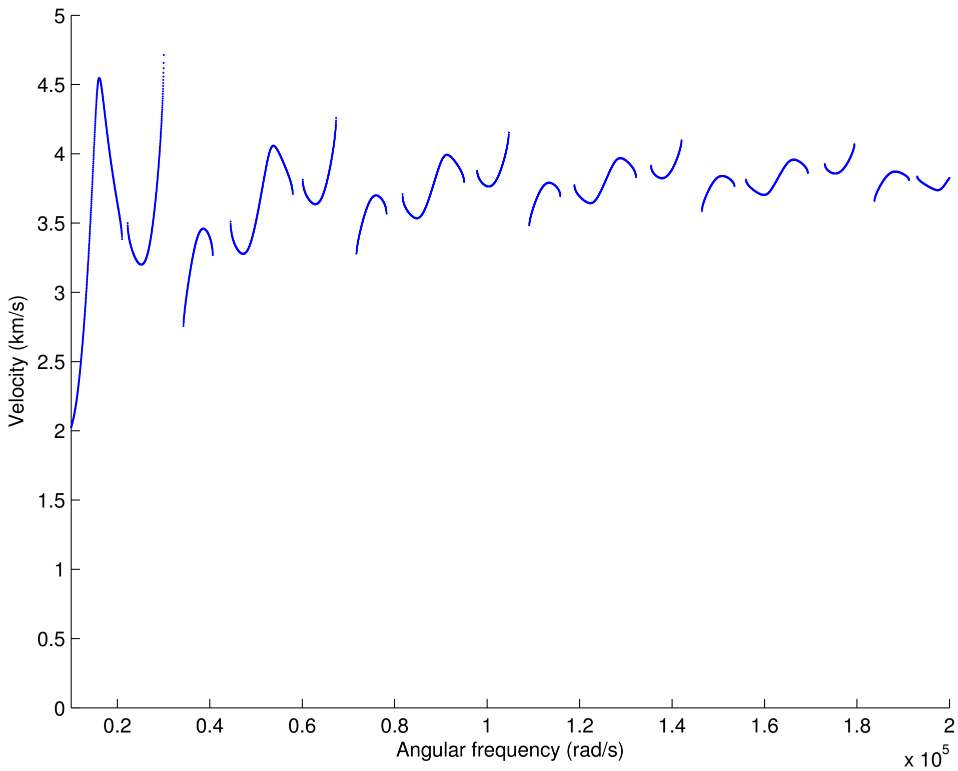

Figure 3.7: Angular frequency vs velocity with propagation normal to layers for alternating solid and fluid layer.

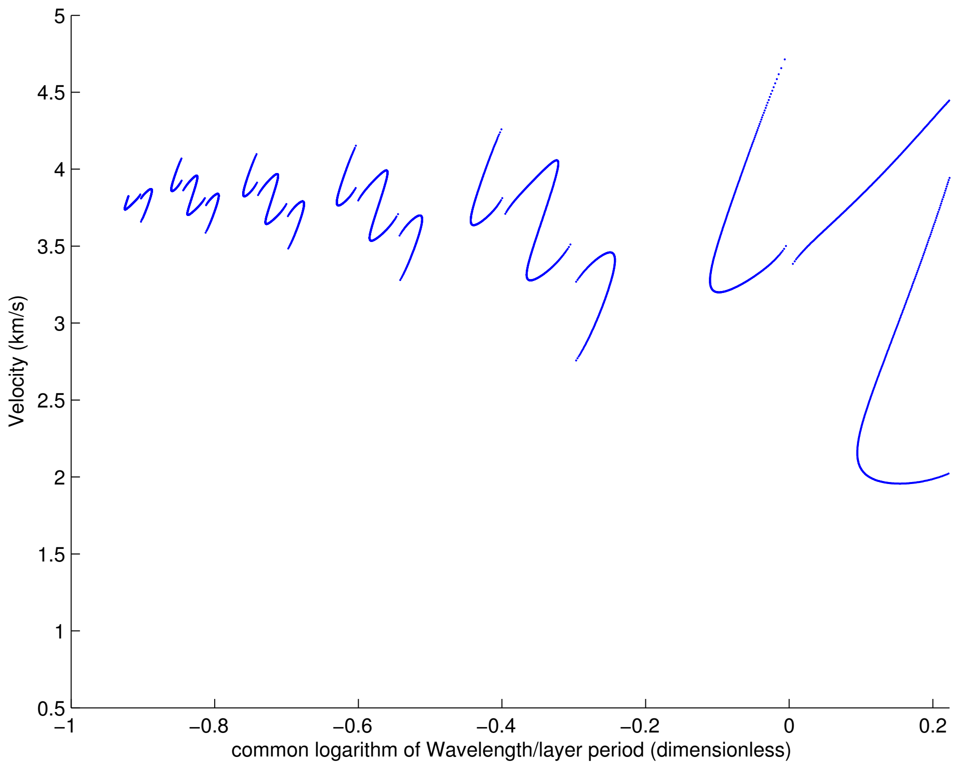

Figure 3.8: λ/H vs velocity with propagation normal to layers for alternating solid and fluid layer.

exact result about how contrast of one parameter affects the dispersion behavior, each parameter will be studied separately. Figures 3.9 - 3.14 show how varied bulk modulus contrast influences behavior of phase velocity as a function of frequency with density and thickness constant. Figures 3.15 - 3.20 show the cases that only density contrast varies, Figures 3.21 - 3.25 show cases in which only thickness contrast varies.

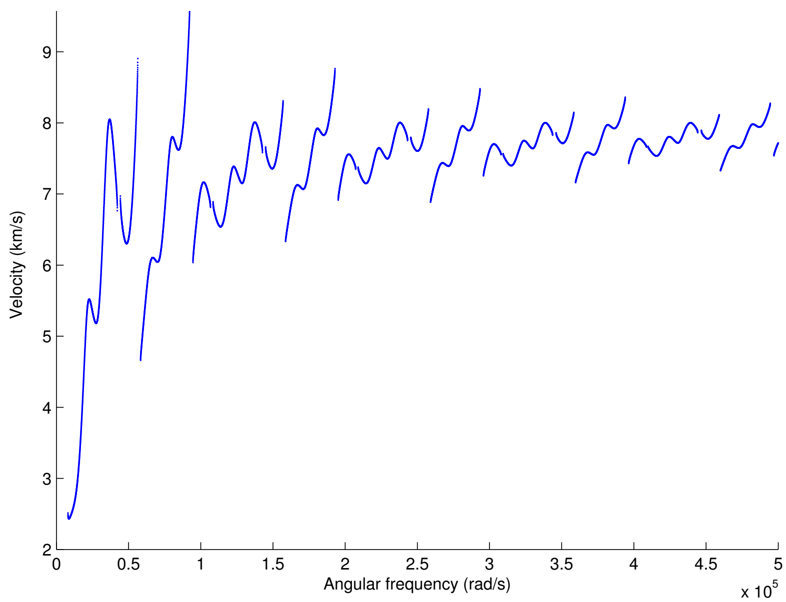

Figure 3.9: Dispersion of P-wave phase velocity, with K contrast = 1:1. solid layer: $K = 7.13\,GPa; \mu = 0.95\,GPa; \rho = 2.1\,g/cm^3$; thickness $h = 0.5\,m$; fluid layer: $\mu = 0\,GPa; \rho = 1\,g/cm^3$; thickness $h = 0.5\,m$.

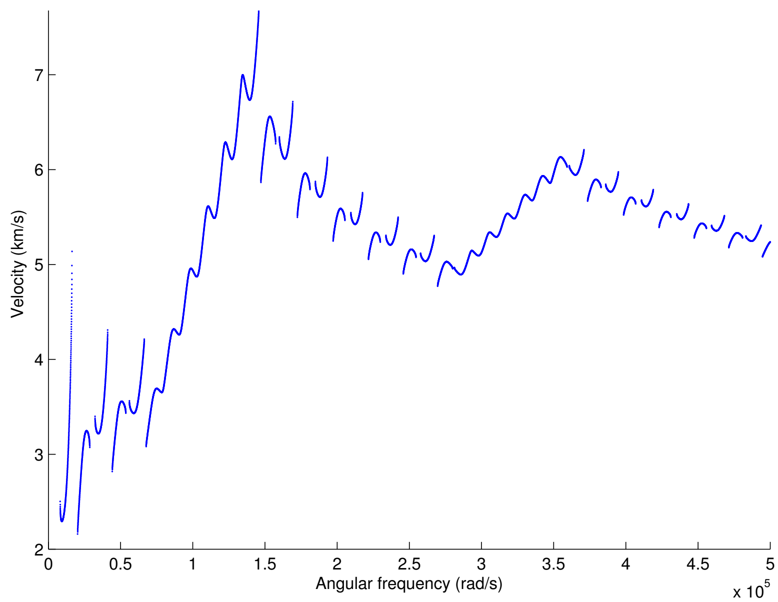

Figure 3.10: Dispersion of P-wave phase velocity, with K contrast = 2:1. solid layer: $K = 7.13\,GPa; \mu = 0.95\,GPa; \rho = 2.1\,g/cm^3$; thickness $h = 0.5\,m$; fluid layer: $\mu = 0\,GPa; \rho = 1\,g/cm^3$; thickness $h = 0.5\,m$.

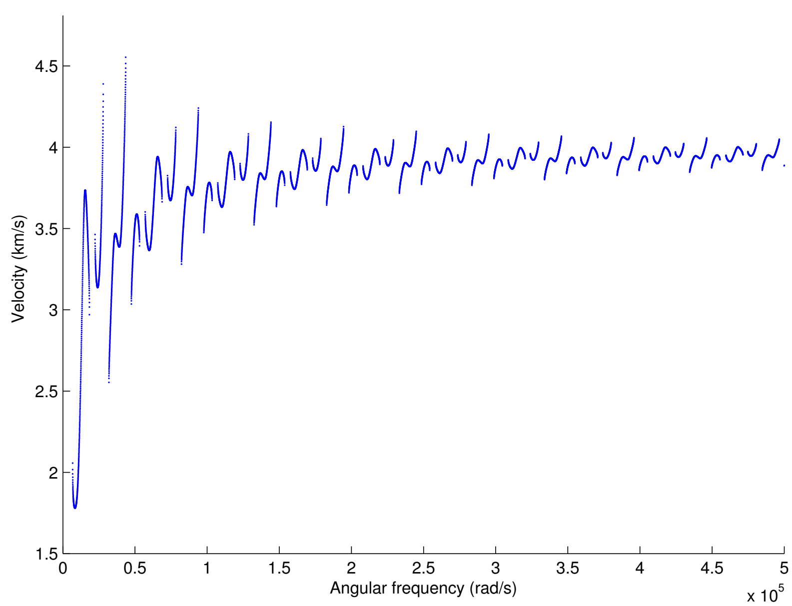

Figure 3.11: Dispersion of P-wave phase velocity, with K contrast = 4:1. solid layer: $K = 7.13\,GPa; \mu = 0.95\,GPa; \rho = 2.1\,g/cm^3$; thickness $h = 0.5\,m$; fluid layer: $\mu = 0\,GPa; \rho = 1\,g/cm^3$; thickness $h = 0.5\,m$.

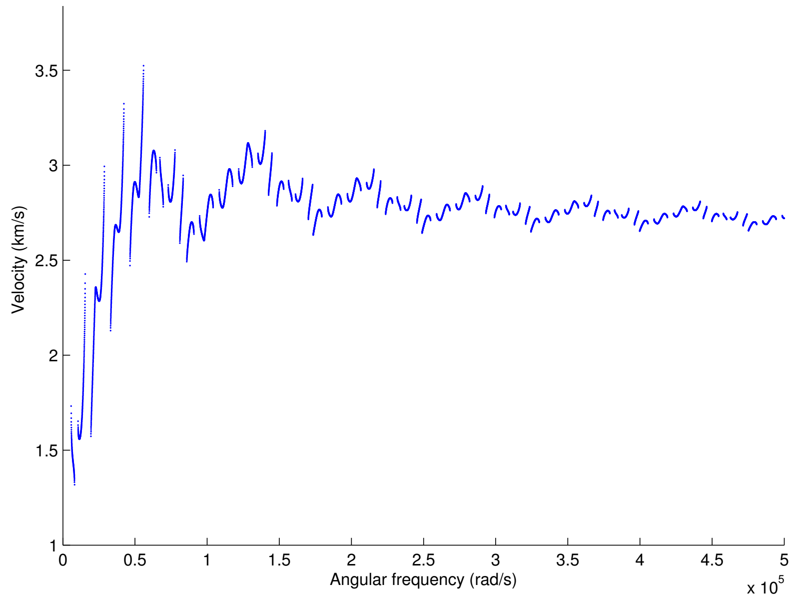

Figure 3.12: Dispersion of P-wave phase velocity, with K contrast = 6:1. solid layer: $K = 7.13\,GPa; \mu = 0.95\,GPa; \rho = 2.1\,g/cm^3$; thickness $h = 0.5\,m$; fluid layer: $\mu = 0\,GPa; \rho = 1\,g/cm^3$; thickness $h = 0.5\,m$.

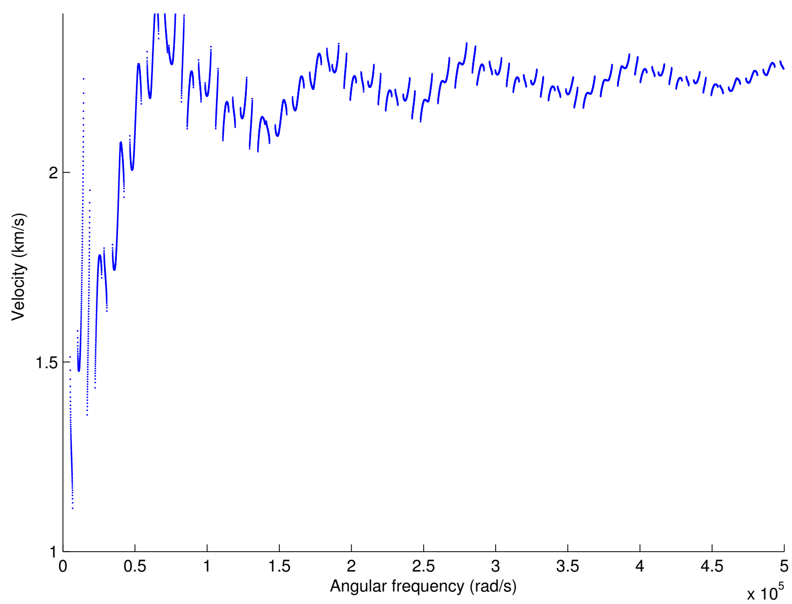

Figure 3.13: Dispersion of P-wave phase velocity, with K contrast = 8:1. solid layer: $K = 7.13\,GPa; \mu = 0.95\,GPa; \rho = 2.1\,g/cm^3$; thickness $h = 0.5\,m$; fluid layer: $\mu = 0\,GPa; \rho = 1\,g/cm^3$; thickness $h = 0.5\,m$.

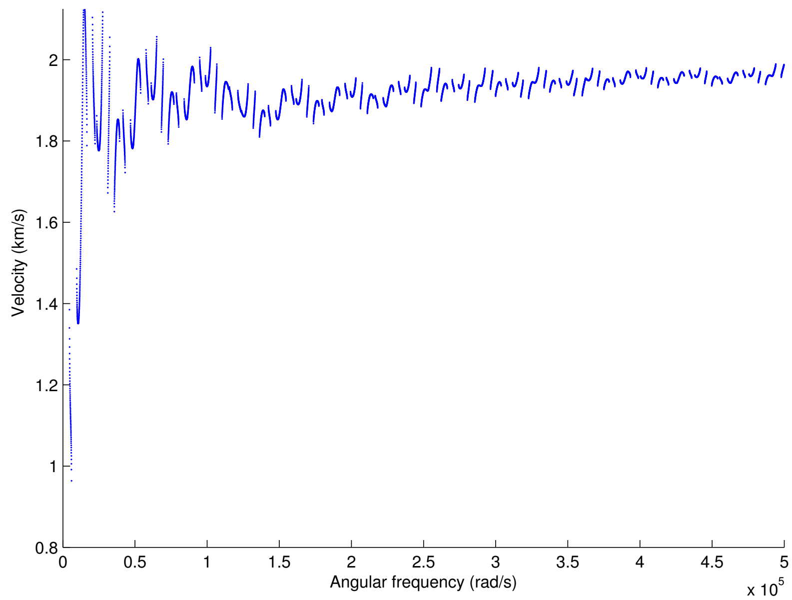

Figure 3.14: Dispersion of P-wave phase velocity, with K contrast = 10:1. solid layer: $K = 7.13\,GPa; \mu = 0.95\,GPa; \rho = 2.1\,g/cm^3$; thickness $h = 0.5\,m$; fluid layer: $\mu = 0\,GPa; \rho = 1\,g/cm^3$; thickness $h = 0.5\,m$.

The parameters of solid layers are set constant, with bulk modulus $K = 7.13GPa$, shear modulus $\mu = 0.95\,GPa$, and density $\rho = 2.1\,g/cm^3$. While K and ρ of fluid layers change respectively, to achieve different contrasts, μ of fluid layers is always 0. For the study of K contrast and density contrast, the thickness of both layers are equal. From all those cases, it is indicated that phase velocity converges at a value as frequency approaches positive infinity, corresponding to ray velocity. Additionally, the figures clearly show the stop-bands, which are the frequency bands at which a real velocity value does not exist.

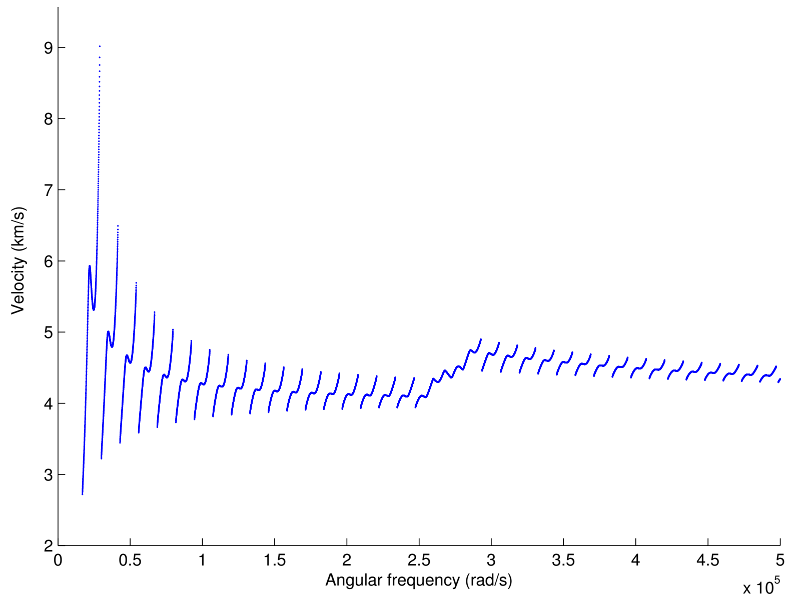

Figure 3.15: Dispersion of P-wave phase velocity, with density contrast = 1:1. solid layer: $K = 7.13\,GPa; \mu = 0.95\,GPa; \rho = 2.1\,g/cm^3$; thickness $h = 0.5\,m$; fluid layer: $K = 2.2\,GPa; \mu = 0\,GPa$; thickness $h = 0.5\,m$.

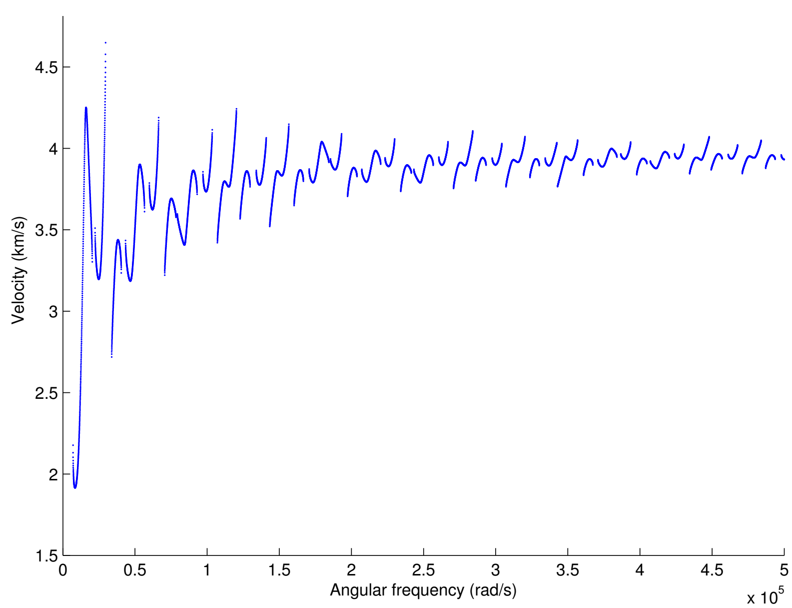

Figure 3.16: Dispersion of P-wave phase velocity, with density contrast = 2:1. solid layer: $K = 7.13\,GPa; \mu = 0.95\,GPa; \rho = 2.1\,g/cm^3$; thickness $h = 0.5\,m$; fluid layer: $K = 2.2\,GPa; \mu = 0\,GPa$; thickness $h = 0.5\,m$.

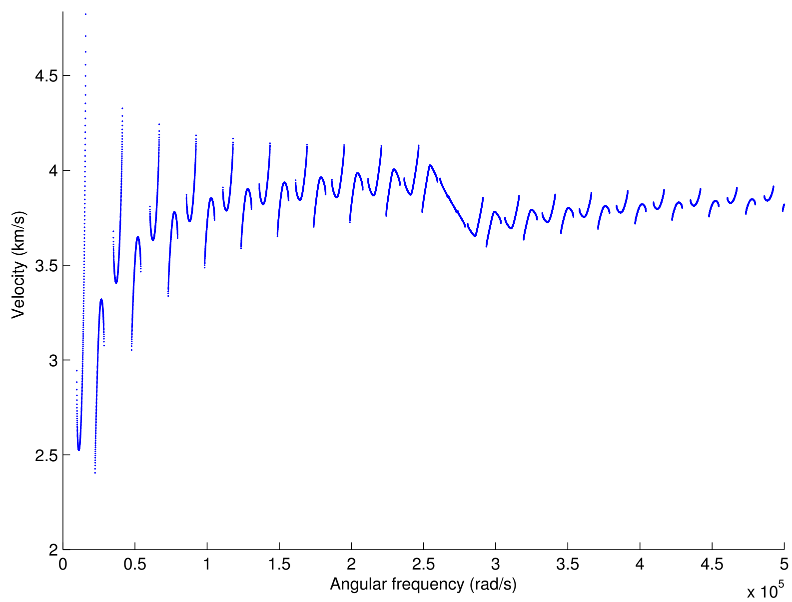

Figure 3.17: Dispersion of P-wave phase velocity, with density contrast = 4:1. solid layer: $K = 7.13\,GPa$; $\mu = 0.95\,GPa$; $\rho = 2.1\,g/cm^3$; thickness $h = 0.5\,m$; fluid layer: $K = 2.2\,GPa$; $\mu = 0\,GPa$; thickness $h = 0.5\,m$.

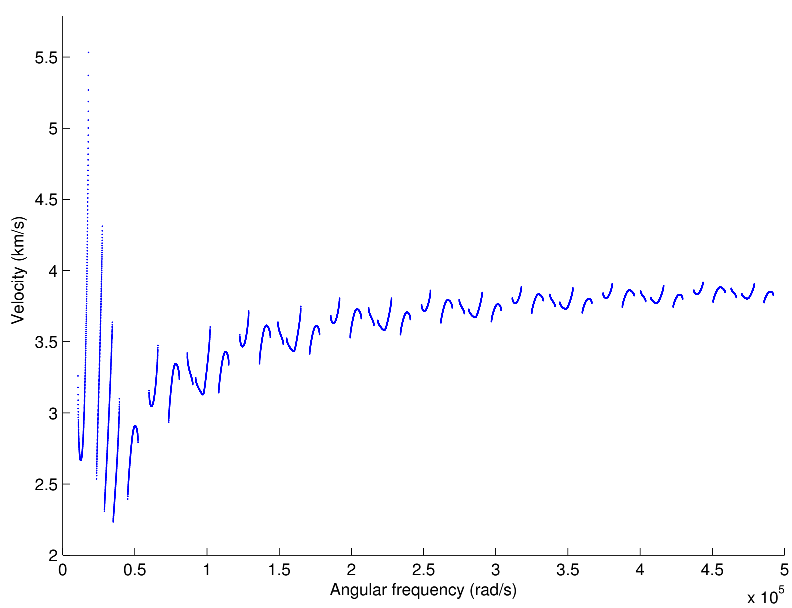

Figure 3.18: Dispersion of P-wave phase velocity, with density contrast = 6:1. solid layer: $K = 7.13\,GPa$; $\mu = 0.95\,GPa$; $\rho = 2.1\,g/cm^3$; thickness $h = 0.5\,m$; fluid layer: $K = 2.2\,GPa$; $\mu = 0\,GPa$; thickness $h = 0.5\,m$.

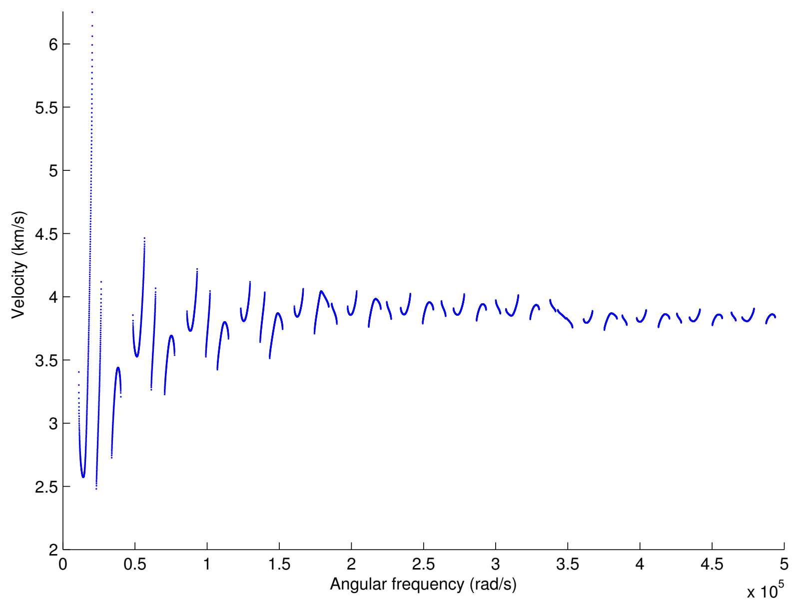

Figure 3.19: Dispersion of P-wave phase velocity, with density contrast = 8:1. solid layer: $K = 7.13\,GPa; \mu = 0.95\,GPa; \rho = 2.1\,g/cm^3$; thickness $h = 0.5\,m$; fluid layer: $K = 2.2\,GPa; \mu = 0\,GPa$; thickness $h = 0.5\,m$.

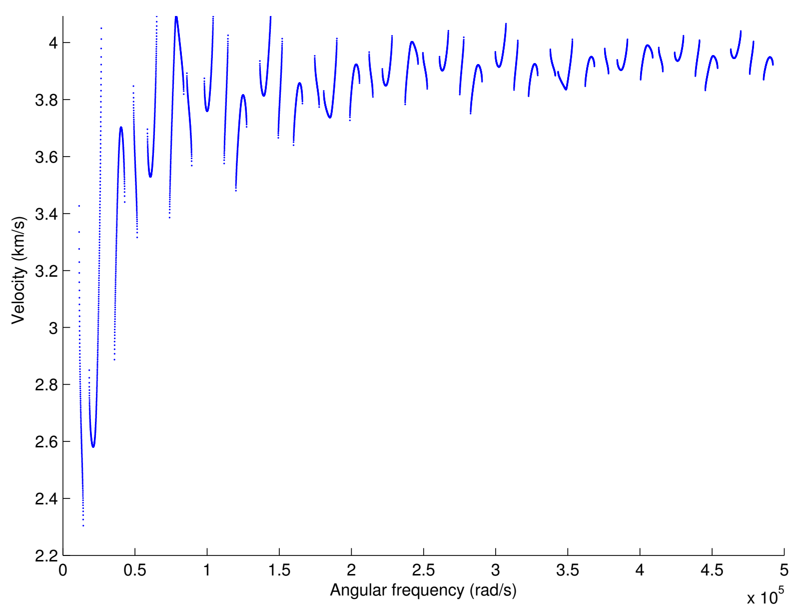

Figure 3.20: Dispersion of P-wave phase velocity, with density contrast = 10:1. solid layer: $K = 7.13\,GPa; \mu = 0.95\,GPa; \rho = 2.1\,g/cm^3$; thickness $h = 0.5\,m$; fluid layer: $K = 2.2\,GPa; \mu = 0\,GPa$; thickness $h = 0.5\,m$.

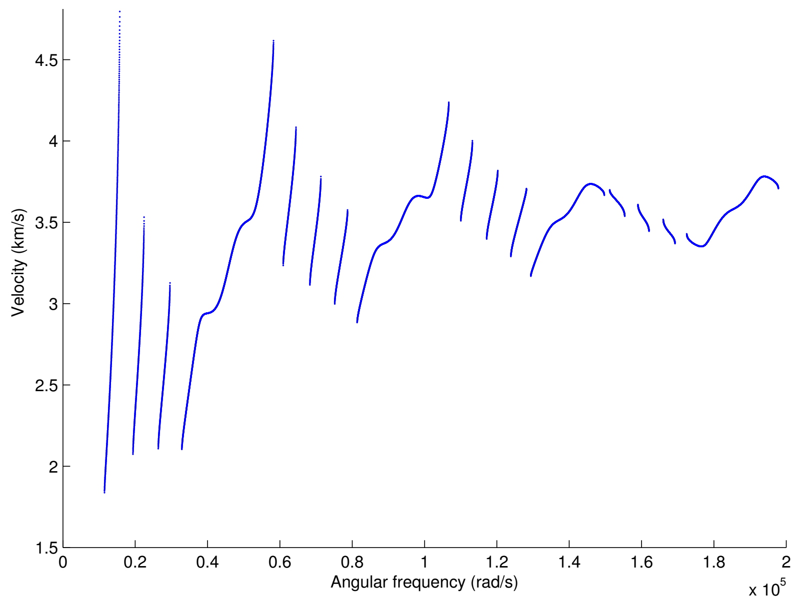

Figure 3.21: Dispersion of P-wave phase velocity, with thickness contrast = 1:9. solid layer: $K = 7.13\,GPa; \mu = 0.95\,GPa; \rho = 2.1\,g/cm^3$; fluid layer: $K = 2.2\,GPa; \mu = 0\,GPa$; $\rho = 1\,g/cm^3$. The thickness of period is 1 m.

3.4 Stop-bands at direction normal to the layering

Two major phenomena of scattering in periodic layered media are dispersion and stop-bands. The stop-bands are generated due to destructive interference (Rich, 2006). The characteristics of stop-bands are affected by two factors, namely the relative thickness of layers, and the impedance contrast between the solid and the fluid layers. The impedance is the product of the velocity and the density, with the impedance of P-wave $I_p = v_p \times \rho$, and the impedance of S-waves $I_s = v_s \times \rho$. Figures 3.26 - 3.28 show the stop-bands on a plane of angular frequency and impedance contrast for P-waves propagating or decaying normal to the layering.

In Figure 3.26, the varied impedance contrast is produced by the variation of bulk modulus of fluid layers; in Figure 3.27, it is produced by the variation of density

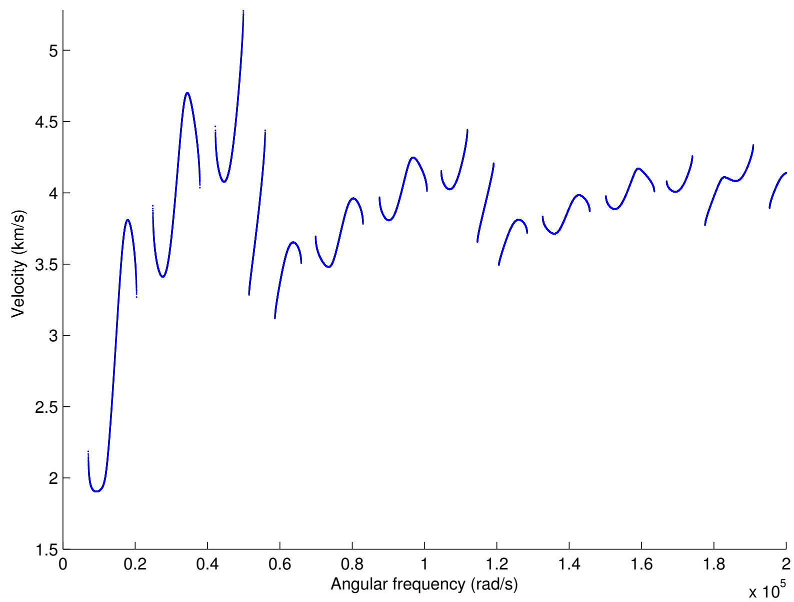

Figure 3.22: Dispersion of P-wave phase velocity, with thickness contrast = 3:7. solid layer: $K = 7.13\,GPa; \mu = 0.95\,GPa; \rho = 2.1\,g/cm^3$; fluid layer: $K = 2.2\,GPa; \mu = 0\,GPa$; $\rho = 1\,g/cm^3$. The thickness of period is 1 m.

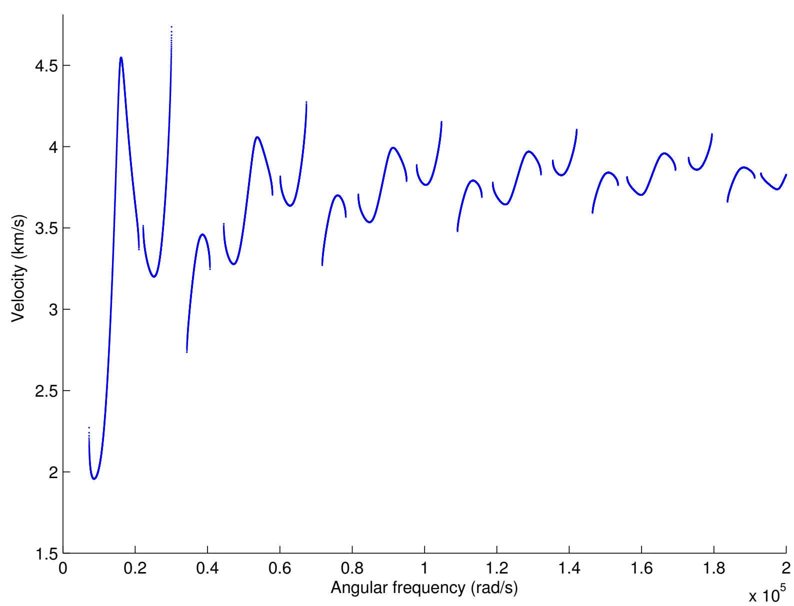

Figure 3.23: Dispersion of P-wave phase velocity, with thickness contrast = 5:5. solid layer: $K = 7.13\,GPa; \mu = 0.95\,GPa; \rho = 2.1\,g/cm^3$; fluid layer: $K = 2.2\,GPa; \mu = 0\,GPa$; $\rho = 1\,g/cm^3$. The thickness of period is 1 m.

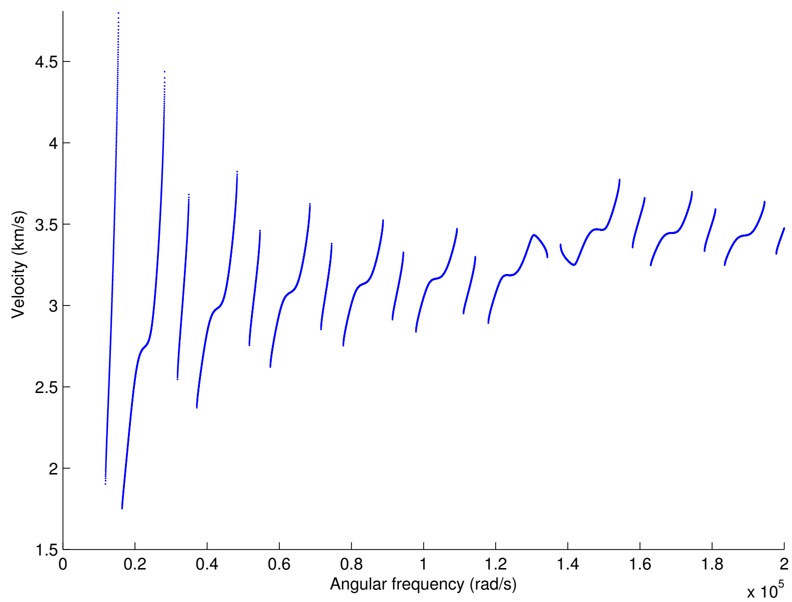

Figure 3.24: Dispersion of P-wave phase velocity, with thickness contrast = 7:3. solid layer: $K = 7.13\,GPa; \mu = 0.95\,GPa; \rho = 2.1\,g/cm^3$; fluid layer: $K = 2.2\,GPa; \mu = 0\,GPa$; $\rho = 1\,g/cm^3$. The thickness of period is 1 m.

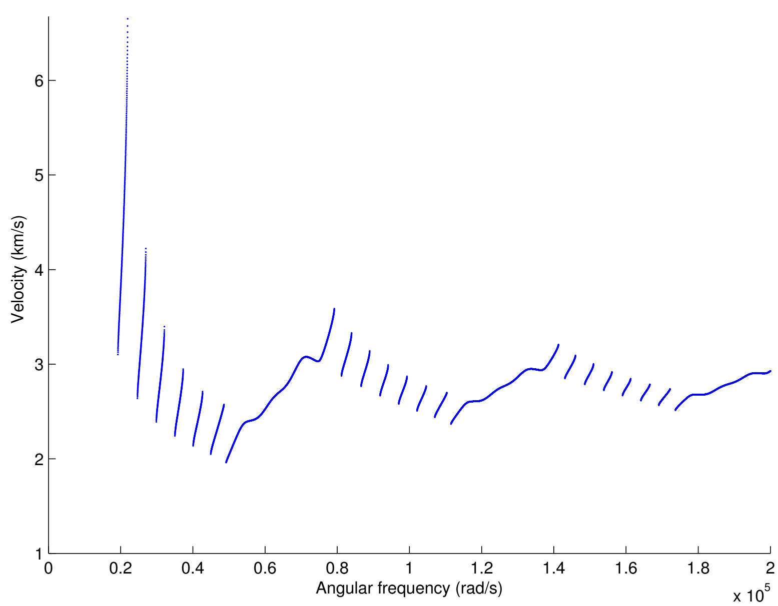

Figure 3.25: Dispersion of P-wave phase velocity, with thickness contrast = 9:1. solid layer: $K = 7.13\,GPa; \mu = 0.95\,GPa; \rho = 2.1\,g/cm^3$; fluid layer: $K = 2.2\,GPa; \mu = 0\,GPa$; $\rho = 1\,g/cm^3$. The thickness of period is 1 m.

of fluid layers. In Figure 3.28, the porosity is the ratio of the volume of fluid layers to the total volume. This is also equal to the thickness of fluid layer divided by thickness of the whole period, since the fluid layers are regarded as inclusion.

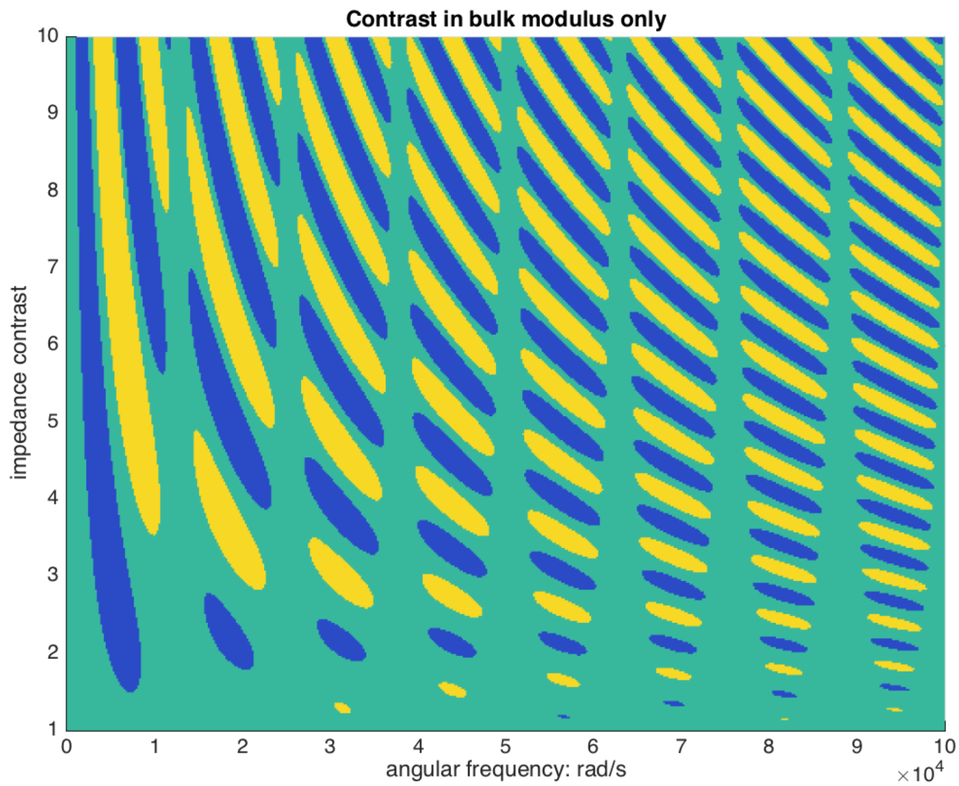

Figure 3.26: stop-band as a function of angular frequency and impedance contrast with change of contrast of bulk modulus only. solid layer: $K = 7.13\, Gpa, \mu = 0.95\, Gpa, \rho = 2.1\, g/cm^3$, thickness: 0.5 m; liquid layer: $\rho = 1\, g/cm^3$, thickness: 0.5 m. The green zones are regions within which propagating waves exist; the yellow zones and the blue zones are stop-bands. In the yellow zones, waves are evanescent with no phase change between adjacent periods, while in the blue zones, waves are evanescent with a 180° phase change between adjacent periods.

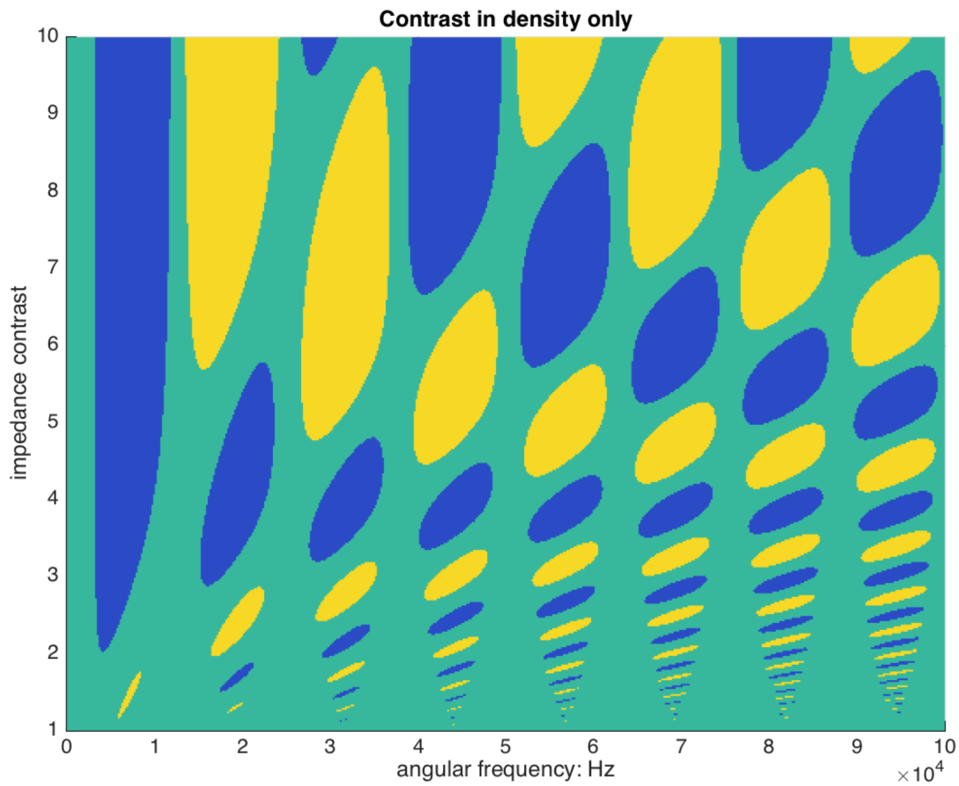

Figure 3.27: stop-band as a function of angular frequency and impedance contrast with change of contrast of density only. solid layer: $K = 7.13Gpa, \mu = 0.95Gpa, \rho = 2.1\,g/cm^3$, thickness: 0.5 m; liquid layer: $K = 2.2\,GPa$, thickness: 0.5 m. The green zones are regions within which propagating waves exist; the yellow zones and the blue zones are stop-bands. In the yellow zones, waves are evanescent with no phase change between adjacent periods, while in the blue zones, waves are evanescent with a 180° phase change between adjacent periods.

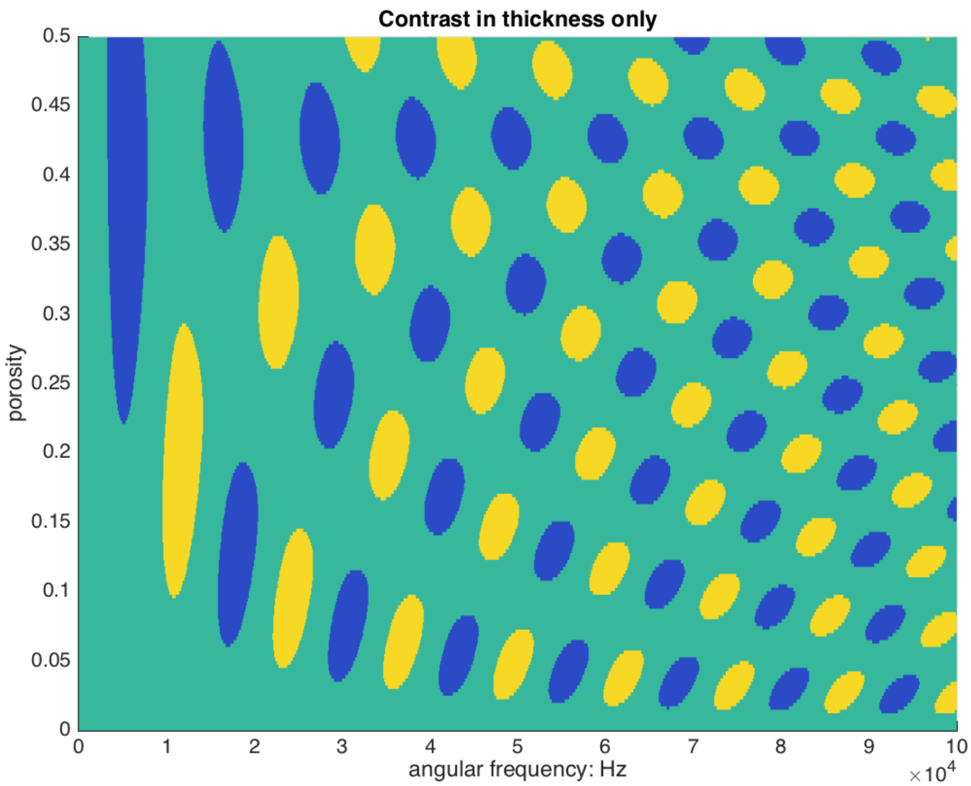

Figure 3.28: stop-band as a function of angular frequency and porosity. solid layer: $K = 7.13\, Gpa, \mu = 0.95\, Gpa, \rho = 2.1\ g/cm^3$, thickness: 0.5 m; liquid layer: $K = 2.2\, GPa; \rho = 1\ g/cm^3$, thickness: 0.5 m. The green zones are regions within which propagating waves exist; the yellow zones and the blue zones are stop-bands. In the yellow zones, waves are evanescent with no phase change between adjacent periods, while in the blue zones, waves are evanescent with a 180° phase change between adjacent periods.

Chapter 4

The Low Frequency Limit for Elastoacoustic Medium

4.1 Schoenberg's theory for the low frequency limit

4.1.1 Phase velocity

In order to discuss the case of long wavelength in which the widths of layers are much thinner than a wavelength, it is then required to take the limit as angular frequency, ω, to approach zero. From Equation 3.16

$$\lim_{\omega \to 0} \frac{\xi}{(\omega h_s H)^2} = \lim_{\omega \to 0} \frac{\kappa}{\omega h_s H} = 1 - 4(1 - \frac{\beta^2}{\alpha^2})\beta^2 s_1^2 \equiv 1 - \alpha_{pl}^2 s_1^2 \tag{4.1}$$

where $\alpha_{pl} = 2(1 - \beta^2/\alpha^2)^{\frac{1}{2}}\beta < \alpha$, the long wavelength velocity of extensional plate wave with S-wave velocity, β, and P-waves velocity, α. Therefore, from Equations 4.1, 3.16, and 3.21, in the low frequency regime, it follows:

$$
\begin{aligned}
\overline{q}_f(h_f H) &= \begin{bmatrix} 1 - \frac{1}{2}(\omega s_f h_f H)^2 + O(\Omega^4) & -i\omega\rho_f h_f H + O(\Omega^3) \\ -i\omega s_f^2 h_f H/\rho_f + O(\Omega^3) & q_{f_{11}}(h_f H) \end{bmatrix} \\
\overline{q}_s &= \begin{bmatrix} 1 - \frac{(\omega s_p h_s H)^2}{2(1-\alpha_{pl}^2 s_1^2) + O(\Omega^4)} & -i\omega\rho h_s H + O(\Omega^3) \\ -\frac{i\omega s_p^2 h_s H}{\rho(1-\alpha_{pl}^2 s_1^2)} + O(\Omega^3) & q_{s_{11}} \end{bmatrix}
\end{aligned}
\tag{4.2}
$$

where Ω is a parameter that is ωH divided by some convenient material speed, indicating a dimensionless frequency. Then C, half of the trace of $\overline{Q}$ is

$$
\begin{aligned}
C =& 1 - \frac{(\omega H)^2}{2} f(s_1^2) + O(\Omega^4) \\
f(s_1^2) =& (h_f\rho_f + h_s\rho)\left[h_f \frac{s_f^2}{\rho_f} + h_s \frac{s_p^2}{\rho(1-\alpha_{pl}s_1^2)}\right] \\
=& < \rho > \left\langle \frac{\alpha^{-1} - s_1^2}{\rho(1-\alpha_{pl}^2 s_1^2)} \right\rangle
\end{aligned}
\tag{4.3}
$$

where the plate velocity of the fluid layer is zero, and $<>$ represents the thickness weighted average. For long wavelengths and a solid-fluid medium, the overall wave slowness is $[f(s_1^2)]^{\frac{1}{2}} + O(\Omega^2)$, with eigenvalues of $\overline{Q}$ equal to $e^{\pm i\omega H\sqrt{f(s_1^2)}} + O(\Omega^3)$. The relation of components of slowness for the long wavelength case in elastoacoustic medium is

$$
F_0(s_3^2, s_1^2) = s_3^2 - f(s_1^2) = 0 \tag{4.4}
$$

For the discussion below, multiplying the equation on both sides by $(\alpha_{pl}^{-2} - s_1^2)$

$$
(\alpha_{pl}^{-2} - s_1^2)\left[\frac{s_3^2}{< \rho >} + s_1^2\left\langle\frac{1}{\rho}\right\rangle - \left\langle\frac{1}{\rho\alpha^2}\right\rangle\right] = \frac{1}{\rho} s_1^2 h_s(\alpha^{-2} - s_1^2) \tag{4.5}
$$

the solution to this slowness equation are indicated by the slowness surfaces. In Figure 4.1, the solid line denotes the real value of s_3 as a function of s_1 for the model that portrays a low contrast Plexiglas-water combination. For the parameters of the model, $\alpha/\alpha_f = 1.8, \beta/\alpha_f = 0.92, \rho/\rho_f = 1.2$. All slowness and velocities are normalized with respect to the speed of water.

In Figure 4.2, we have a case for a high contrast aluminum-water combination. For the parameters of the model, $\alpha/\alpha_f = 4.3, \beta/\alpha_f = 2.1, \rho/\rho_f = 2.7$.

There are two solid lines in each graph, of which the one closer to origin of the coordinate system represents the fast P-wave and the other one represents the slow P-wave. For every real value of s_1^2, only one real value of s_3^2 exists, except when s_1^2 equals $1/\alpha_p l^2$. $s_1 = 0$, denotes the case of normal incidence. $s_3^2 =< \rho > \cdot < 1/\rho\alpha^2 >$ satisfies the theory of propagation through layered media in cases of normal incidence. s_3^2 decreases monotonically as s_1 increases, until s_1 equals the slowness of fast P-wave, when $s_3^2 = 0$. As s_1 continues to increase and becomes greater than $\alpha^{-1}, f(s_1^2)$ becomes negative and grows to negative infinity as s_1 approaches α_{pl}^{-1}. When $s_{fast} < s_1 < \alpha^{-1}, s_3^2$ is negative, so that s_3 is imaginary, showing that when horizontal slowness equals such value of s_1, it is not possible that propagation wave exists through the medium. This indicates what is then called stop-band in horizontal slowness. As s_1 approaches α_{pl}^{-1} from the negative side, the rate of decay of the evanescent wave in x_3 direction approaches infinity.

When s_1 is greater than α_{pl}^{-1}, it corresponds to the regime of slow P-wave. As s_1 approaches α_{pl}^{-1} from the positive side, $f(s_1^2)$ and thus s_3^2 approaches positive infinity. As s_1 increases, s_3^2 decreases monotonically until $s_1 = s_{slow}$, when s_3^2 equals zero. The velocity of the slow wave propagation parallel to the layering is always slower than the P-wave velocity of the fluid. When s_1 is greater than $s_{slow}, s_3^2 < 0$, there is no propagating wave in the x_3 direction, and yet as s_1 approaches infinity, the rate of decay of the evanescent wave approaches infinity.

Transforming Equation 4.4 into polar coordinates, with $s_1 = s\ sin\,\theta$ and $s_3 =$

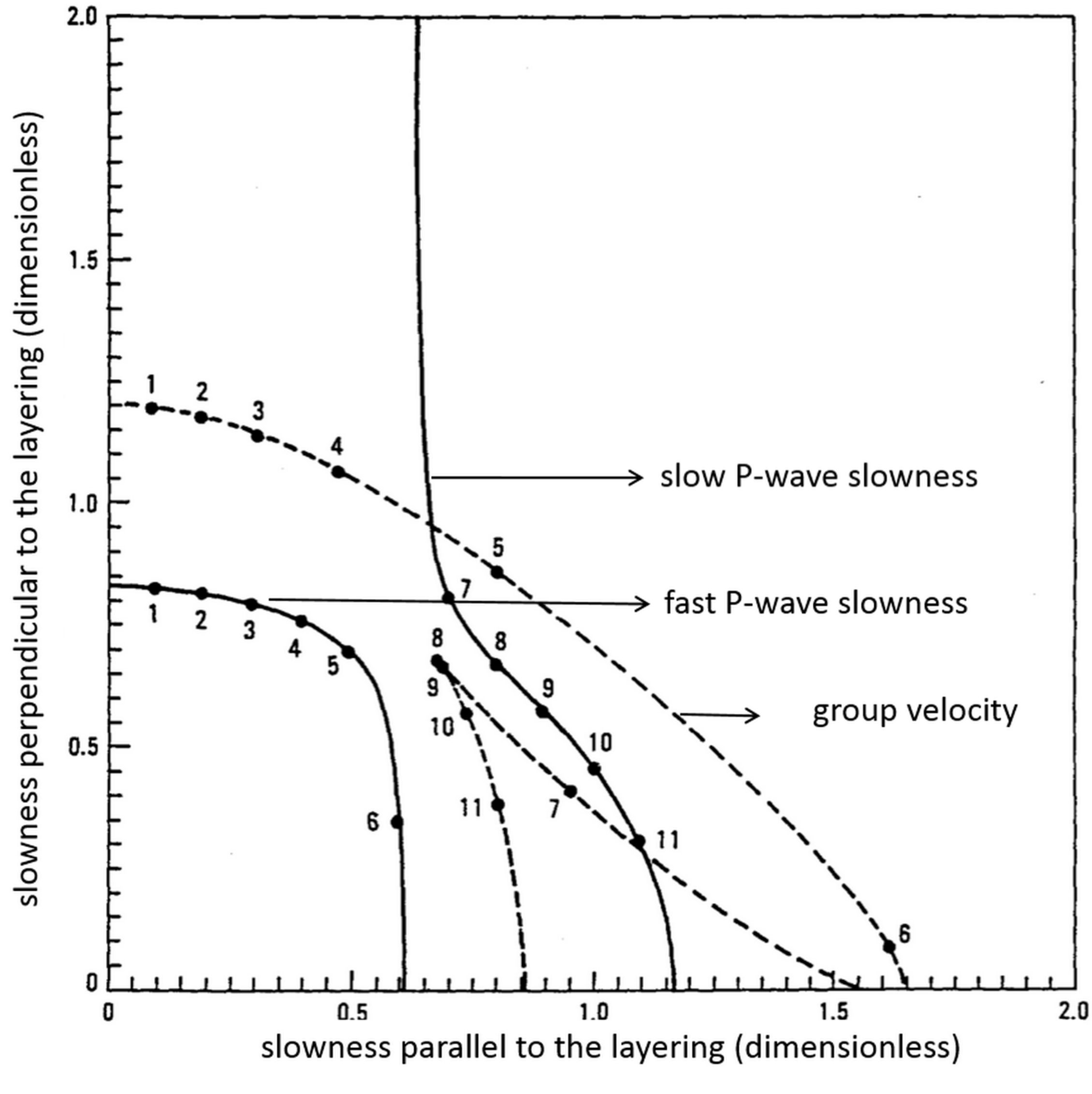

Figure 4.1: long wavelength phase slowness surfaces (solid lines) and group velocity surfaces (dashed lines) for Plexiglas and water with layers of equal thickness (Schoenberg, 1984)

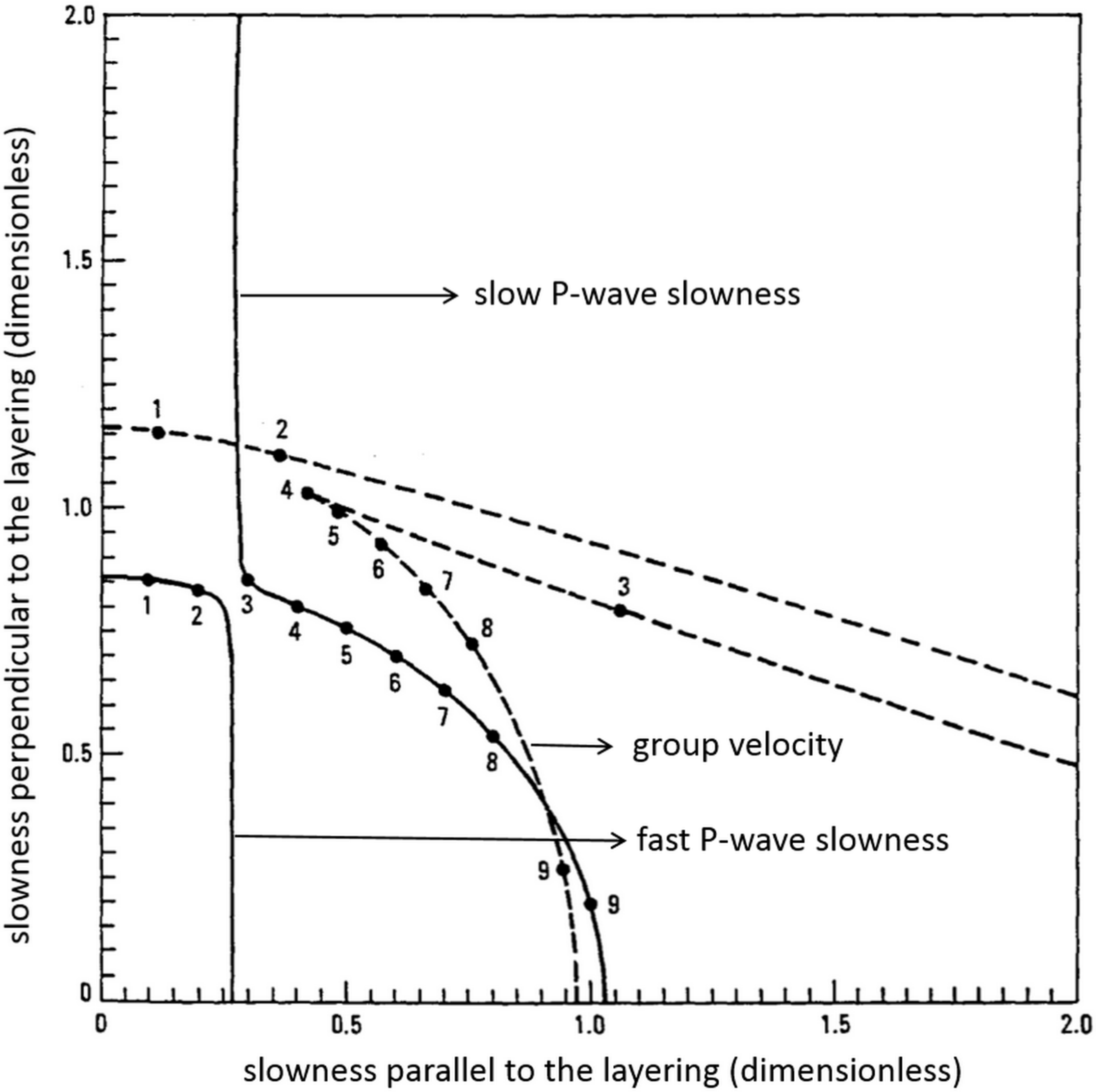

Figure 4.2: long wavelength phase slowness surfaces (solid lines) and group velocity surfaces (dashed lines) for aluminum and water with the solid layers twice the thickness of the fluid layers (Schoenberg, 1984)

$s\ cos\ \theta$, then

$$
\begin{aligned}
&(s^2)^2 \alpha_{pl}^2\ sin^2\ \theta \left(\frac{h_f\ sin^2\ \theta}{\rho_f} + \frac{cos^2\ \theta}{<\rho>} \right) \\
-s^2 &\left[\frac{cos^2\ \theta}{<\rho>} + sin^2\ \theta \left(\left\langle \frac{1}{\rho} \right\rangle + \frac{h_f \alpha_{pl}^2}{\rho_f \alpha_f^2} \right) \right] + \left\langle \frac{1}{\rho \alpha^2} \right\rangle = 0
\end{aligned}
\tag{4.6}
$$

This is a quadratic equation of s^2, which gives the relation of s and θ for all values of θ except when $\theta = 0$, in a case of normal incidence. At all other angle of wave propagation, there are two real positive roots, one corresponding to a fast mode, and the other to a slow mode of propagation respectively. From Equation 4.4 in the interval $s_1 > \alpha_{pl}^{-1}$, the line representing slowness surface of slow wave approaches an ellipse with the semiaxis α_f^{-1} in the x_1 direction and $(<\rho> h_f/\rho_f)^{\frac{1}{2}}$ in the x_3 direction. As shown in Figure 4.2, there is a solution $s_1 \approx \alpha_{pl}^{-1}$ for almost all values of θ; the stop-band then almost vanishes.

4.1.2 Group velocity

For periodic media, propagation exists when $|C| < 1$. In this case, s_3 is calculated by Equation 3.9 within a phase ambiguity of an integer number multiplyed by 2π. Therefore, the dispersion is described with the form

$$
F(\mathbf{k}, \omega) \equiv F(\mathbf{s}, \omega) = C(s_1^2, \omega) - cos\ \omega s_3 H = 0 \tag{4.7}
$$

For anisotropic media, it it more convenient to describe the wave behavior in terms of slowness instead of wavenumber, ($\mathbf{k} \equiv \omega \mathbf{s}$). The group velocity, $\mathbf{v}_g \equiv -\nabla_k F / F_{,\omega}$, with change occurring from $\mathbf{k}$ to $\mathbf{s}$, is

$$
\mathbf{v}_g = \frac{\nabla_s F}{s \cdot \nabla_s F - \omega F_{,\omega}} \tag{4.8}
$$

Then, from Equation 4.7, we get

$$\mathbf{v}_g = \frac{2\mathbf{e}_1 s_1 \frac{\partial C}{\partial s_1^2} + \mathbf{e}_3 \omega H \; sin \, \omega s_3 H}{2s_1^2 \frac{\partial C}{\partial s_1^2} - \omega \frac{\partial C}{\partial \omega}} \tag{4.9}$$

where $\mathbf{e}_i$ is a unit vector in the x_i direction. For propagating waves, characterized by $C(s_1^2, \omega)$ when $|C| < 1$, the value of group velocity is unique, as given by Equaion 4.9. The sign of the term $sin\, \omega s_3 H$ is given by the sign of the imaginary part of λ_i.

For the scenario involving low frequency waves, substitute C from Equation 4.3 into Equation 4.9; we then obtain the result of the group velocity,

$$\begin{aligned} \mathbf{v}_g &= \frac{-f' s_1 \mathbf{e}_1 + s_3 \mathbf{e}_3}{-f' s_1^2 + s_3^2} + O(\Omega^2), \\ f' &\equiv \frac{df}{d(s_1^2)} = - < \rho > \left[\frac{h_f}{\rho_f} + \frac{h_s}{\rho_s} \left(\frac{1 - \beta^2/\alpha^2}{1 - \alpha_{pl}^2 s_1^2} \right)^2 \right] \end{aligned} \tag{4.10}$$

As $\omega \to 0$, this expression becomes,

$$\mathbf{v}_g \equiv \frac{\nabla_s F_0}{s \cdot \nabla_s F_0} = \frac{\mathbf{e}_n}{|s| \; cos \, \angle(\mathbf{s}, \mathbf{e}_n)} \tag{4.11}$$

where $\mathbf{e}_n$ is the outward unit vector perpendicular to the slowness surface. And thus the modulus of the group velocity equals the reciprocal of the projection of $\boldsymbol{s}$ on the direction perpendicular to the slowness surface at $\boldsymbol{s}$, and the direction of the group velocity is then normal to the slowness surface, as shown in Figure 4.3 (Schoenberg, 1984).

4.2 Anisotropy at low frequency limit and material contrast

In order to study the sensitivity of angular dependent velocities to material contrast, the effect of each parameter set will be examined separately. While this is not based

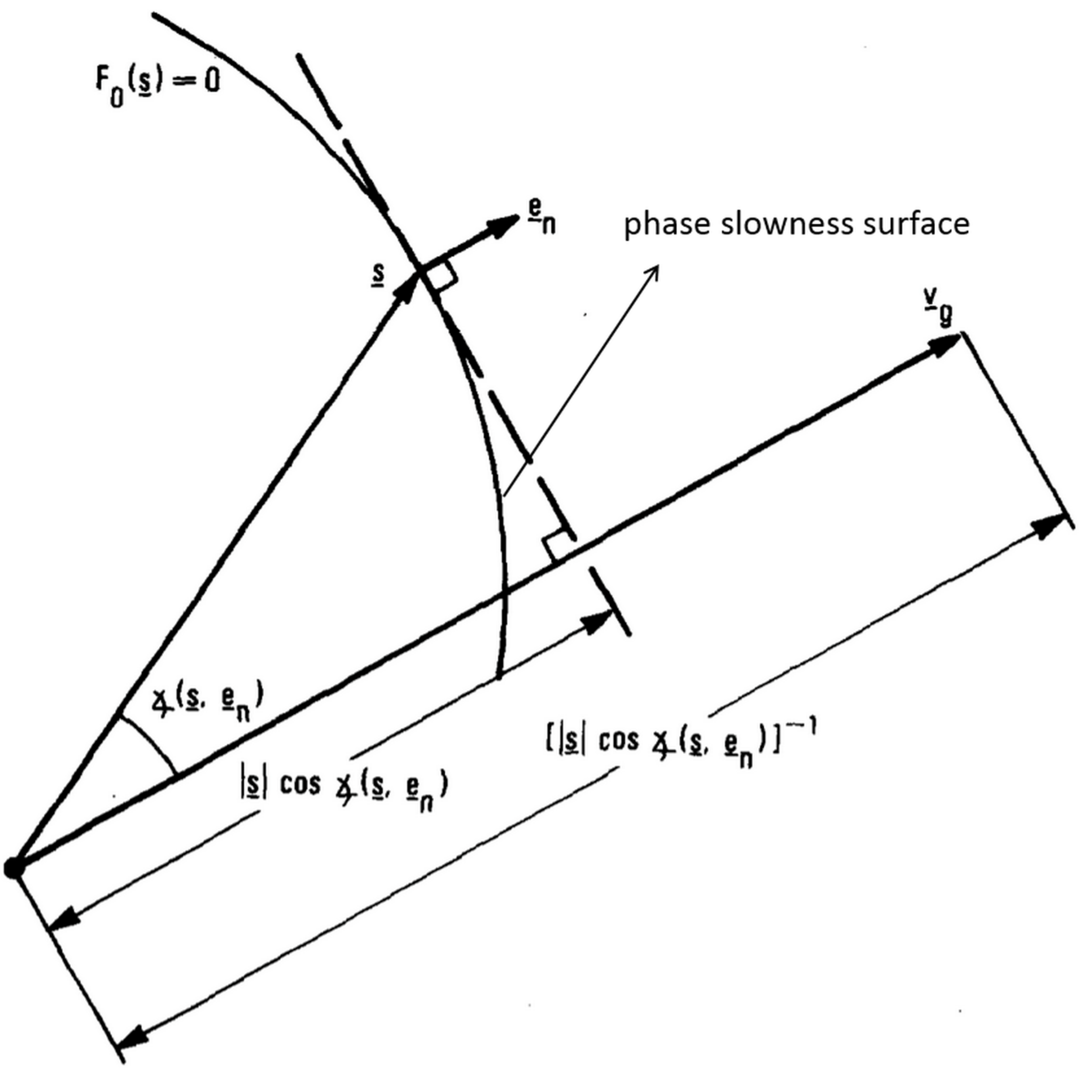

Figure 4.3: Geometrical relation between phase slowness and group velocity showing the polar reciprocal nature of the slowness and wave surface (Schoenberg, 1984)

on a geologically realistic situation, it is designed for understanding how physical rock and fluid properties control layer-induced anisotropy. In this numerical model, there are two layers in each period, again a solid layer and a fluid layer. In the following study, the physical parameters of the solid layer are constant, thus each parameter of the fluid varies respectively to produce different parameter contrast in each situation. In order to describe the anisotropy, an anisotropy coefficient is defined in Equation 2.14. However, for the model with alternating solid and fluid layers, the slow P-wave at 0° (perpendicular to the layer) is 0; therefore the anisotropy coefficient must be redefined as follow:

$$anisotropy\ coefficient = \frac{velocity(\theta) - velocity(\theta = 90^\circ)}{velocity(\theta = 90^\circ)} \tag{4.12}$$

First, the influence of bulk modulus contrast is researched. In all figures below in this chapter, the solid lines represent the velocities of the fast P-wave, and the dashed lines represent the velocities of the slow P-wave. Figure 4.4 describes the effect of varied bulk modulus contrast between solid and the fluid layers on angular dependent phase velocities . Figure 4.5 shows the effect of varying contrasts in which there is an anisotropy coefficient given. Figure 4.6 then shows what effect may occur on group velocities. As Figure 4.5 shows, as bulk modulus contrast increases, the angle where there is a turning point shifts to that of a smaller value. Figure 4.6 denotes that the range of angle in which a slow P-wave exists becomes wider as the bulk modulus contrast increases. In a case of very high contrast, however, the relatively constant parts of fast and slow waves tend to be continuous, with any expected gap almost vanishing.

Figures 4.7 to 4.9 denote the influence of different density contrasts. As shown in Figure 4.8, at low density contrast, the anisotropy coefficient of slow wave from 90° to 0° increases slightly first and then decreases. Thus the anisotropy coefficient

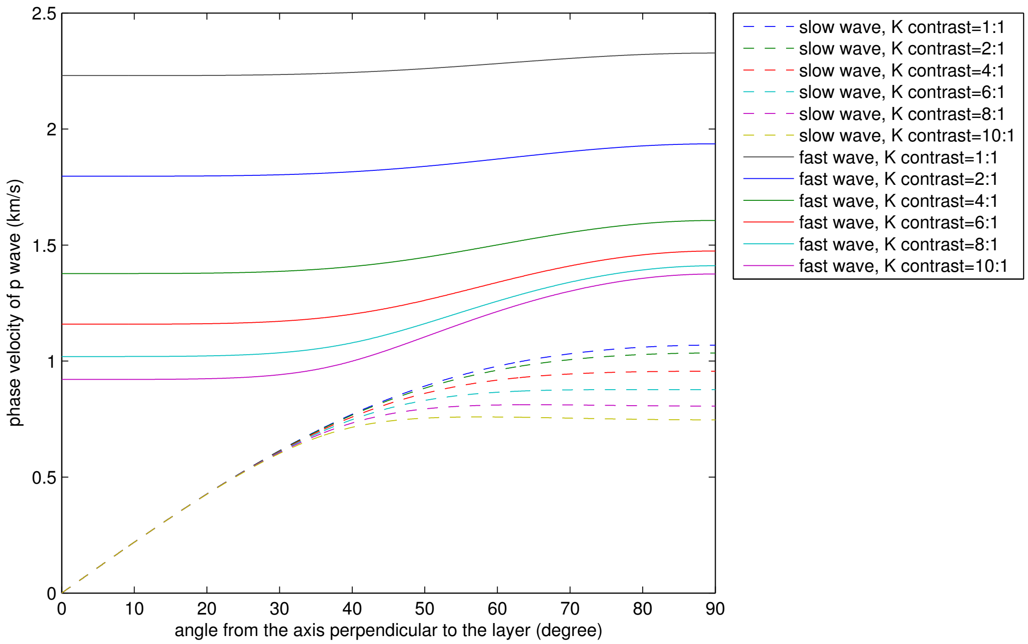

Figure 4.4: effect of varying bulk modulus contrast on angular dependent phase velocity. solid layer: K=7.13 GPa; μ=0.95 GPa; density=2.1 g/cm^3; fluid layer: μ=0 GPa; density=1 g/cm^3

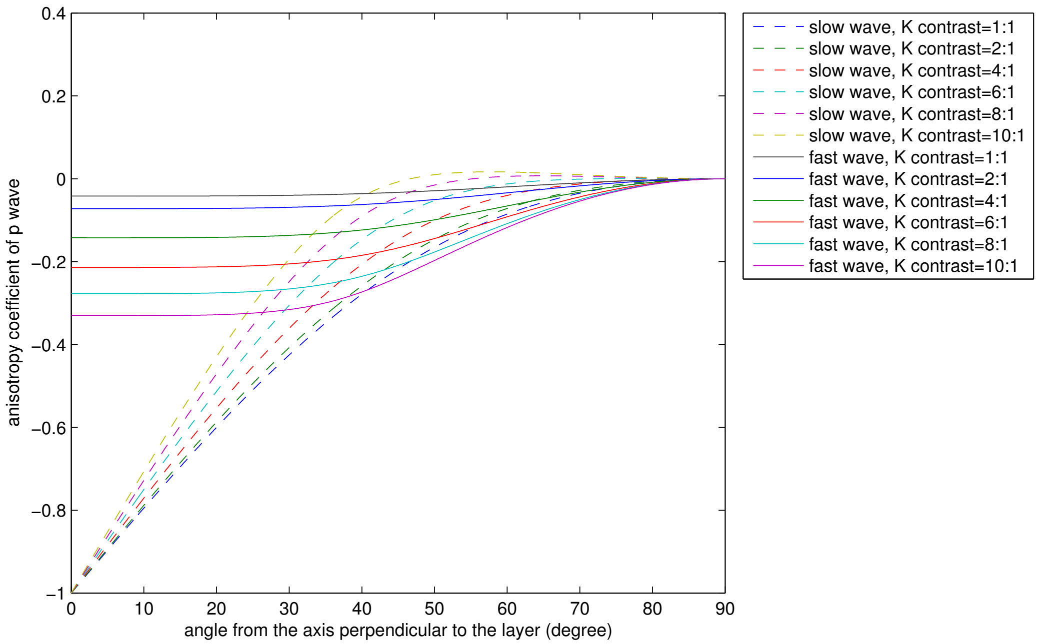

Figure 4.5: effect of varying bulk modulus contrast on anisotropy. solid layer: K=7.13 GPa; μ=0.95 GPa; density=2.1 g/cm^3; fluid layer: μ=0 GPa; density=1 g/cm^3

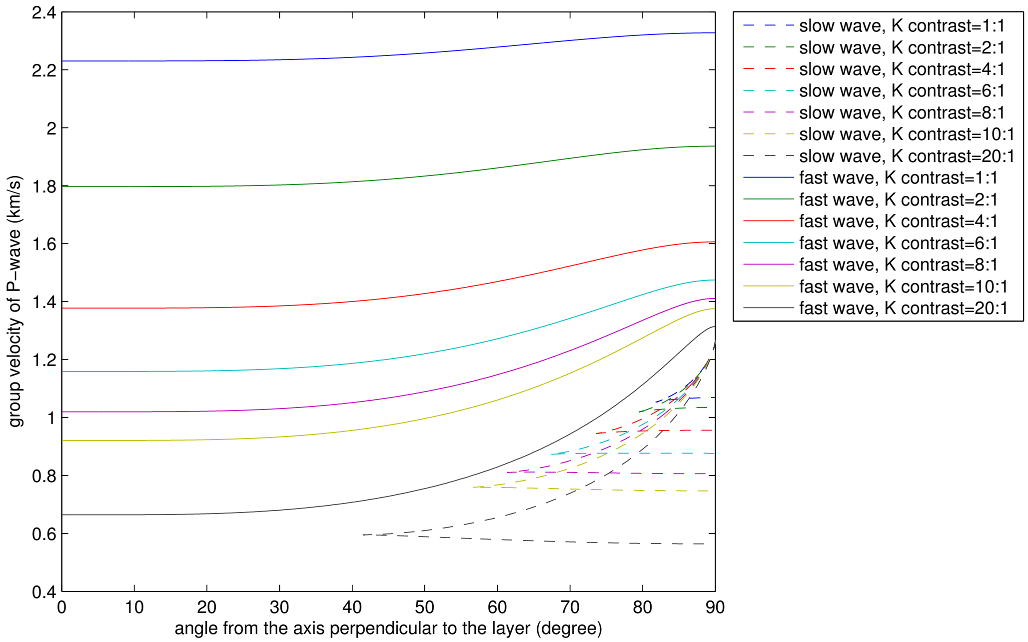

Figure 4.6: effect of varying bulk modulus contrast on angular dependent group velocity. solid layer: K=7.13 GPa; μ=0.95 GPa; density=2.1 g/cm^3; fluid layer: μ=0 GPa; density=1 g/cm^3

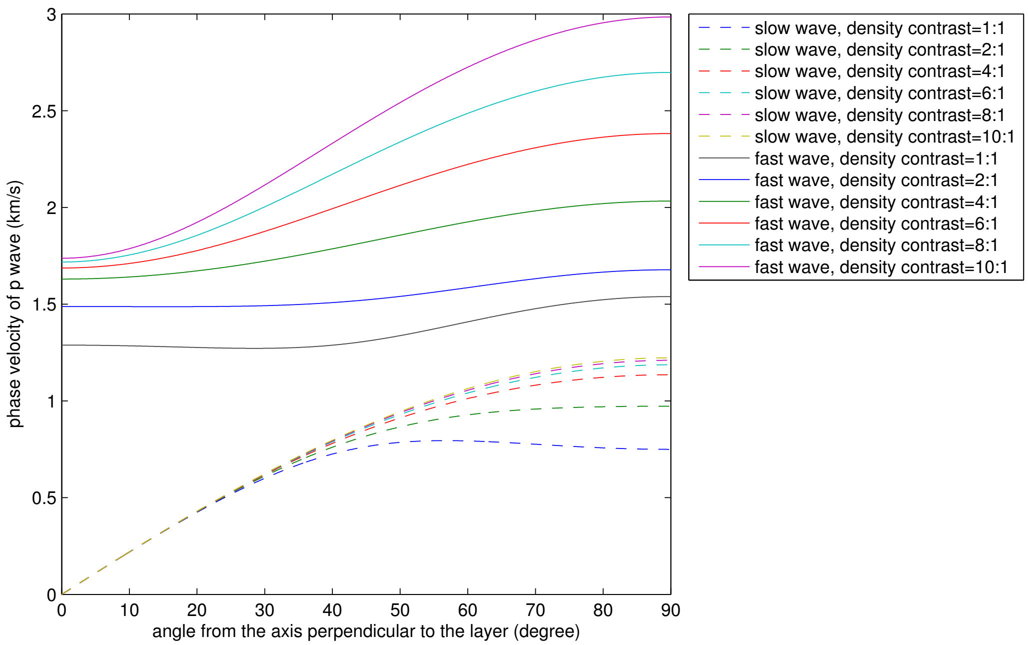

Figure 4.7: effect of varying density contrast on angular dependent phase velocity. solid layer: K=7.13 GPa; μ=0.95 Gpa; density=2.1 g/cm^3; fluid layer: K=2.2 GPa; μ=0 GPa;

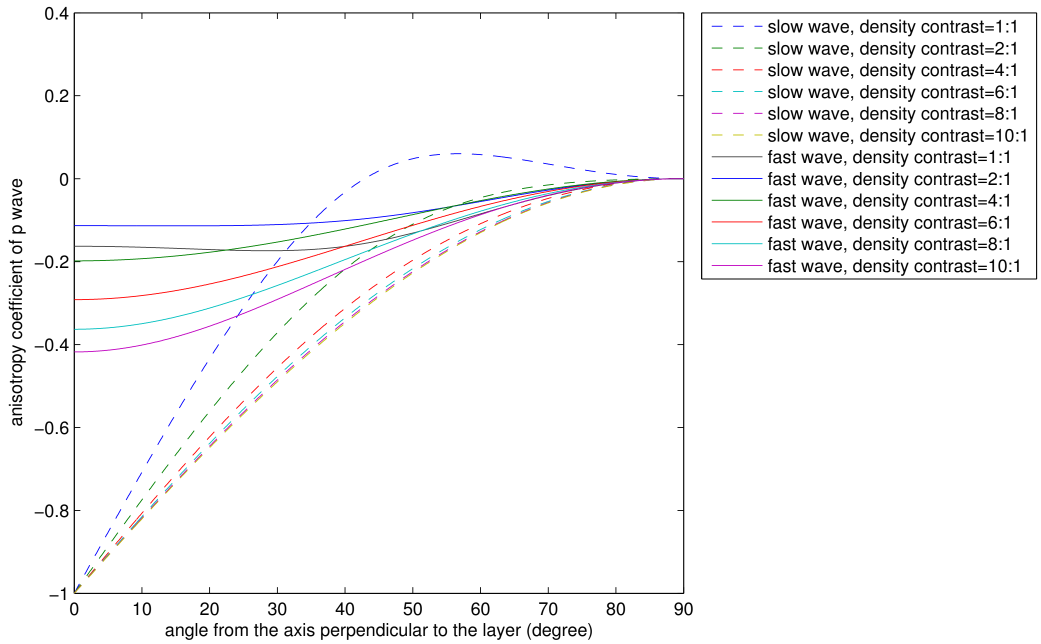

Figure 4.8: effect of varying density contrast on anisotropy. solid layer: K=7.13 GPa; μ=0.95 Gpa; density=2.1 g/cm^3; fluid layer: K=2.2 GPa; μ=0 GPa;

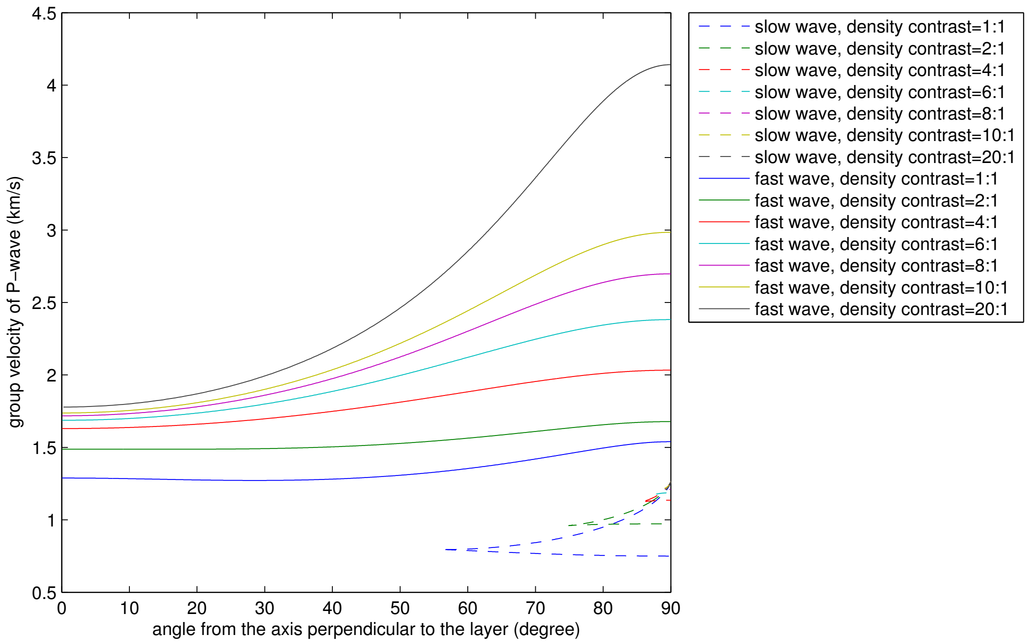

Figure 4.9: effect of varying density contrast on angular dependent group velocity. solid layer: K=7.13 GPa; μ=0.95 Gpa; density=2.1 g/cm^3; fluid layer: K=2.2 GPa; μ=0 GPa;

of fast wave at low density contrast first decreases and then increases slightly. It is given then, that the behavior of lines with higher density contrasts, which are almost monotonic, differs from how lines with lower density contrasts behave. It is already discussed in a previous chapter that in a case involving the solid-solid medium, the effective anisotropy is not influenced by density contrast; again from Equation 2.3 this can be examined. However, in the case of alternating solid and liquid layers, density contrast has an effect on the anisotropy of the effective medium. This phenomenon can be described by the effective medium theory of an elastoacoustic medium at long wavelength (Schoenberg, 1984). The effective medium is described as fluid, so S-wave cannot propagate through it, and it is anisotropic with more than one P-wave. The particle velocity, ν, is related to negative pressure σ through an equation of motion

$$\nabla\sigma = \overline{\rho}\frac{\partial \boldsymbol{\nu}}{\partial t} \equiv \begin{bmatrix} \rho_{\parallel} & 0 \\ 0 & \rho_{\perp} \end{bmatrix} \begin{bmatrix} \frac{\partial \nu_1}{\partial t} \\ \frac{\partial \nu_3}{\partial t} \end{bmatrix} \tag{4.13}$$

which shows anisotropy through the second rank tensor of density. In Figure 4.9, it can be observed that the range of angle in which the slow wave exists becomes narrower as the density contrast increases.

Figure 4.10 and Figure 4.11 indicate the effect of thickness on behavior of the angular dependent velocity and given anisotropy coefficient.

4.3 Comparison between Backus' and Schoenberg's method in extreme thickness contrast

Both Backus' and Schoenberg's method can be used to predict the behavior of angular dependent phase velocity for a periodic layered medium when wavelength

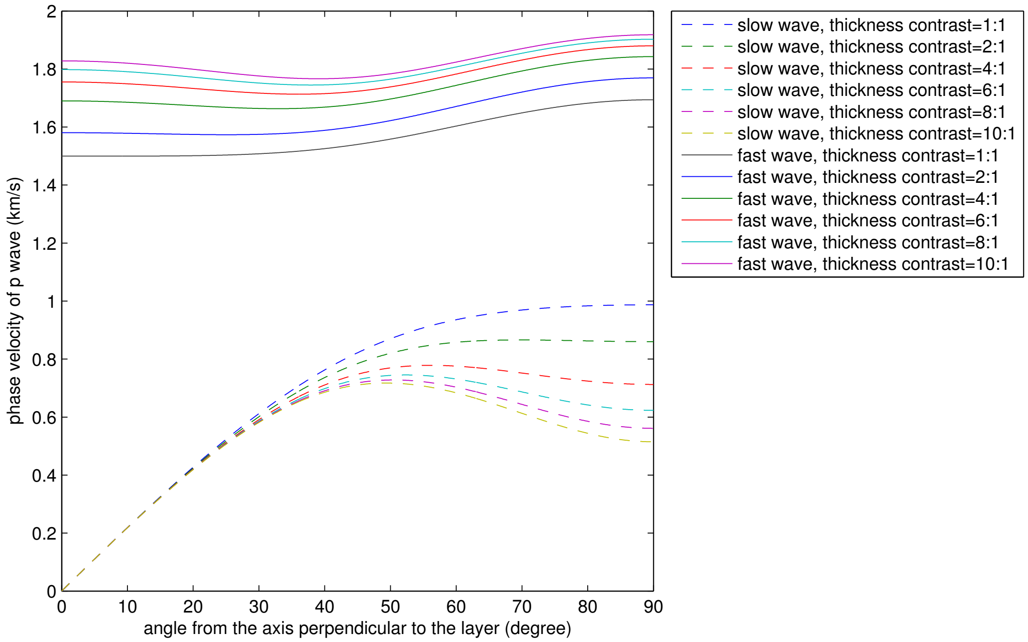

Figure 4.10: effect of varying thickness contrast on angular dependent phase velocity. solid layer: K=7.13 Gpa; μ=0.95 Gpa; density=2.1 g/cm^3; fluid layer: K=2.2 Gpa; μ=0 Gpa; density=1 g/cm^3

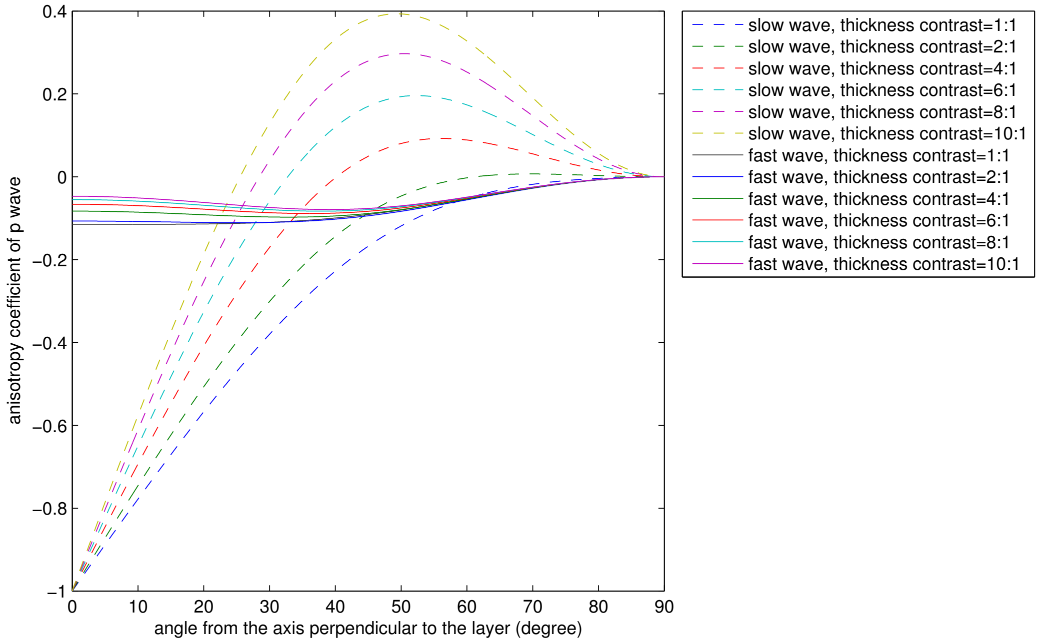

Figure 4.11: effect of varying thickness contrast on anisotropy. solid layer: K=7.13 Gpa; μ=0.95 Gpa; density=2.1 g/cm^3; fluid layer: K=2.2 Gpa; μ=0 Gpa; density=1 g/cm^3

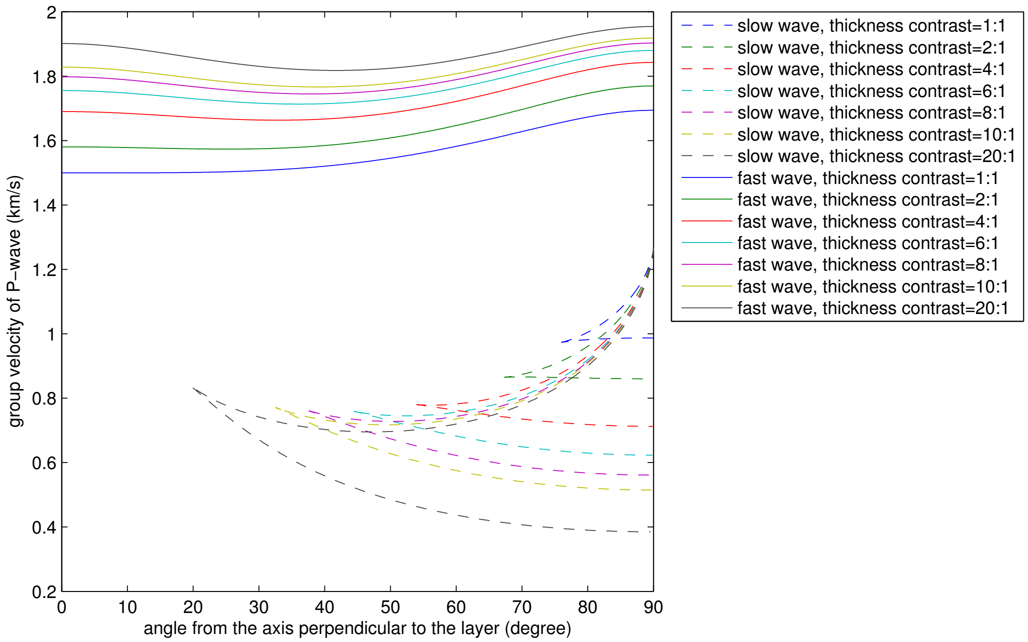

Figure 4.12: effect of varying thickness contrast on angular dependent group velocity. solid layer: K=7.13 Gpa; μ=0.95 Gpa; density=2.1 g/cm^3; fluid layer: K=2.2 Gpa; μ=0 Gpa; density=1 g/cm^3

is much greater than the spatial period of the medium. Backus' method can be only used for a medium that consists of all solid layers; by contrast, Schoenberg's method can handle a case of a medium consisting of alternating solid and fluid layers. However, if the thickness of the solid layer is much greater than that of the fluid layer, the effective whole medium will be closer to a medium with all solid layers. In this case, how the prediction of Backus' method works out compared with that of Schoenberg's method is an interesting question. On the other hand, if the thickness of the fluid layer is much greater than that of the solid layers, will Schoenberg's method yield a plausible prediction? What then is the result of Backus's method even if the behavior that results is not what is expected or thought to be correct?

We set a medium consisting of two kinds of isotropic media periodically, with alternating solid and fluid layers. Equation 2.4 is applied to get results from Backus's method, and Equation 4.6 is used to calculate Schoenberg's prediction. There are two models. The physical parameters of the models are shown in Table 4.1.

Table 4.1: The physical parameters of the models

physical parameters	Model I		Model II	
	solid layer	fluid layer	solid layer	fluid layer
$K(GPa)$	7.13	2.2	20.35	2.2
$\mu(GPa)$	0.95	0	13.24	0
$\rho(g/cm^3)$	2.1	1	2.37	1

Figures 4.13 - 4.22 give the predictions from Backus' and Schoenberg's methods at different thickness contrasts, in which the solid lines represent the result of Backus's method, and the dashed lines denote the result of Schoenberg's method. Figures 4.13 - 4.17 concern Model I, and Figures 4.18 - 4.22 concern Model II.

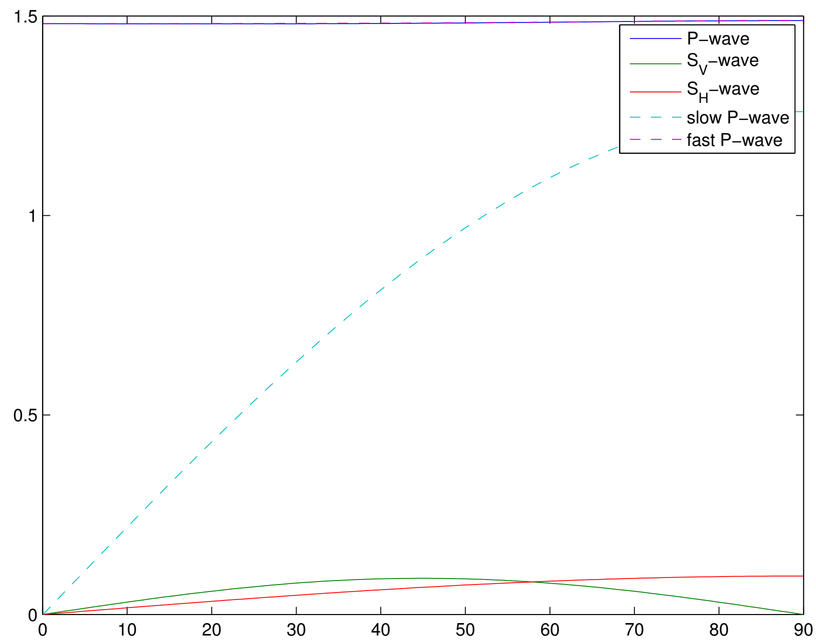

Figure 4.13: Model I: thickness contrast: 1:100. The physical parameters are given in Table 4.1.

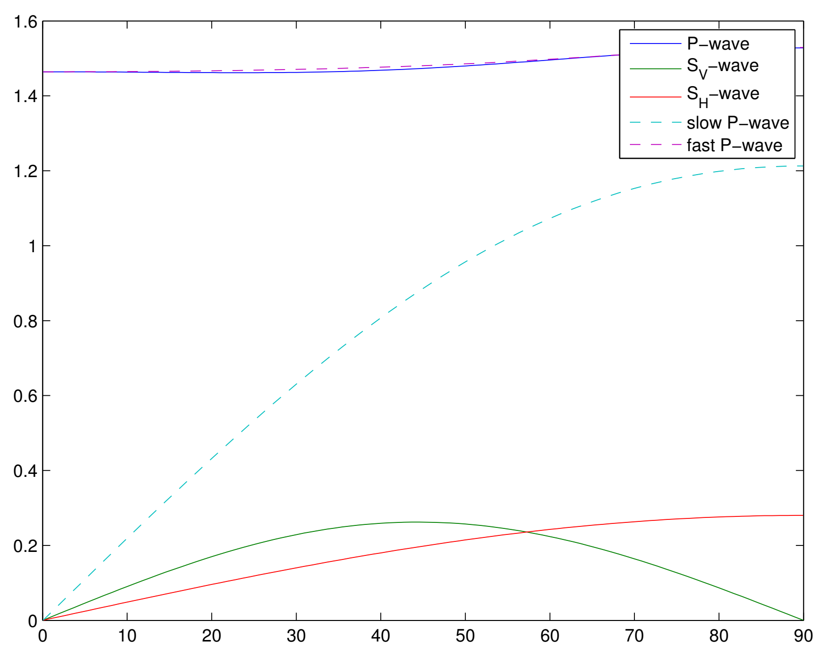

Figure 4.14: Model I: thickness contrast: 1:10. The physical parameters are given in Table 4.1.

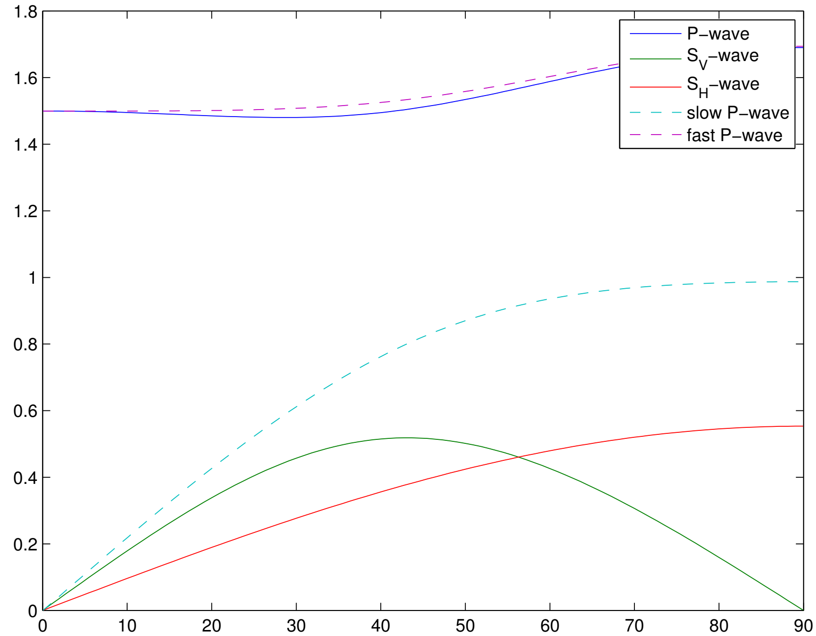

Figure 4.15: Model I: thickness contrast: 1:1. The physical parameters are given in Table 4.1.

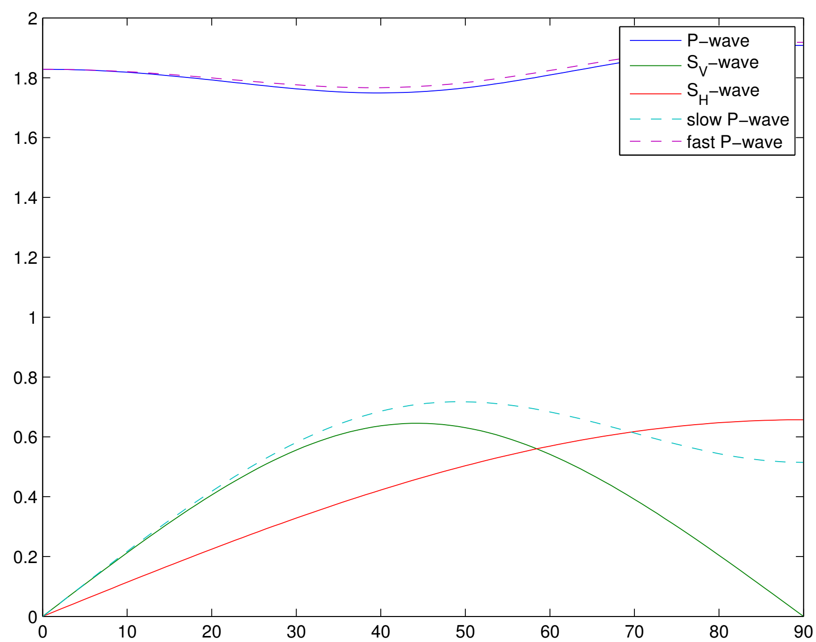

Figure 4.16: Model I: thickness contrast: 10:1. The physical parameters are given in Table 4.1.

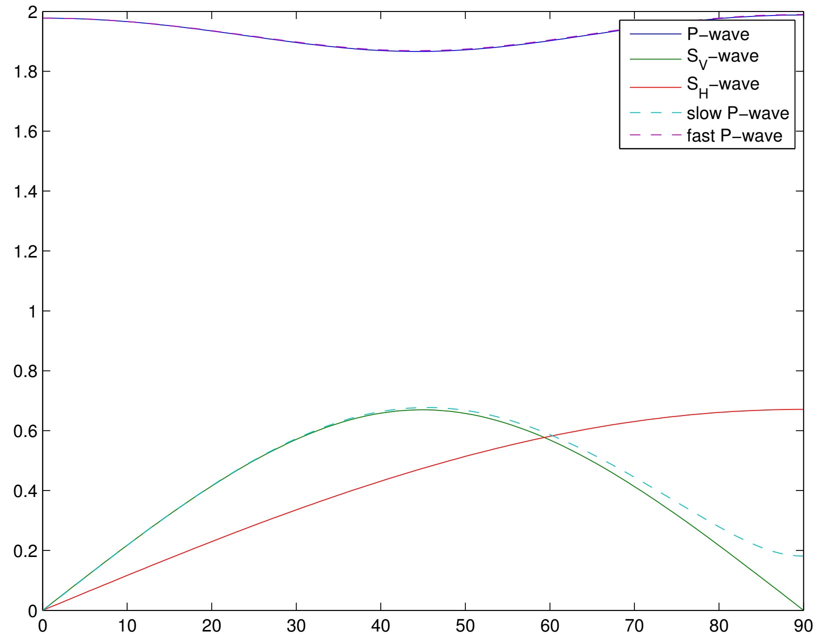

Figure 4.17: Model I: thickness contrast: 100:1. The physical parameters are given in Table 4.1.

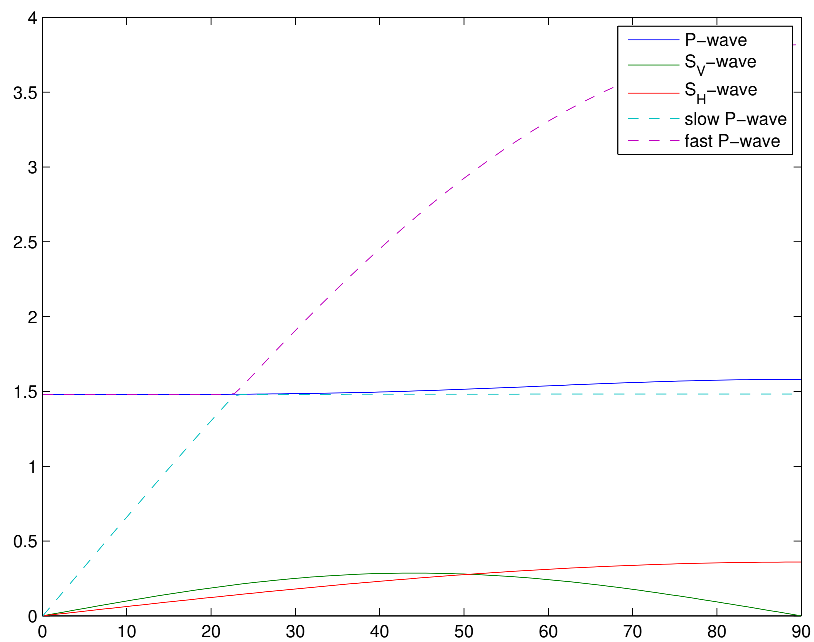

Figure 4.18: Model II: thickness contrast: 1:100. The physical parameters are given in Table 4.1.

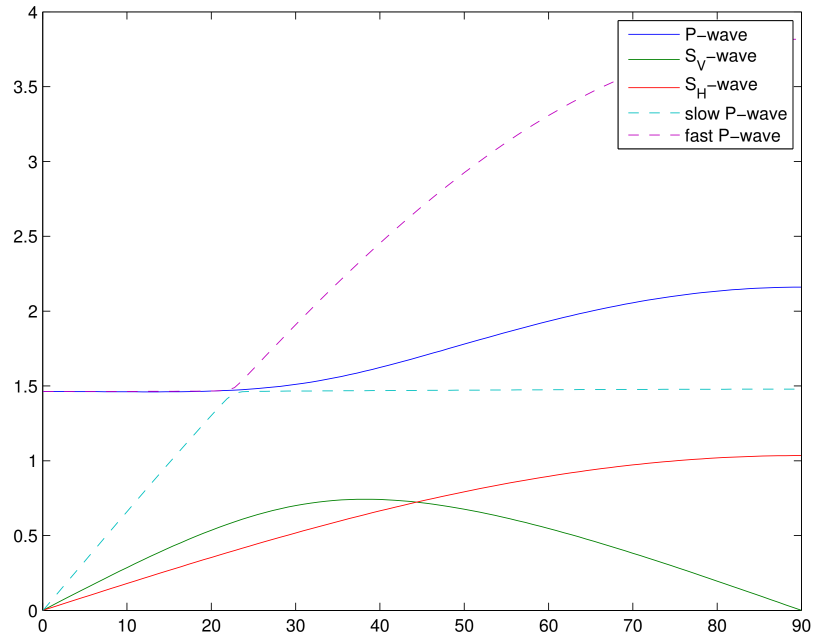

Figure 4.19: Model II: thickness contrast: 1:10. The physical parameters are given in Table 4.1.

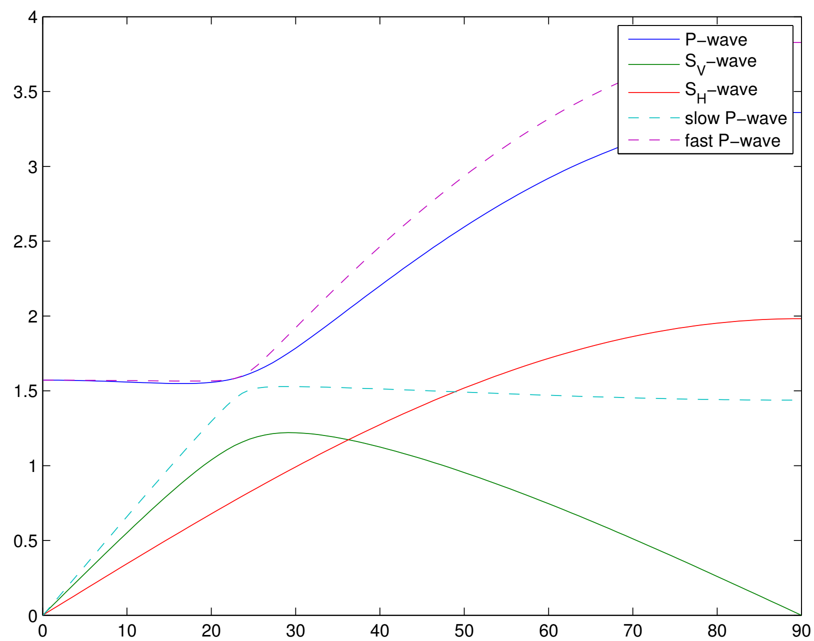

Figure 4.20: Model II: thickness contrast: 1:1. The physical parameters are given in Table 4.1.

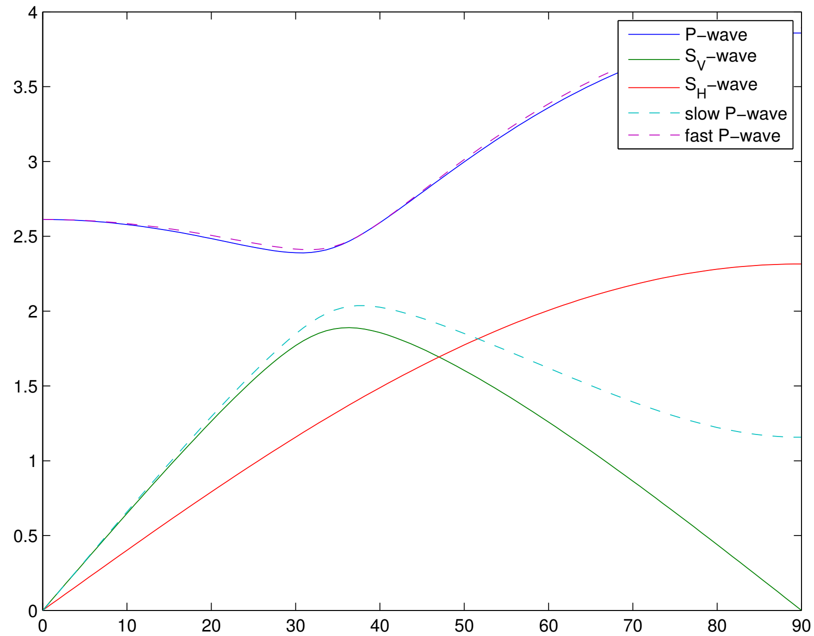

Figure 4.21: Model II: thickness contrast: 10:1. The physical parameters are given in Table 4.1.

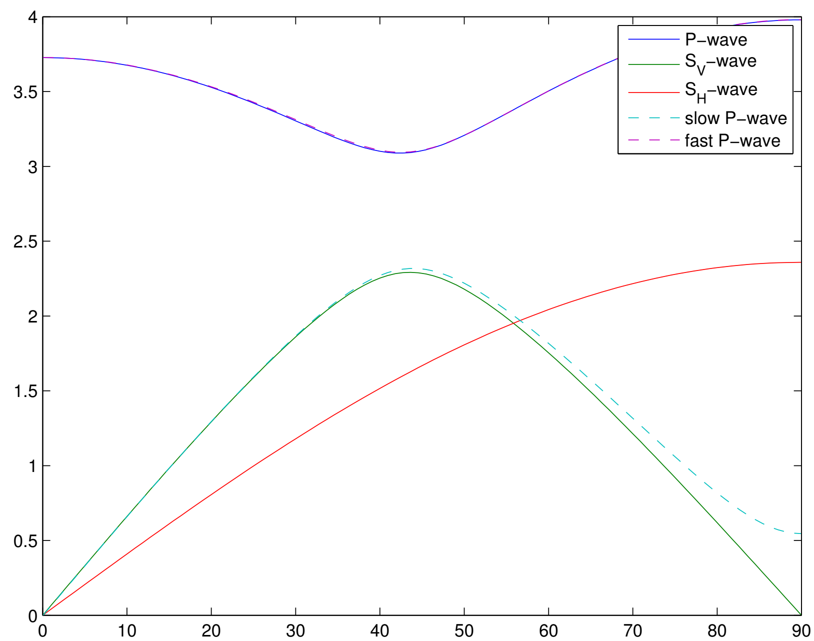

Figure 4.22: Model II: thickness contrast: 100:1. The physical parameters are given in Table 4.1.

Chapter 5

The Medium with Aligned Fractures in Low Crack Density

5.1 Introduction

The periodic layered medium with alternating solid and fluid layers is an model approximating a matrix with aligned fractures. In this approximation, the fluid layers are supposed to simulate the aligned fractures which are flat and contain high fracture density. However, for aligned fractures with relatively high aspect ratio and low fracture density, another model instead of periodic layered medium will be considered. J. D. Eshelby's inclusion theory provides the basic theory for building this model (Eshelby, 1957).

5.2 Eshelby's inclusion

Eshelby (1957) devised a set of problems involving ellipsoidal elastic inclusions in an infinite elastic body. According to Eshelby's thinking, for a linear elastic body to contain an inclusion, the inclusion must have undergone a transformation (such as localized thermal expansion or crystal twinning), but also the change of its shape and size is restricted by the surrounding material. In this situation, the inclusion and the surrounding material still occur in a stressed state. Eshelby provides the thought that using a “sequence of imaginary cutting, straining and welding operations.”, it is then found that the strain and stress fields inside the ellipsoidal inclusion are uniform and thus provide a closed-form solution. In order to solve the transformation problem, we shall make use of the set of imaginary cutting, straining and welding operations. The first step, to cut around the target region (i.e. the inclusion) and then remove it from the matrix, is shown in Figure 5.1(a). The second step is to apply certain surface stress on the region to restore it to its original form, then to put it back in the original position in the matrix to reintegrate the involved material across the cut. Now the stress in the matrix equals zero, with a known constant value as the inclusion. The surface traction is set along lines generated by a layer of body force spread over the interface between the matrix and the inclusion. The third step, this unwanted layer should be removed in order to complete the solution by applying a layer of body force with equal and opposite values. The second and third steps are shown in Figure 5.1(b) (Glas, 2011). As a result, the stress and strain in the inclusion do not satisfy Hooke’s law, because part of the strain is generated by a non-elastic twinning or other transformation within which no stress is involved.

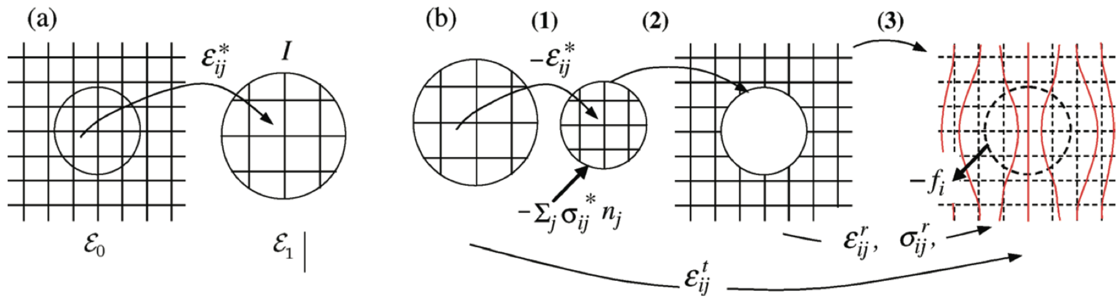

Figure 5.1: (a) Stress-free strain relative to the inclusion. (b) The three stages of an Eshelbys process. (Glas, 2011)

5.3 Effective transversely isotropic medium of crack model

Using this theory, we can obtain an exact solution of strain inside an ellipsoidal inclusion in an isotropic matrix, with constant stress or strain applied, thus giving us a static solution. Considering the potential energy of the total system, effective elastic moduli are obtained with volume V under a constant applied strain e^A (Cheng, 1993):

$$\frac{1}{2}c_{ij}^* e_i^A e_j^A V = \frac{1}{2}c_{ij}^0 e_i^A e_j^A V + E_{int} \tag{5.1}$$

where c^* is the stiffness matrix of the effective medium, c^0 is the stiffness matrix of the background matrix, and E_{int} is the change in the energy resulting from presence of the crack:

$$E_{int} = -\frac{1}{2}c_{ij}^0 e_i^A e_j^T V_{int} \tag{5.2}$$

e_j^T is the "stress-free" strain of the inclusion - the strain necessary to restore the inclusion to its original shape under the applied strain e_j^A. This strain is associated with the applied strain through a matrix, and thus a function of the volume, the aspect ratio of the inclusion, and its elastic properties. V_{int} is the volume of the inclusion. The result is that

$$c_{ij}^* = c_{ij}^0 - \phi c_{ij}^1 \tag{5.3}$$

where ϕ is the porosity.

For a medium with isotropic matrix and horizontally aligned fractures evenly distributed in a vertical direction, the effective elastic moduli have the form (subscript 3 represent the vertical axis) as follows:

$$\begin{aligned}
c_{11}^1 =& \lambda(s_{31} - s_{33} + 1) \\
&+ \frac{2\mu(s_{33}s_{11} - s_{31}s_{13} - (s_{33} + s_{11} - 2C - 1) + C(s_{31} + s_{13} - s_{11} - s_{33}))}{D(s_{12} - s_{11} + 1)} \\
c_{33}^1 =& \frac{(\lambda + 2\mu)(-s_{12} - s_{11} + 1) + 2\lambda s_{13} + 4\mu C}{D} \\
c_{13}^1 =& \frac{(\lambda + 2\mu)(s_{13} + s_{31}) - 4\mu C + \lambda(s_{13} - s_{12} - s_{11} - s_{33} + 2)}{2D} \\
c_{44}^1 =& \frac{\mu}{1 - 2s_{1313}} \\
c_{66}^1 =& \frac{\mu}{1 - 2s_{1212}}
\end{aligned} \tag{5.4}$$

with

$$
\begin{aligned}
D =& s_{33}s_{11} + s_{33}s_{12} - 2s_{31}s_{13} - (s_{11} + s_{12} + s_{33} - 1 - 3C) \\
& - C(s_{11} + s_{12} + 2(s_{33} - s_{13} - s_{31})) \\
s_{11} =& QI_{aa} + RI_a \\
s_{33} =& Q(\frac{4\pi}{3} - 2I_{ac}\alpha^2) + I_c R \\
s_{12} =& QI_{ab} - RI_a \\
s_{13} =& QI_{ac}\alpha^2 - RI_a \\
s_{31} =& QI_{ac} - RI_c \\
s_{1212} =& QI_{ab} + RI_a \\
s_{1313} =& \frac{Q(1+\alpha^2)I_{ac}}{2} + \frac{R(I_a + I_c)}{2} \\
C =& \frac{K_f}{3(K - K_f)}
\end{aligned}
\tag{5.5}
$$

and

$$
\begin{aligned}
I_a =& \frac{2\pi\alpha(cos^{-1}\alpha - \alpha S_a)}{S_a^3} \\
I_c =& 4\pi - 2I_a \\
I_{ac} =& \frac{I_c - I_a}{3S_a^2} \\
I_{aa} =& \pi - \frac{3I_{ac}}{4} \\
I_{ab} =& \frac{I_{aa}}{3} \\
\sigma =& \frac{3K - 2\mu}{6K + 2\mu} \\
S_a =& \sqrt{1 - \alpha^2} \\
R =& \frac{1 - 2\sigma}{8\pi(1 - \sigma)}
\end{aligned}
\tag{5.6}
$$

where K and μ are the bulk modulus and shear modulus of the matrix respectively, K_f is the bulk modulus of fluid in inclusions, and α is aspect ratio of the inclusion.

5.4 Property contrast between the matrix and the fluid in inclusions and aspect ratio of the inclusion

In this section, the main point to articulate is to explain how the property contrast between the matrix and the inclusion and the aspect ratio of the inclusion affects the phase and group velocities in all directions. The effective elastic constants are calculated with Equations 5.3 and 5.4. This algorithm is reliable only on condition that the crack density of inclusion is small; therefore, the crack density is set to be 0.05. The relation between crack porosity, aspect ratio, and crack density is

$$\phi = \frac{4}{3}\pi \, N_c \, \alpha \tag{5.7}$$

where ϕ is the crack porosity, α is the aspect ratio, and N_c is the crack density.

For this model, the properties of the matrix are constant, and variation in properties of the fluid in the crack produces different property contrasts. Figure 5.2 and 5.3 show that the anisotropy increases as bulk modulus contrast increases, except in cases involving the S_H-wave; the S_H-wave velocities only depend on c_{44} and c_{66}. Besides, the triplication of group velocity occurs when bulk modulus contrast is high. From Figure 5.4 and 5.5, it can be seen that density contrast does not have any effect on anisotropy of the effective medium. As shown in Figure 5.6 and 5.7, a higher aspect ratio of cracks generates a higher degree of anisotropy on velocities of the P-waves and S_V-waves.

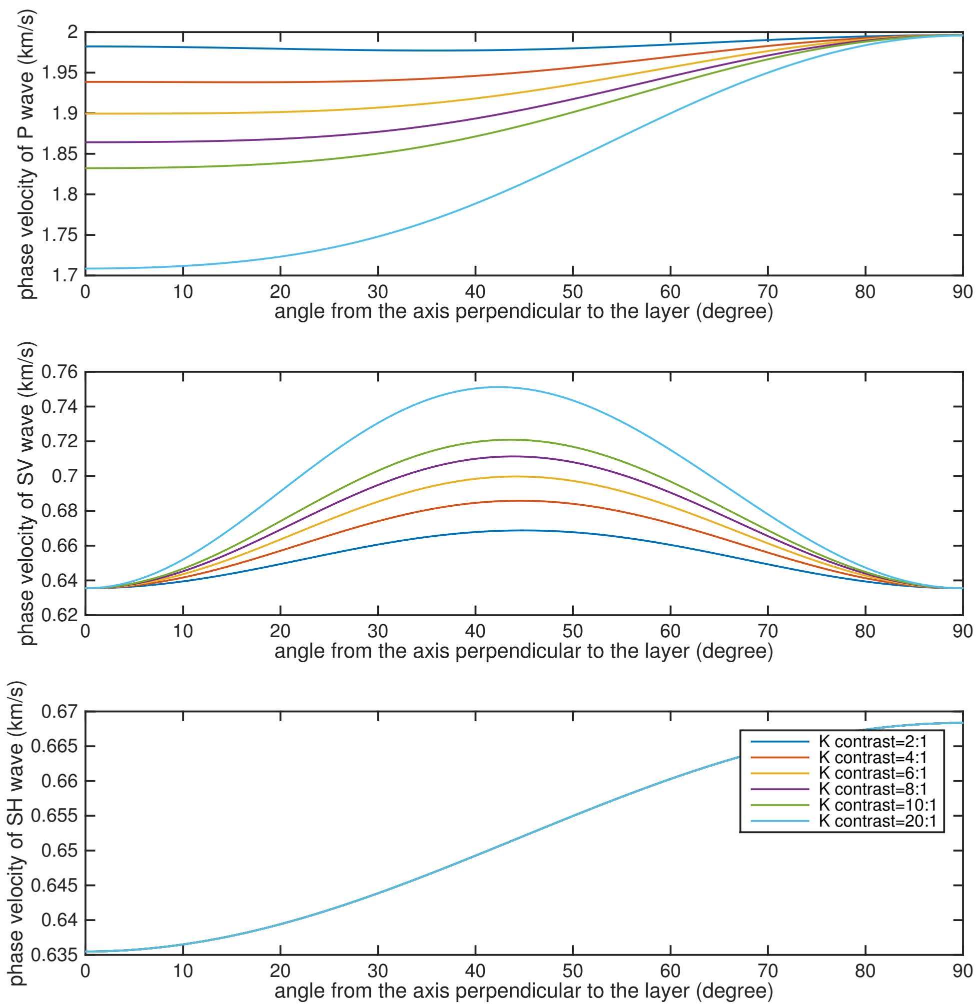

Figure 5.2: Effect on angle dependent phase velocities of variation of contrast of bulk moduli. matrix: $K = 7.13\, GPa$; $\mu = 0.95\, GPa$; density $\rho = 2.1\ g/cm^3$; fluid in the inclusion: $\mu = 0\, GPa$; density $\rho = 1\ g/cm^3$; aspect ratio $= 0.1$; crack density $=$ 0.05

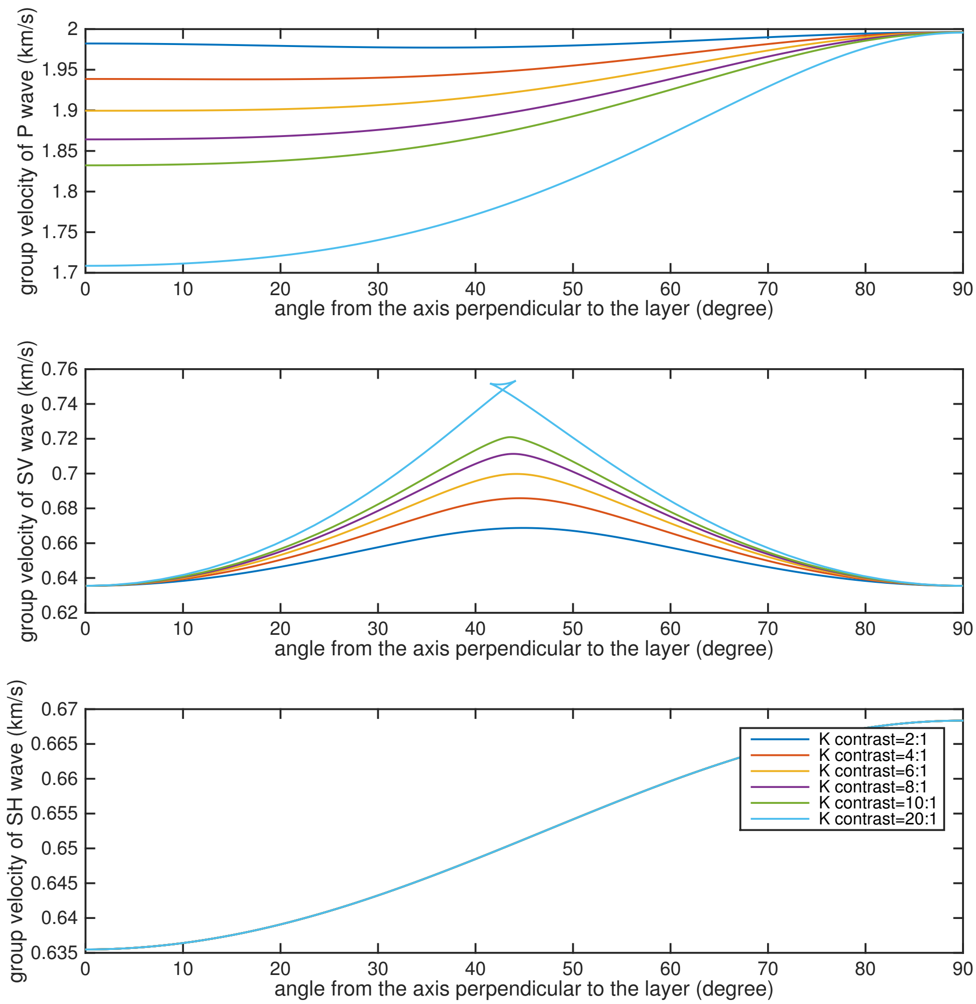

Figure 5.3: Effect on angle dependent group velocities of variation of contrast of bulk moduli. matrix: $K = 7.13\, GPa; \mu = 0.95\, GPa$; density $\rho = 2.1\, g/cm^3$; fluid in the inclusion: $\mu = 0\, GPa$; density $\rho = 1\, g/cm^3$; aspect ratio $= 0.1$; crack density $=$ 0.05

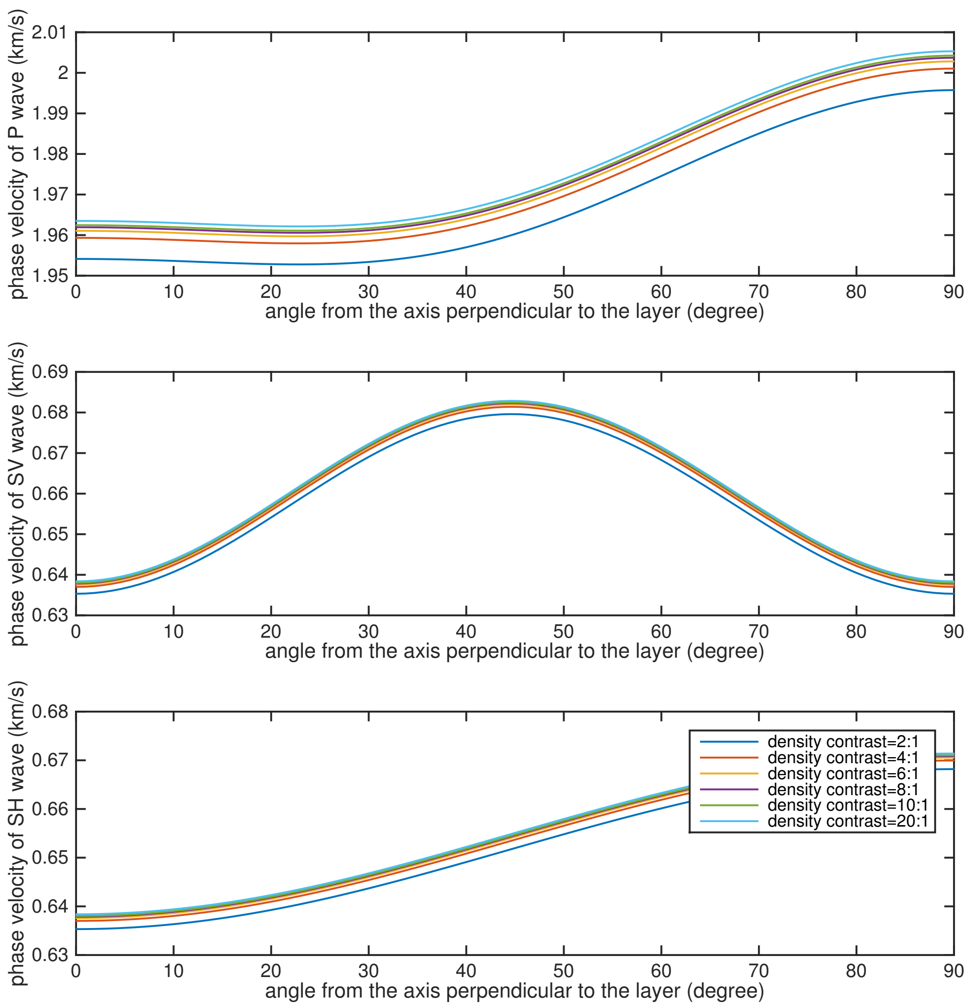

Figure 5.4: Effect on angle dependent phase velocities of variation of contrast of density. matrix: $K = 7.13\,GPa; \mu = 0.95\,GPa$; density $\rho = 2.1\,g/cm^3$; fluid in the inclusion: $\mu = 0\,GPa$; $K = 2.2\,Gpa$; aspect ratio $= 0.1$; crack density $= 0.05$

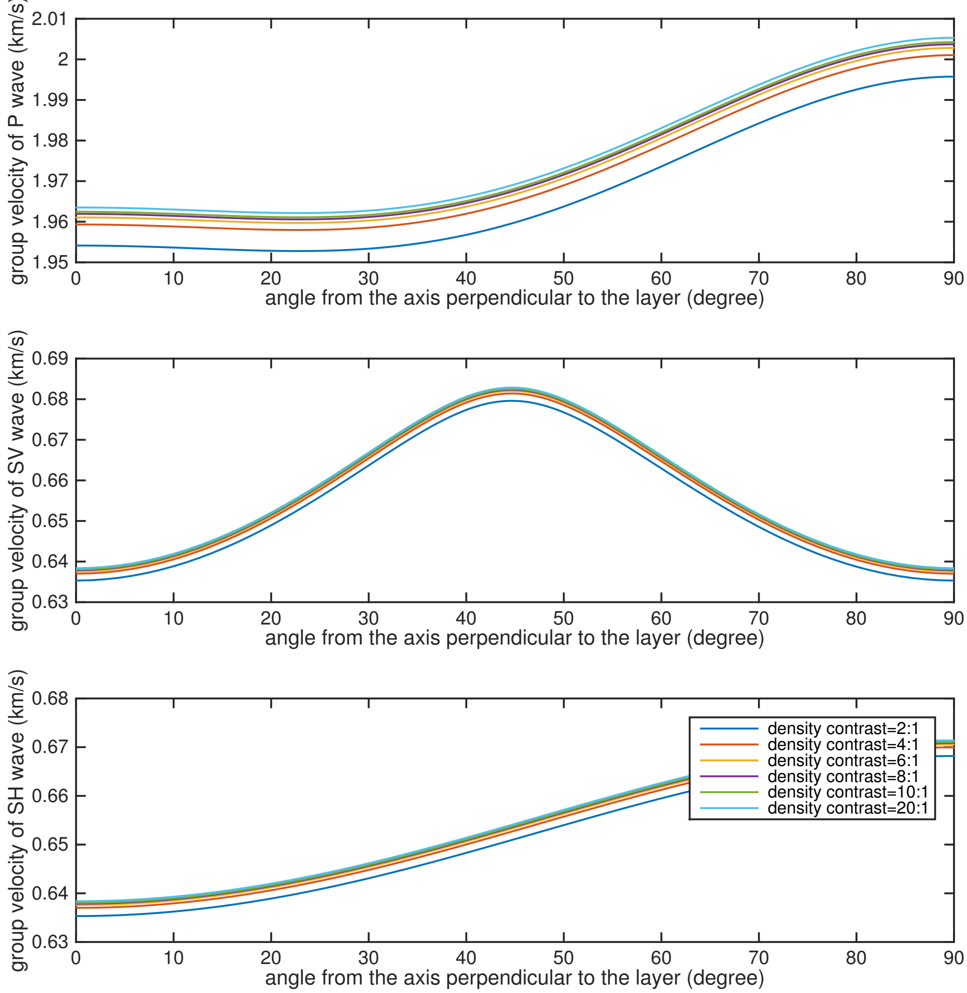

Figure 5.5: Effect on angle dependent group velocities of variation of contrast of density. matrix: $K = 7.13\,GPa; \mu = 0.95\,GPa$; density $\rho = 2.1\,g/cm^3$; fluid in the inclusion: $\mu = 0\,GPa$; $K = 2.2\,Gpa$; aspect ratio = 0.1; crack density = 0.05

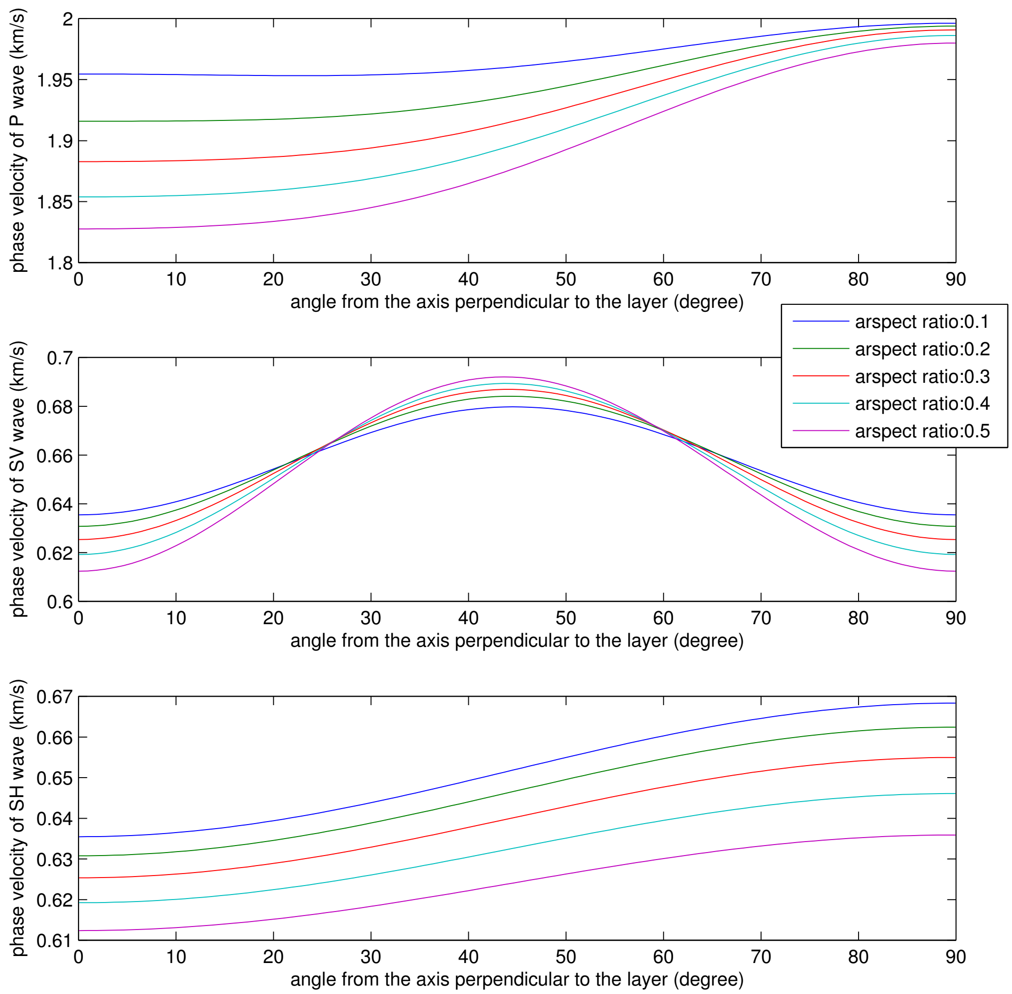

Figure 5.6: Effect on angle dependent phase velocities of variation of aspect ratio. matrix: $K = 7.13\,GPa; \mu = 0.95\,GPa$; density $\rho = 2.1\,g/cm^3$; fluid in the inclusion: $\mu = 0\,GPa$; $K = 2.2\,Gpa$; density $\rho = 2.1\,g/cm^3$; crack density $= 0.05$

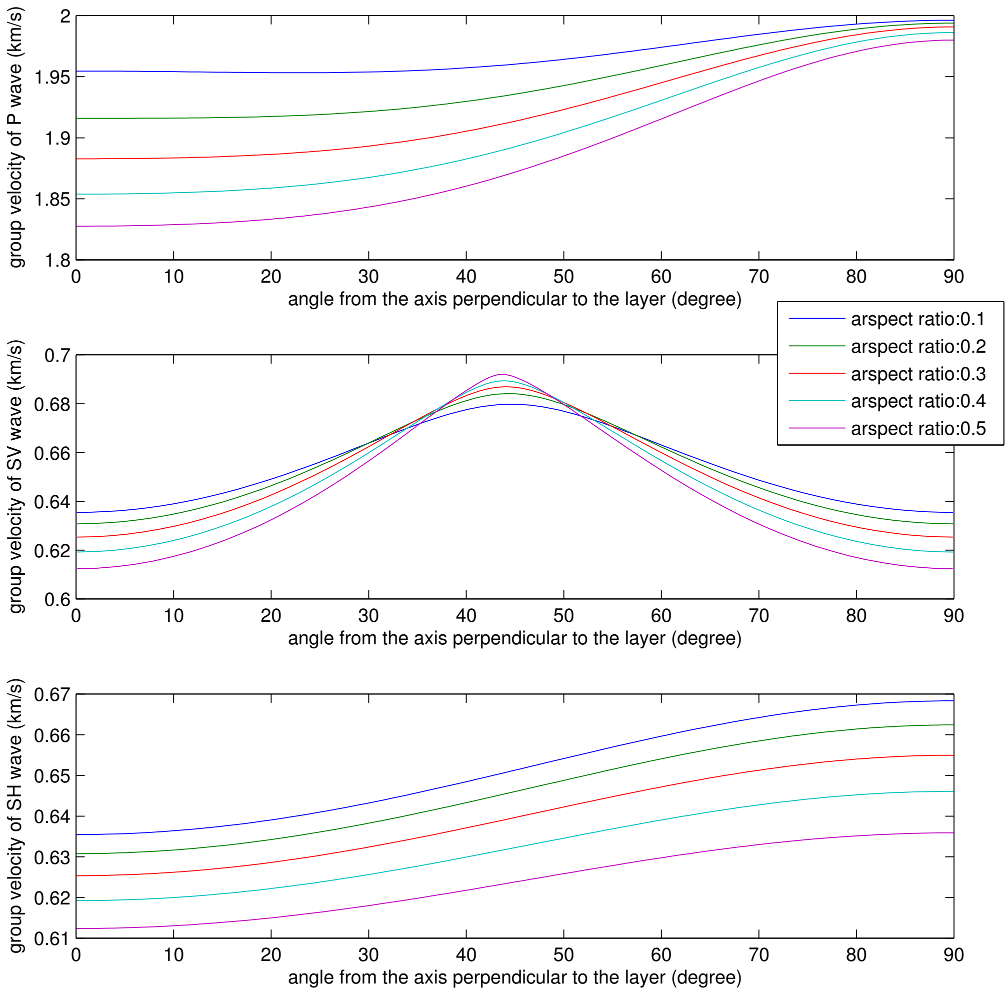

Figure 5.7: Effect on angle dependent group velocities of variation of aspect ratio. matrix: $K = 7.13\,GPa; \mu = 0.95\,GPa$; density $\rho = 2.1\,g/cm^3$; fluid in the inclusion: $\mu = 0\,GPa$; $K = 2.2\,Gpa$; density $\rho = 2.1\,g/cm^3$; crack density $= 0.05$

5.5 Porous layered periodic medium

Consider a layered periodic medium whose layer itself is not homogeneous, for instance, where aligned fractures exist. The model can be constructed that the layered medium is composed alternately and periodically of two kinds of layers. The first layer is porous, formed by water-saturated penny-shaped elliptical inclusions and an isotropic background matrix; the second layer is isotropic and a homogeneous solid. If the wavelength is much greater than the spatial period of the layered medium and the crack density of the porous layer is lower than 0.1, the effective elastic constants of the porous layer can be calculated using Cheng (1993)'s method.

By using Cheng's method, we can obtain the effective transversely isotropic medium with five independent elastic constants. However, this medium can be further simplified. The effective transversely isotropic medium can be described by two sets of effective isotropic medium, which are thus the Voigt average and Reuss average (Chesnokov). The Voigt average is the effective bulk modulus and shear modulus calculated based on assumption that the strain is uniform within the medium, whereas the Reuss average is obtained under an assumption of uniform stress.

For the medium with hexagonal (transversely isotropic) and trigonal symmetry, the relations between the effective isotropic elastic constants and the original elastic constants are

$$\begin{aligned}
K_V &= \frac{1}{9}(2c_{11} + c_{33} + 4c_{13} + 2c_{12}) \\
\mu_V &= \frac{1}{30}(7c_{11} + 2c_{33} - 5c_{12} - 4c_{13} + 12c_{44}) \\
K_R^{-1} &= 2s_{11} + s_{33} + 2s_{12} + 4s_{13} \\
\mu_R^{-1} &= \frac{2}{15}(7s_{11} - 5s_{12} - 4s_{13} + 2s_{33} + 3s_{44})
\end{aligned} \tag{5.8}$$

In order to make a comparison between the effect in layered periodic media of the effective transversely isotropic media constructed by Cheng's method and the effective isotropic media produced by Voigt and Reuss average, the model shown in Figure 5.8 can be used.

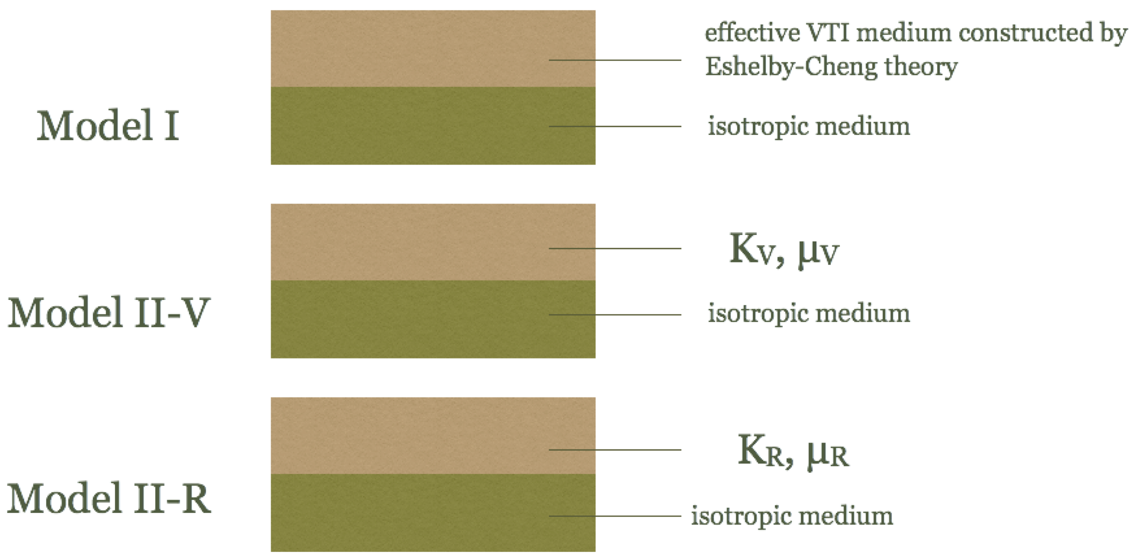

Figure 5.8: The three models of layered periodic media

As Figure 5.8 shows, each spatial period consists of two layers. The first layer is the effective medium and the second layer is the isotropic medium. And the effective elastic constants of the whole medium is calculated by Backus Average, given in Equation 2.4. The physical properties of the matrix of the first layer and the isotropic second layer are: bulk modulus $K = 20.35\ GPa$, shear modulus $\mu = 13.24\ GPa$, density $\rho = 2.37\ g/cm^3$; the fluid in the inclusions of the first layer is: $K = 2.2\ GPa, \rho = 1\ g/cm^3$. Figuress 5.9 - 5.11 show the behavior of angular dependent phase velocity of these three models, giving different aspect ratio of the inclusion in the porous layers. All three model have the same crack density assumed to be 0.05.

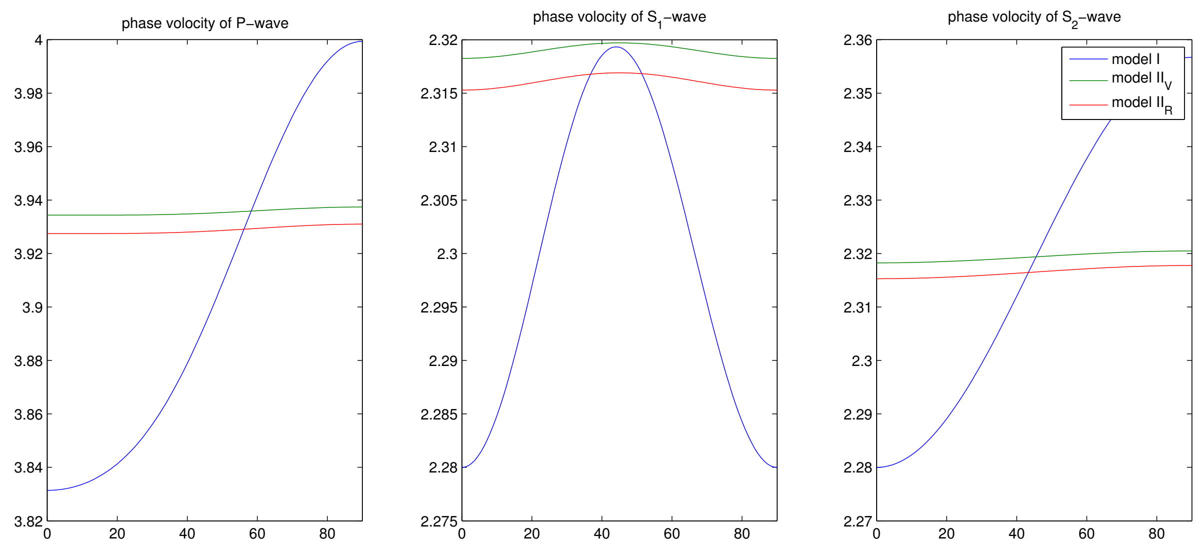

Figure 5.9: The behavior of angular dependent phase velocity of the three models. Aspect ratio of the inclusions: 0.1

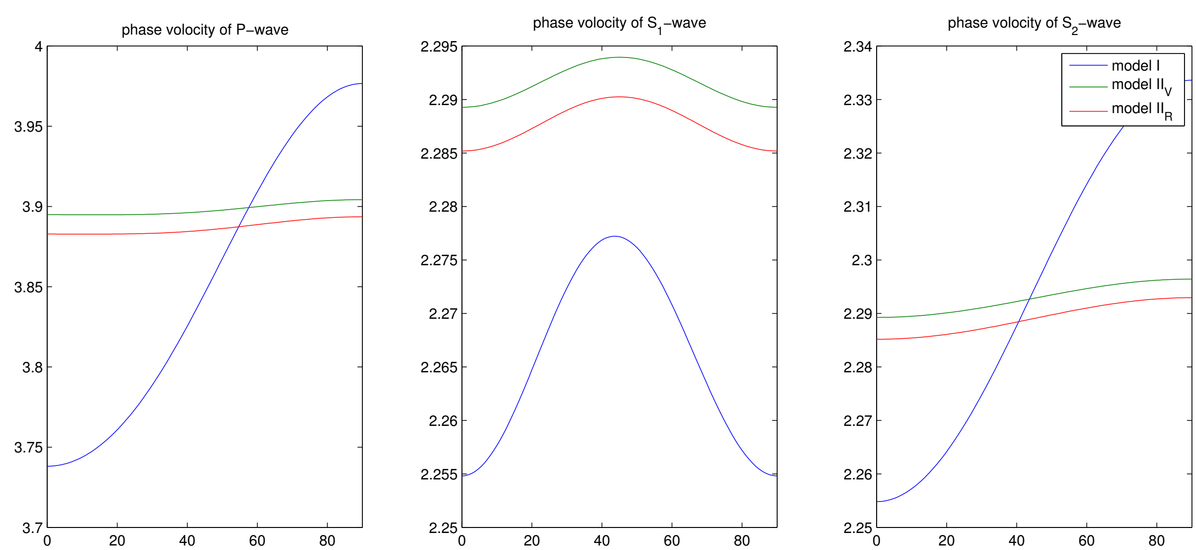

Figure 5.10: The behavior of angular dependent phase velocity of the three models. Aspect ratio of the inclusions: 0.3

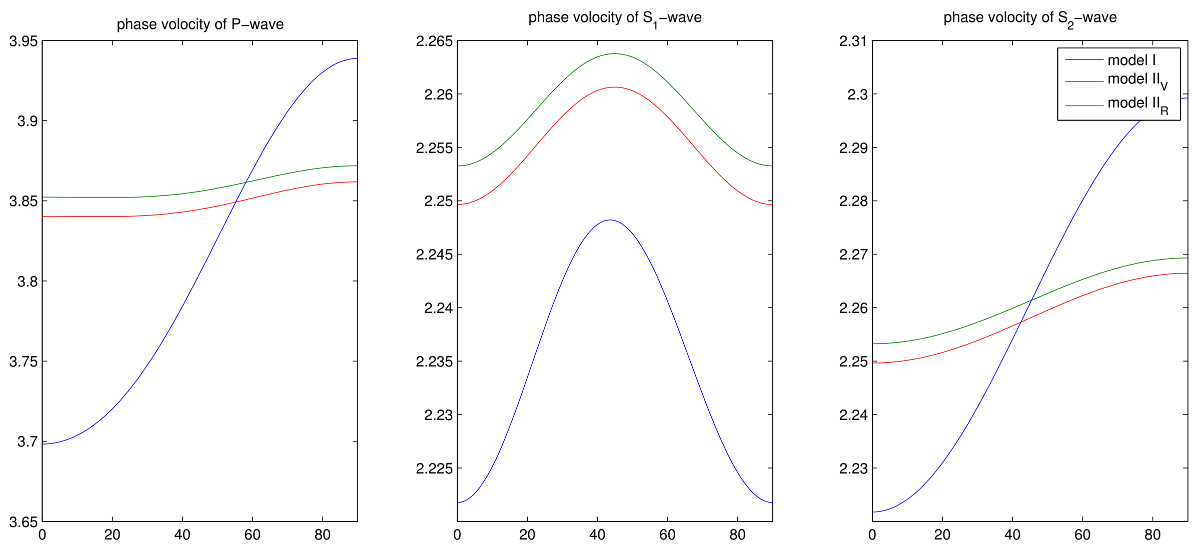

Figure 5.11: The behavior of angular dependent phase velocity of the three models. Aspect ratio of the inclusions: 0.5

Chapter 6

Conclusion and Discussion

In this thesis, the main result sought here is the numerical modeling in the forward problem of both a layered periodic medium and a medium with evenly distributed aligned penny-shape fractures. The model of layered periodic medium with alternating solid and fluid layers given approximates media with aligned fractures which have high crack density and low aspect ratio. The effects of different material contrasts on the behavior of anisotropy of phase and group velocity and the dispersion of phase velocity at direction normal to the layering are examined.

For the model of layered periodic medium with all solid layers based on condition of there being long wavelength, the effect of shear modulus contrast on anisotropy is essential. If shear moduli of two layers are equal, the effective medium is isotropic. The increase of bulk modulus contrast shifts the maximum S_V-wave velocity point to that of smaller angle.

For given model of elastoacoustic medium, there will be dispersion for propagating P-wave, and thereby stop-bands exist. For some wavelength values, there may then be more than one corresponding value of velocity to be expected. The limit of the velocity when frequency approaches infinity is equal to ray velocity. When wavelength is much greater than the spatial period of the medium, there are two modes of P-wave, the fast and the slow P-wave. Different from the layered periodic medium with all solid layers, the density contrast significantly influences anisotropy of the velocity in this situation.

For the model of medium with aligned fluid-saturated fractures which have low crack density, the increase of bulk modulus contrast will increase the anisotropy of the effective medium. As the aspect ratio increases from 0.1 to 0.5, the anisotropy of P-wave and S_V-wave increases.

Future work will focus on randomly layered media, meaning that from layer to layer there is no periodic change other than at random.

Bibliography

Backus, G. E., 1962, Long-wave elastic anisotropy produced by horizontal layering: Journal of Geophysical Research, **67**, 4427–4440.

Baird, A. F., J.-M. Kendall, and D. A. Angus, 2013, Frequency-dependent seismic anisotropy due to fractures: Fluid flow versus scattering: Geophysics, **78**, WA111–WA122.

Berryman, J. G., 1979, Long-wave elastic anisotropy in transversely isotropic media: Geophysics, **44**, 896–917.

———, 2005, Fluid effects on shear waves in finely layered porous media: Geophysics, **70**, N1–N15.

Brillouin, L., 1946, Wave propagation in periodic structures: McGraw-Hill Inc.

———, 1953, Wave propagation in periodic structures: electric filters and crystal lattices: Dover.

Cheng, C. H., 1993, Crack models for a transversely isotropic medium: Journal of Geophysical Research: Solid Earth (1978–2012), **98**, 675–684.

Coe, A. L., 2003, The sedimentary record of sea-level change: Cambridge University Press.

Delph, T., G. Herrmann, and R. Kaul, 1978, Harmonic wave propagation in a periodically layered, infinite elastic body: antiplane strain: Journal of Applied Mechanics, **45**, 343–349.

Eshelby, J. D., 1957, The determination of the elastic field of an ellipsoidal inclusion, and related problems: Proceedings of the Royal Society of London. Series A. Mathematical and Physical Sciences, **241**, 376–396.

Gilbert, F., and G. E. Backus, 1966, Propagator matrices in elastic wave and vibration problems: Geophysics, **31**, 326–332.

Glas, F., 2011, Elastic strain relaxation: Thermodynamics and kinetics: Mechanical Stress on the Nanoscale: Simulation, Material Systems and Characterization Techniques, 1–26.

Lee, E., and W. H. Yang, 1973, On waves in composite materials with periodic structure: SIAM Journal on Applied Mathematics, **25**, 492–499.

Lynn, H., and L. Thomsen, 1990, Reflection shear-wave data collected near the principal axes of azimuthal anisotropy: Geophysics, **55**, 147–156.

Mavko, G., T. Mukerji, and J. Dvorkin, 2009, The rock physics handbook: Tools for seismic analysis of porous media: Cambridge University Press.

Perdomo, J. P., 2012, Scale-frequency effect in elastic periodical multi-layered media: Master's thesis, University of Houston.

Postma, G., 1955, Wave propagation in a stratified medium: Geophysics, **20**, 780–806.

Rich, J., 2006, Quantitative analysis of material contrasts and wave propagation in periodic layered media: PhD thesis, University of Oklahoma.

Rytov, S., 1956, Acoustical properties of a thinly laminated media: Soviet Physics: Acoustics, **2**, 68–80.

Schoenberg, M., 1984, Wave propagation in alternating solid and fluid layers: Wave motion, **6**, 303–320.

Thomsen, L., 1986, Weak elastic anisotropy: Geophysics, **51**, 1954–1966.

Van Wagoner, J. C., R. Mitchum, K. Campion, and V. Rahmanian, 1990, Siliciclastic sequence stratigraphy in well logs, cores, and outcrops: concepts for high-resolution correlation of time and facies: AAPG Special Volumes.

Vernik, L., and A. Nur, 1992, Ultrasonic velocity and anisotropy of hydrocarbon source rocks: Geophysics, **57**, 727–735.

Ziman, J. M., 1972, Principles of the theory of solids: Cambridge University Press.